Robust Topological Design of Low Frequency Electromagnetic Devices

Min Li

B.Eng., M.Eng

Department of Electrical and Computer Engineering

McGill University

Montreal, Quebec, Canada

Dec. 11, 2013

A thesis submitted to the Faculty of Graduate and Postdoctoral Studies in partial fulfillment of the requirements for the degree of Doctor of Philosophy

ACKNOWLEDGMENTS

This work would never have been possible without the inspiration and guidance of my thesis supervisor, Prof. David A. Lowther. I am also grateful to the members of my Ph.D. committee: Prof. Hannah Michalska and Prof. Dennis D. Giannacopoulos, for their help and knowledge during the development of my research proposal.

I would also like to show my appreciation to Prof. Frederico G. Guimarães, a mentor and true friend, for the help during my visit in Brazil and the constant mind stimulating discussions.

Finally, I would like to express all my sincere gratitude to my wife Jun Xu, for her continuous loving support and abiding faith in me over the whole period of my Ph.D. studies.

Finally, I would like to thank the financial supports from les Fonds Québécois de la Recherche sur la Nature et les Technologies (FQRNT), the Natural Sciences and Engineering Research Council of Canada (NSERC), and the Canada-Brazil awards from Coordenação de

Aperfeiçoamento de Pessoal de Nível Superior and the Department of Foreign Affairs and International Trade CAPSE-DFAIT.

TABLE OF CONTENTS

LIST OF TABLES

LIST OF FIGURES

ABSTRACT

This thesis presents an automated topological design system for low frequency electromagnetic devices, e.g. an interior permanent magnet motor. The automated design is carried out through a topological shape optimization process: first, the system employs a topological sensitivity analysis to examine the design domain and to determine the optimal topology (distribution of source and materials); second, the system uses a shape optimizer to further improve the design; these two steps are performed alternately until the optimality condition is satisfied.

The robustness of a topology with respect to small variations on its geometries is studied and a robustness measure is defined, originally in the thesis, as the worst case performance of an objective function for the topology and shape optimization. Therefore, the idea of robust design can be applied to the conceptual design (topological design) of electrical machines. Other than the application to motor design, the topology optimization algorithm developed in the thesis, was used originally in the non-destructive testing for quickly location and accurately shape reconstruction of cracks.

ABRÉGÉ

Cette thèse présente un système automatique de conception topologique pour les dispositifs électromagnétiques à basse fréquence, par exemple, un moteur à aimant permanent intérieur. La conception automatisée est effectuée par un processus d'optimisation topologique de la forme : d'abord, le système emploie une analyse de sensibilité topologique pour examiner le domaine de la conception et déterminer la topologie optimale (répartition des sources et des matériaux); Deuxièmement, le système utilise une optimisation de forme pour améliorer la conception, les deux étapes étant effectuées alternativement jusqu'à ce que la condition d'optimalité est satisfaite.

La robustesse de la topologie par rapport à de petites variations est étudiée et une mesure de robustesse est défini, à l'origine dans cette thèse, comme la performance de la fonction objectif, dans le pire des cas, pour l'optimisation topologique de la forme. Le concept de conception robuste peut donc être appliquée à la conception (conception topologique) des machines électriques. Autre que l'application de la conception du moteur, l'algorithme d'optimisation topologique, développé dans la thèse,

a été utilisé à l'origine dans le contrôle non destructif pour trouver rapidement les fissures et preciser la forme optimale.

Chapter 1 INTRODUCTION

1.1 Research Objectives

The purpose of this research work is to implement an efficient and robust process of automating the design of low-frequency (frequencies below several tens of kHz) electromagnetic devices using CAD/CAE software. The automated design system is a software framework which accepts a set of device specifications as the input and produces the description (i.e. dimensions and material layout) of a device as the output. In addition, the actual output of the system is a simulation model of the real device against which the performance can be verified. The design automation is achieved by an iterative procedure of solving direct problems until the desired performance is obtained. At each iteration, the performance of the device is determined based on the field solution computed numerically. A topological design scheme is employed to explore all the possible design candidates under only the assumption of physical principles. The robust design formulation is also applied to guarantee the stability of the actual

performance of realistic devices under variations in manufacturing and working environment.

1.2 Background

Computational methods have been extensively applied to electromagnetic (EM) field analysis for decades. With the advent of high performance computing facilities and advanced software, accurate field results can be obtained by a variety of numerical methods, such as the Finite Element Method (FEM), the Boundary Element Method (BEM), and the Finite Difference Method (FDM). However, when dealing with an Inverse Electromagnetic Problem (IEP) where a device is required to produce certain specified global quantities (such as force or torque) or field values, i.e. an optimal design synthesis, the conventional approach to solving such a problem is to find the desirable device by “trial and error”, which, in effect, is a random search procedure, involving a computationally costly process of solving the field problem many times.

In recent years, Computer-Aided-Design (CAD) has become the first choice of design engineers when new electromagnetic devices are

needed. More specifically, the automation of the design process can be achieved by first modeling the physical problem with CAD tools; and then all the feasible design candidates are mapped into a search space using parameterization; finally the search for an optimal result is conducted through a mathematical optimization programming process, such as gradient based search direction algorithms which converge within an affordable number of iterations in most cases. This is extremely cost-efficient compared to the conventional trial and error approach.

Topological design of EM devices

The design parameterization of a low-frequency electromagnetic device usually contains three major categories of problems: the Sizing, Shape and Topology design (Bendsoe and Sigmund, 2003). Unlike the first two (sizing and shape) problems which only play with a limited number of specifications, topology design optimization can start with an empty space which is free of assumptions (on shape and topology) and provides the possibility of achieving innovative design results. In fact, designing an electrical machine can be interpreted as finding the physical layout and connectivity of different materials (Topological design) and sources and determining the boundary between different components (shape design)

under certain requirements of performance and manufacturing constraints (Dyck and Lowther, 1996). From a systematic point-of-view of the engineering design (Pahl et al., 2007), topological design can be considered as a conceptual design tool for determining solutions that can be used for the embodiment and detail design phase (which are equivalent to shape design).

Uncertainties and robust design

The job of design cannot be considered as complete until a physical device or prototype can be produced. If the newly designed device is to be manufactured, the tolerance problem must be taken into account. For example, one can run the simulated model in the computer several times and the results are always the same; but, in reality, the manufacturing process often generates small variations to the product. Sometimes, these variations can cause serious deterioration in the performance of a device. Therefore, in order to prevent such performance deterioration, perturbations of the design variables need to be handled and integrated into the mathematical formulation of optimal design, and such a procedure is usually referred to as “Robust Design” since the performance of the resulting product is more robust, i.e. reliable.

Although the concept of robust design, which was pioneered by Dr. Genichi Taguchi (Taguchi, 1993), has been widely used in quality engineering for several decades, the criteria of “Robustness”, particularly in the context of topological design, has rarely been discussed except in (Al-Widyan and Angeles, 2005). Different definitions maybe found in the literature developed by different authors based on their individual applications. Therefore, we must first clarify the meaning of “robustness” discussed within the scope of this thesis.

Other than the definition from its semantics perspective by the dictionary, the word “Robustness” was originally described by Taguchi in (Taguchi et al., 2000), as:

The state where the technology, product, or process performance is minimally sensitive to factors causing variability (either in the manufacturing or user’s environment) and aging at the lowest unit manufacturing cost.

From Taguchi’s definition, it is worth noting that sensitivity is considered as a key to the measurement of the robustness being sought in robust design. Yet another question being raised is how to measure the

robustness of a design in a quantitative way or in mathematical terms. While there exist many metrics to express robustness, such as the signal to noise (S/N) ratio, meeting specifications, reliability data, etc., a comprehensive expression of robustness is to use the standard deviation (or scatter) of the performance with respect to the probabilistic distribution of the design parameters. Figure 1.1 shows the comparison of the performance distributions between two products (A and B).

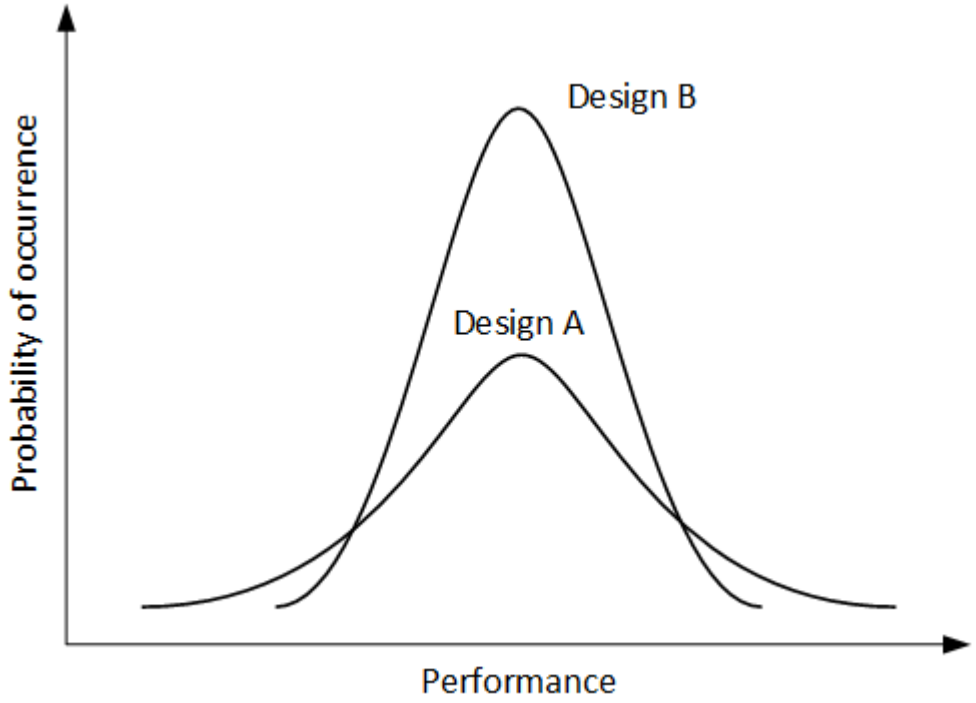

Figure 1.1 Definition of robustness

From the above figure, we can easily tell that the performance of design B is more robust than that of design A, because the standard deviation of design B is smaller than that of A, which means design B has higher

reliability (in the sense of avoiding performance deterioration) than design A, despite the fact that designs A and B have the same mean value of performance. In other words, from the point of view of a probabilistic distribution of the performance under manufacturing uncertainties, design B yields better qualified products with the target performance.

A robust design solution should be less sensitive to the uncertainties in the design variables. In some cases, the solution from a conventional optimization process might not be optimal any more in the sense of robustness. Figure 1.2 illustrates the objective function taking account of the variations in the design variables.

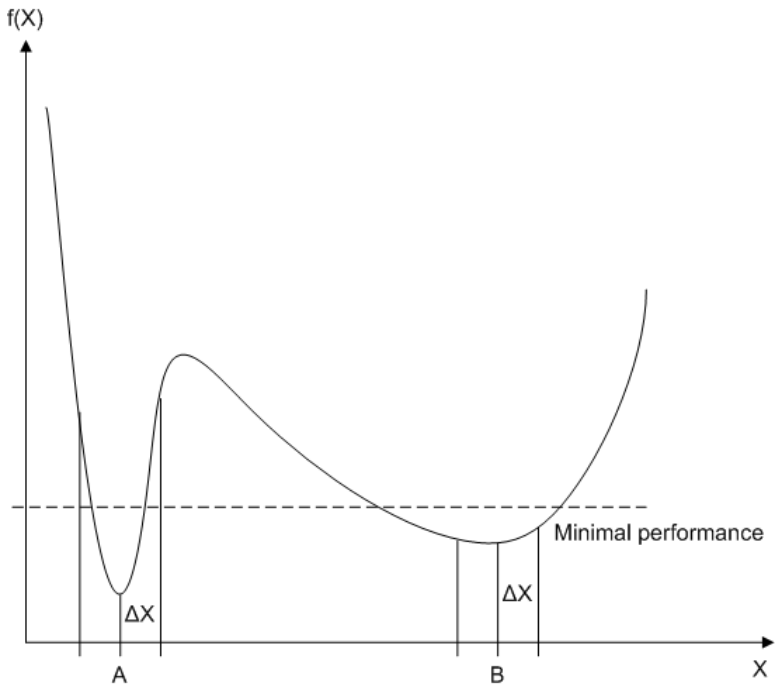

Figure 1.2: Robustness of the solution

As shown in figure 1.2, point A is the local minimum of the deterministic design, and point B is the robust optimum. Although the nominal value of the objective function at point A is smaller than that of point B, the performance varies drastically in a small neighborhood of the point A, therefore if a prescribed minimum performance criterion is specified, which is the dashed line in the above figure, the performance of design B is also acceptable and it is more robust since the performance variation is much smoother around its nominal design. In conclusion, a robust solution is found in a flat region in the search space instead of narrow valleys around minima.

Unfortunately, the evaluation of the variance of the performance or objective function requires probability information. If a stochastic model based on statistics is used, some drawbacks may occur. First, the probability information about the distribution of design variables is not usually available or could be hard to retrieve (Parkinson et al., 1993, Yoon et al., 1999). Even if it is available, it is computationally expensive to compute the variance of the performance, which usually requires many evaluations of FEM solutions. Therefore, although such analyses can be used *a posteriori* for robustness evaluation, it is not practical to use the

stochastic model to deal with the problems when there is a large number of design variables. On the other hand, it is desirable to build the robustness measurement into the mathematical formulation of the design system, thus we need an approach to estimate the robustness of any design and to guide the search in the direction of a more robust solution. This information about the robustness must be easy to obtain and can be efficiently computed to approximate the variance of the performance function. Among many methods, sensitivity analysis is an effective tool for numerical analysis, and it provides a good measure of the robustness. Minimum sensitivity indicates the smallest likelihood of failure in the linear case of the response with respect to the uncertain variables.

Interval mathematics provides an alternate and straightforward approach of expressing the robustness of the device performance (Lowther, 2003). For example, any variable in the design that is subject to uncertainty can be transformed to an interval variable, i.e. representing a range of values. If the interval is defined using the nominal value of the design variable plus its tolerance, the range of the values can be propagated through the equation network, and the tolerance of the device performance can be obtained through the propagation. Hence, the robustness and validity of

the design can be evaluated using the information provided by an analysis based on interval mathematics.

Another important issue in robust design is the violation of the constraints. In constrained optimization problems, optima are often found near the boundary of the feasible set and if a small variation exists in the design variables, the values may no longer be feasible. Some treatment of the constraint function is required to guarantee the feasibility as well as the robustness of the solution.

Combining robust design with topology optimization

Optimal topology design has been studied extensively in the field of structural and mechanical engineering. It is used to design the optimal topological structure for supporting systems. Due to the similarity between the two disciplines, some of the recently developed techniques in structural engineering can be migrated to the area of electric machine design.

A topological design system can provide size and geometry of the target device as well as its topological structure. As a result of the advance of

design technologies, target devices are more and more complex; some have really delicate structures such as MEMS. It has been noted that both the structure and performance of the optimal topological solution are quite sensitive to the variation situation, but so far very little work has been done to merge the topological design with robust design considerations taking into account the uncertainties in design and state variables.

In the context of a robust topological design, the uncertainties can be categorized as noise in the measurement, material properties and geometry of the body. Unfortunately, in the conventional formulation of topology optimization based on the theory of homogenization or material distribution, the design variables are the material densities in the discretized cells, thus it is difficult to associate the performance variation with respect to geometrical or topological uncertainties, and only uncertainties in the material properties or noise in the measurement can possibly be handled using uncertainty sets defined on these design variables.

Recent research shows that the concept of topological sensitivity analysis is a very promising tool to enhance the topology design. The so-called

topological derivative or topological gradient (TG) is derived from the topological asymptotic expansion for partial differential equation (PDE) systems. The physical implication of TG presents the sensitivity of the design performance when a hole is created in the material domain. Thus, the topological gradient can be used to determine whether a topological change is necessary. Topological sensitivity analysis can be applied in conjunction with the classical shape gradient in the optimization, which allows the simultaneous change of shape and topology. Compared to the conventional topology optimization methods in the area of EM device design, which suffer from a series of drawbacks, such as non-smooth boundaries, checkerboard situations and high computational costs, topological shape optimization is more flexible and powerful in handling the delicate shape and structure of EM devices. Most importantly, the topological shape optimization approach provides the possibility of incorporating robust design with topology optimization since the design variables are no longer density functions in discretized cells, as in the case of the conventional topology optimization methods. Hence, by combining topological design and robust modeling, a solution which is less sensitive to the discretization and measurement error can be found.

1.3 Literature Review

Engineering design processes are often described as iterative feed-back loops. For example, in the model developed by (French, 1999), the design process is divided into four major stages: analysis of problem; conceptual design; embodiment of schemes and detailing. In addition to French's model, (Pahl et al., 2007) added some detailed working steps to each stage and implemented a complete strategic guideline for mechanical design. Two most important components in computer-based design packages (based on the aforementioned design models) for the design of electromagnetic devices are synthesis and optimization. In the synthesis phase, a parametric definition of the physical device is provided by the design environment in order to create the design space, instead of sketches using pencil and paper; while in the optimization phase, a variety of mathematical formulations and programming algorithms are applied to search for the final design which is optimal and feasible in terms of the imposed conditions and constraints. The state of the art methodologies and techniques are reviewed in the following four areas: design parameterization, topology design, design sensitivity analysis, and robust design.

Design parameterization

Design parameterization generates design variables for any piece of data that changes during the design process, such as material properties, electromagnetic quantities and geometry information that describes the size, position and shape of the physical device. From the design perspective, modification of the values of the corresponding design variables changes the design target and the performance of the device. Constraints in the design are also represented by the lower and upper bounds on the design variables and some of their combinations. As a result, this creates a search space for the optimization process and these variables are used as specifications of the realistic device in the final design. During the early development of EM device design assisted by the field solutions from FEM, the design variables are usually associated with the nodes or elements of the FEM mesh (Hoole and Subramaniam, 1992). It was revealed by (Weeber and Hoole, 1992b) that the choice of the proper design variables is critical to the success of an optimization procedure using parametric design. Various approaches to defining the parameterization are possible for the shape optimization. One of those uses the various dimensions of the device as the design variables (Mohammed et al., 1993); another one uses the coordinates of a set of

nodes as the design variables, with the interface surface defined by segments connecting the nodes (Preis and Ziegler, 1990); another approach uses a linear combination of basis functions to represent the shape in which case the design variables are the weights associated with the basis functions (Preis et al., 1990). The design element method (Weeber and Hoole, 1992c) has imposed itself in solving shape optimization problems, where the analysis domain is divided into several sub-domains and the finite element is distortable but the topology is kept constant. Interpolation methods, such as Hermite, B-Spline and Bezier, were used to generate smooth boundaries, allowing at least C^1 continuity (Weeber and Hoole, 1992a). It must be emphasized that different interpolation techniques applied to the same design nodes, generate interfaces with different shapes. An important development in this field was the creation of a design environment that provided user interface and facilities for non-expert designers (Biddlecombe et al., 1994) and would eventually replace the conventional sketching work of a human (Mohammed et al., 2001); (Parker et al., 1996). It is of particular importance to review the technologies developed for design parameterization since the robustness of the design is linked to the variation in the design parameters.

An alternative machine representation scheme was proposed in (Dyck and Lowther, 1996), where the design region was divided into thousands of small cells and the EM device was described as distribution of material and sources. The automated design system requires no *a priori* knowledge but the physical principles, and yields a global optimum for the design. This work belongs to the area of topological optimization and more details will be elaborated later.

Topological optimization

Topology optimization techniques can be used to predict the optimal lay-out of the device structure as well as the size and shape. In practice, topology optimization is often used as a preprocessing stage before shape optimization. As a result, novel designs of a device can be generated through topological optimization and further refined by the shape optimization method. The early concept of topological design was developed in the 1900s in the area of lay-out design based on analytical methods and was referred to as generalized shape optimization in the literature (Michell, 1904). Over the last two decades, significant development was achieved in both the theoretical study and the applications. Most of these achievements can be divided into two

categories: the Microstructure technique and Macrostructure technique (Eschenauer and Olhoff, 2001). The fundamental difference between the two techniques lies in the material model employed; the former uses a microstructure of material or material density, while the later focuses on solid isotropic materials, i.e. the topology optimization is closely linked with a shape optimizer. In 1988, Bendsoe first presented a grey-scale pixel-like image of device representation and applied it in the field of structural engineering (Bendsoe and Kikuchi, 1988); (Bendsoe, 1989). The design space was extended to include the solutions of composite materials and this guaranteed the existence of the solution through a regularization of the objective function based on the method of homogenization (Kohn and Strang, 1986). In formulations based on the material distribution, the physical device is treated as the combination of a set of distributed functions of material properties or sources with continuously varying values. Uniform and rectangular elements in the mesh are commonly used to represent the material or empty space. The density of material within each finite element is used as a design variable defined between 0 (no material) and 1 (solid material). One possible treatment of the composite material was known as Solid Isotropic Material with Penalization (SIMP), where the intermediate values of material (between 0 and 1) are penalized

and the optimal solid structure is obtained through a procedure known as solidification (Sigmund, 1999). Some recent research effort has been focused on combining topology and shape design (Campelo et al., 2008).

On the other hand, the Macrostructure approaches to topology optimization work are based on the constitutive laws for solid, isotropic materials. Among many techniques based on the concept of the Macrostructure, it is important to emphasize the so-called bubble method (Eschenauer et al., 1994). This method combines a fixed method with the natural extension of the classical shape sensitivity inside the domain of the material. The concept of topological gradient was developed by Schumacher, and it allows the calculation of the sensitivity to topological changes (i.e. infinitesimal holes) to the design domain. (Sokolowski and Zochowski, 1999a); (Sokolowski and Zochowski, 1999b) provided mathematical justification of topological sensitivity analysis, where the topological gradient was derived in the case of homogeneous Neumann boundary conditions on a hole with various objective functions, and (Masmoudi et al., 2005) extended the definition of topological gradient to the case of more generalized boundary conditions. Various algorithms were later developed by (Cea et al., 2000) and (Stephane et al., 2001)

based on the concept of the topological gradient of a functional that depends on the solution to a PDE for a large class of problems.

In particular, topological optimization has been employed in the design of electrical machines. The Optimal Material Distribution (OMD) method was adopted from structural engineering by (Dyck and Lowther, 1996) and applied in the automated design of magnetic devices. Later, in (Choi et al., 1998), the material distribution representation from the topology design was converted to a conventional shape optimization problem by the application of image processing techniques, which resulted in the significant reduction of the design space. The performances of two different design approaches, using Artificial Neural Networks (ANN) and deterministic optimization based on OMD, were compared by (Lowther et al., 1998). Various applications exploiting sensitivity information in the topological optimization of different electromagnetic devices, such as an electrostatic actuator and nonlinear magnetostatic devices, can be found in (Byun et al., 1999); (Byun et al., 2000); (Byun et al., 2002); (Wang and Kang, 2002). A modified density method based on the homogenization design concept was developed by (Yoo, 2004), and the results were compared between the density method and the homogenization design

method. A novel material updating scheme based on continuum design sensitivity analysis was applied in the optimal design of the coil configuration in a MRI device, where no intermediate states of the material are required in the optimal source distribution (OSD) formulation (Dong-Hun et al., 2005). Most recently, Kim presented a smooth boundary topological shape design algorithm based on the idea of topological gradient, where the shape optimization and the topology design were performed simultaneously (Kim et al., 2008); (Kim et al., 2009).

An alternative design scheme is to treat the topological design of EM devices as a combinatorial optimization process for which each element in the design space has a discrete value representing a different material that can be used in the design. In this case, Ant Colony Optimization (ACO) algorithms can be applied to find the optimal topology. The combinatorial topological design of a magnetic actuator and interior permanent magnetic machines were solved by the ACO (Batista et al. 2011); (Batista et al. 2012).

Design sensitivity analysis

In the context of design optimization, “sensitivity” is defined as the change of the objective function with respect to a small perturbation of the design variables. The procedure for obtaining such information is also known as “design sensitivity analysis”. The sensitivity can be computed numerically via a finite difference approach where the derivative is approximated by the ratio of the difference of the objective function and the design variables through perturbation. However, this approach requires many FEA solutions, and is thus not computationally practical. Two major approaches for computing the sensitivity for the EM design optimization problem have been developed over the past few years. The discrete design sensitivity analysis (DDSA) approach, which first became known through Coulomb’s implementation of the virtual work principle (VWP) (Coulomb, 1983), employed a direct differentiation of the algebraic system matrix of the FEM. (Ramirez et al., 1994) applied Tellegen’s theorem (Tellegen, 1952) to the magnetic network model to access sensitivity information and thus successfully obtained the magnetostatic loading force using virtual work with only one solution. The work of (Nguyen and Coulomb, 1999) presented a generalized framework of computing high-order finite element

derivatives with respect to geometric parameters based on the symbolic computation of Taylor's polynomials.

On the other hand, the continuum design sensitivity analysis (CDSA) was first proposed by (Park et al., 1991) in the magnetostatic case for shape optimization. The material derivative concept of continuum mechanics was adopted from structural engineering (Komkov et al., 1986) and the adjoint variable method was applied to derive the explicit sensitivity formula for the interface between two different linear materials, e.g. non-saturating iron and air. Later, Park and Coulomb demonstrated a numerical implementation of CDSA (Park et al., 1993) in conjunction with a standard FEA package, while the adjoint variables are obtained through the computation of an adjoint load based on the existing finite element code. A further derivation of the sensitivity formula, performed by Kim, can be applied together with existing general purpose FEA software (Kim et al., 2003b). The EM implications of the pseudo sources of the adjoint system used in CDSA were discussed by (Kim et al., 2004). Particularly, analytical formulae of the force calculation as the shape design sensitivity of the system energy were derived by coupling the augmented Lagrangian method, the material derivative concept and the adjoint variable method

(Kim et al., 2005). The contribution of different EM sources (such as permanent magnetization and current) to the global forces was indicated in three different cases. The most recent work of (Kim et al., 2007) presented an efficient CDSA based method for global force as well as local force calculation.

The CDSA method is based on the assumption that the material properties are continuous and the derivative of an objective function with respect to the shape design variables can be obtained by differentiating the variational governing equations in integral form. The method is thus able to compute any global quantity of the field problem in terms of the perturbation of a parameter. Unlike the DDSA proposed by (Coulomb, 1983), the implementation of CDSA-based force calculation can easily be coupled with any commercial FEM software package without knowing detailed information about the system matrix and the procedures within the solver. In fact, the CDSA based approach is independent of the numerical field computation tools, and it only requires a set of field values for any force calculation.

Robust design

Robust design is an area that has raised most interest in the field of engineering in recent decades. It originated from the research on design tolerance and improving engineering productivity and quality control for reducing the output variation. The earlier attempt by engineers to handle such problems was to use the Six Sigma Quality strategy (Tennant, 2001) and +−3 standard deviations to guarantee the performance of a product within the range of acceptance. Later, two different fashions of non-deterministic methods became dominant in this area, which are the reliability-based method and robust design method. While the reliability-based method employs risk analysis by computing the probability of failure of the product using the probability distribution of the system's response, the variation is not minimized according to a robustness measurement during the process. Thus, this approach is out of the scope of this thesis. The objective of robust design approaches is different from the reliability approach, and is to optimize the mean performance and minimize its variation, while maintaining feasibility with probabilistic constraints. This is achieved by optimizing the product and process of design to make the performance minimally sensitive to the various causes of variation. In the 1950's and 1960's, Dr. Taguchi developed the foundations of robust

design to meet the challenges of producing high-quality products. The Taguchi method (Taguchi, 1989) is a data driven and design of experiments method and uses the concept of signal-to-noise ratio to estimate the robustness of the product. The applications using Taguchi models are usually pretty accurate around the nominal value of the performance. Later, more robust design methods were developed based on an optimization process trying to find the optimal design with a robust performance with respect to uncertainties in the design (Alotto et al., 2003). Sensitivity was considered as a good approximation to the standard deviation of the performance since the reduction of sensitivity implies the increase of robustness (Belegundu and Zhang, 1992). (Parkinson et al., 1993) proposed a general approach for robust design and addressed the issue of design feasibility where the procedures are developed to account for tolerances during design optimization such that the final design will remain feasible despite variations in parameters or variables. The robust design idea for electromagnetic devices was first introduced by Yoon, where the design was treated as a multi-objective problem with the function value and its derivative as the objectives (Yoon et al., 1999). A robust target function was built through the integration of uncertainty factors and the robustness measure into the optimization

process in (Alotto et al., 2003), including the discussion of the shape of the uncertainty set and the differentiability of the robust target function. The robustness of the feasibility in constrained design problems was further discussed in (Steiner et al., 2004). In addition to the sensitivity-based approaches, genetic algorithms and evolutionary algorithms have been applied to obtain the solution of a multi-objective function based on a worst case approach to the robust design of magnetic devices (Spagnuolo, 2003); (Cioffi et al., 2004). Several robust design formulations were discussed by (Guimaraes et al., 2006), who pointed out that the standard deviation can be approximated using the difference between the worst performance and the nominal performance and the computation cost could be largely reduced. In particular, (Han and Kwak, 2004) defined a gradient index (GI) using the sensitivity of performance functions with respect to stochastic variables. This simple and efficient algorithm was illustrated with an example of a MEMS device where robustness is crucial for a high yield rate. And the performances of a gradient-based worst case optimization (G-WCO), conventional WCO and multi-objective approach using gradient index (GI) were compared by (Ren et al., 2013a). In the recent development of robust design optimization, a second-order sensitivity analysis implemented by the hybrid direct differentiation-adjoint

variable method was employed for the accurate prediction of the worst case for complex and strongly non-linear performance functions (Ren et al., 2013b). Last but not least, the kriging surrogate modelling, which takes advantage of information already found, is a promising method for reducing the computational cost of solving robust design optimization problems (Xiao et al., 2012); (Xiao et al., 2013b); (Xiao et al., 2013a).

1.4 Original Contributions

The objective of this research project is to find an efficient and accurate solution to the non-routine design of electromagnetic devices. In particular, the projected original contribution to knowledge will lie in the following:

1. The introduction of the robust design formulation in the early stage (conceptualization) of the design of an EM device using topology optimization.
2. A quantified definition of robustness of the topological design solution.
3. Sensitivity analysis of the objective performance function with respect to the random variables to determine the critical design parameters in topology optimization.

4. An efficient algorithm for the automated design of EM devices exploring the topological and shape gradient.

Chapter 2 METHODOLOGIES

A design problem involving a low-frequency device is often formulated as a mathematical programming problem where an objective function is minimized or maximized under certain requirements of the performance and physical constraints. As a requirement of robust design, a measurement of the robustness of the objective function needs to be incorporated into the design optimization process in order to provide not the best but the most robust solution in the feasible region.

In this chapter, first, we give the general formulation of robust design using worst case analysis, where a robust design can be formulated using a robust objective function on an uncertainty set. Then a novel method of the topology optimization using topological sensitivity analysis is introduced; and, at the end of this chapter, the two methods are combined and an algorithm for robust topology optimization is presented.

2.1 General Robust Design Formulations

Non-robust objective function

A design problem can be expressed mathematically as an optimization problem. While robustness is not considered, an objective function f(x): $R^n \rightarrow R$, for the design optimization is defined as,

$$\begin{aligned} &\min_x f(x) \\ s.t. \quad &g_i(x) \le 0 \quad i = 1,...,n, \\ &X_L \le x \le X_U \end{aligned} \tag{2.1}$$

where $x = [x_1, x_2, \ldots, x_n]^T$ is a vector of the design variables; f(x) is an objective function defined to evaluate the performance of the target device; the constraints of the design are expressed as the functions g(x); and X_L and X_U are the lower and upper boundaries of the design variables, x, respectively.

The design variables are usually chosen by the design engineer as geometries, physical attributes or material properties of the device; examples are dimensions of the rotor or the currents in the windings of an electrical motor. In general, the objective function, as in (2.1), is an implicit function of the design variables and they can be evaluated after a numerical field analysis. The objective function, f, can be defined as the

performance of a device (e.g. torque in the case of electrical motor design) or the difference between the current state and the target (e.g. squared error in the case of non-destructive crack reconstruction).

Uncertainty set

Unlike the conventional formulation of design optimization, a robust design formulation aims to minimize the variation of the objective function. The concept of an uncertainty set is introduced to take account of the variations of the design variables which can cause the performance variation. An uncertainty set $U(x) \subset R^n$ is defined as a compact sub-domain of the design space containing all the possible combinations of perturbations to the nominal values of the design variables x. For a particular point x_0 of the design variables x, the uncertainty set $U(x_0)$ is given as,

$$U(x_0) = \{\xi \in R^n : x_0 - \Delta \le \xi \le x_0 + \Delta\}. \qquad (2.2)$$

where $\Delta = [\Delta_1, \Delta_2, \ldots, \Delta_n]^T$ represents the variations to the nominal value of point x_0.

Sometimes the variations of the design variables may be defined as proportional to the nominal value of the design variables of every

dimension, especially when the vector of design variables contains different physical quantities. Thus the uncertainty set U(x) of x_0, when x_0 is a positive real number, can also be defined as:

$$U(x_0) = \{\xi \in R^n : (1-\Delta_i)x_{0,i} \le \xi \le (1+\Delta_i)x_{0,i}\}. \quad (2.3)$$

where $\Delta_i x_{0,i}$ represents the largest variation to $x_{0,i}$, the ith component of vector x_0, as shown in figure 2.1. This uncertainty set is modeled as a hyper-rectangular box and figure 2.1 shows the shape of a rectangular uncertainty set in 2-D.

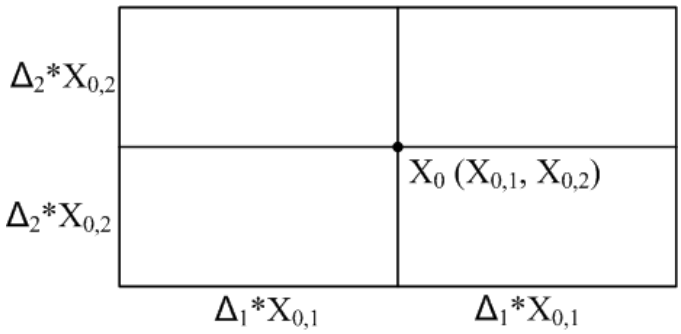

Figure 2.1: 2-D rectangular uncertainty set

While there can be other shapes of the uncertainty set, the advantage of the rectangular uncertainty set is the simplicity of its implementation and it does not require any statistical information about the design variables.

Robust objective function

There are many different formulations of robustness measures existing in

the literature, e.g. the worst case or the statistical tolerance (Parkinson et al., 1993) or the mean value and variance (Yoon et al., 1999). One of the practical ways to treat the robust design problem is to use the worst case scenario. A robust objective function is defined as the worst performance of the objective function f due to the perturbation of the design variables x, as:

$$f_w(x) = \max_{\xi \in U(x)} f(\xi). \tag{2.4}$$

Design feasibility

In a constrained design problem, the robust design formulation must guarantee that the perturbed design does not violate any of the constraints. For example, if a solution x* is located too close to the boundary of the feasible region, variations to x* may not be feasible anymore. Figure 2.2 shows a 2-D solution space of a constrained robust design problem.

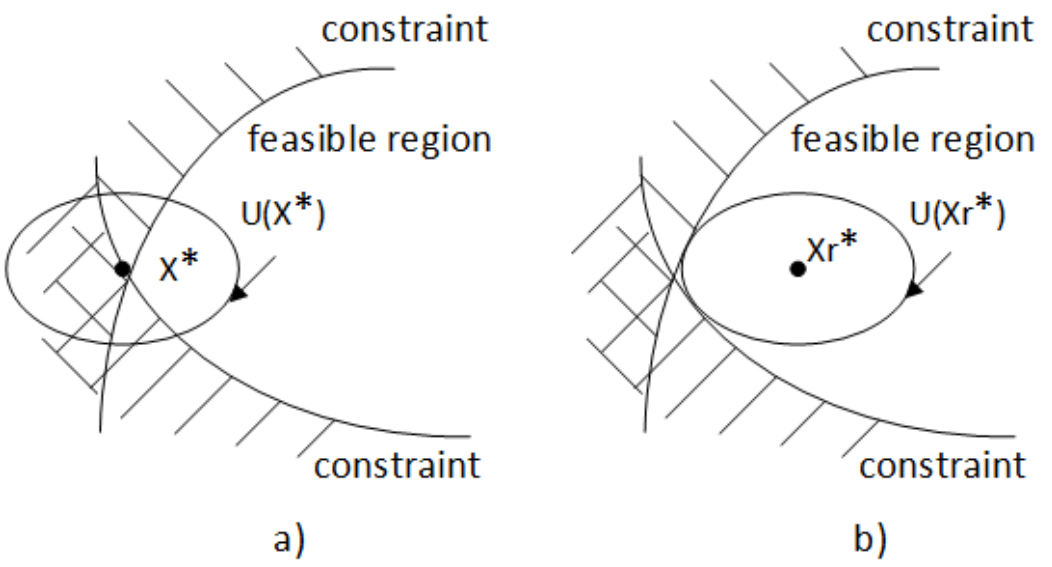

Figure 2.2: Feasibility robustness

Figure 2.2(a) indicates the case where a non-robust optimum x* becomes infeasible. And figure 2.2(b) shows a robust solution x_r* that satisfies the constraints over the entire uncertainty set defined on x_r*. Thus, to ensure feasibility robustness, the shape of the constraint function must be altered by the uncertainty set. A robust constraint function can be defined as:

$$\max_{\xi \in U(x)} g_i(\xi) \leq 0 , \tag{2.5}$$

where any points in the uncertainty set, U(x), must satisfied the constraints.

Overall, a robust design problem can be formulated as minimizing the worst performance of the objective function value within the uncertainty

set:

$$\min_{x} \max_{\xi \in U(x)} f(\xi)$$
$$s.t. \max_{\xi \in U(x)} g_i(\xi) \leq 0 \cdot \tag{2.6}$$

Differentiability of robust objective functions

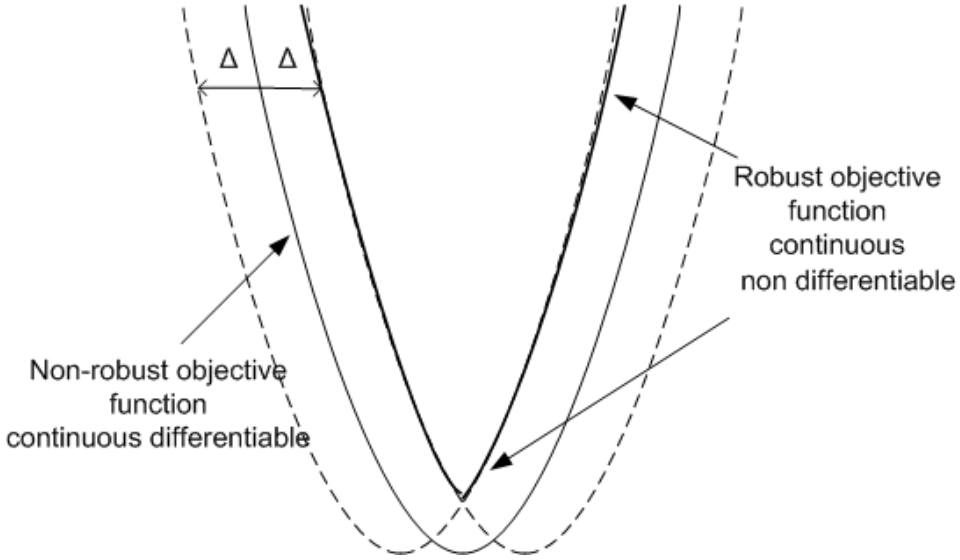

Figure 2.3: Differentiability of the robust objective function

The properties of the robust objective function f_w may be different from the original objective function f and this can be critical for the implementation of the optimization algorithms. If f is continuous on R^n, then it guarantees that f_w is also continuous on R^n. If f is continuously partially differentiable, then the directional derivative exists for f_w, but the differentiability is not guaranteed. In addition, f_w only loses its differentiability at the point where at least one of the partial derivatives of the original objective function

changes its sign, as shown in figure 2.3. Therefore, if deterministic search algorithms are to be applied to the optimization process, some special treatments are required for the gradients of the robust objective functions at those non-differentiable points.

Worst vertex prediction using sensitivity

From the constrained optimization theory (Alotto et al., 2003), the worst value of the objective function f occurs at one of the corners of the uncertainty set U, if f is convex on U, and convexity can always be assumed in a small neighborhood of a local minimum. Unfortunately, evaluating the objective function at every single vertex of the uncertainty set to find the worst value on the uncertainty set is not feasible since the whole procedure has an exponentially increased time complexity with respect to the number of design variables. The total number of function evaluations, K, equals 2^N for an N-dimensional problem. In order to find the worst vertex more efficiently, a worst vertex prediction mechanism can be applied based on the determination of the direction of the ascent of the objective function value, as:

$$x_{pred} = x_0 + \begin{pmatrix} \mathrm{sgn}(f(x_{1+}) - f(x_{1-})) \cdot \Delta_1 \\ \vdots \\ \mathrm{sgn}(f(x_{n+}) - f(x_{n-})) \cdot \Delta_n \end{pmatrix}. \qquad (2.7)$$

Hence the worst performance is approximated by the function value at the worst vertex x_{pred},

$$\max_{\xi \in U(x_0)} f(\xi) \approx f(x_{pred}) . \qquad (2.8)$$

This approximation requires only K = 2N+1 times function evaluations, where N is the number of the design variables. This has seriously reduced the computational cost of the robust design optimization compared to 2^N function evaluations if the value of the objective function is evaluated at every corner of the uncertainty set.

In addition, we may also use the information of the gradient computed at the point x if the gradient can be obtained without a high cost. This can further reduce the computational cost of the robust objective function evaluation. Figure 2.4 gives an example of the worst vertex prediction, for a non stationary point, in R^2, where the opposite direction of the gradient of the objective function points to the worst vertex of the uncertainty set.

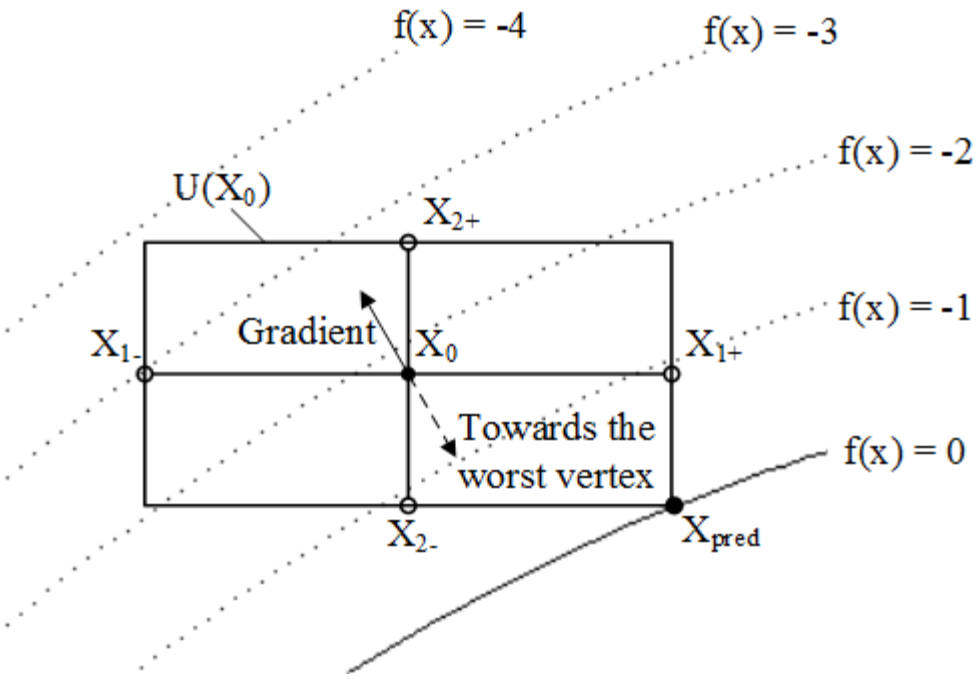

Figure 2.4: Worst vertex prediction using gradient information

2.2 Topological Gradient

In the conventional formulation of topology optimization based on the theory of homogenization or material distribution, the design space is usually divided into cells. And the design variables are the dimensions of the discretized elements. The possible values of these design variables are numbers between 0 and 1 which represent the intermediate states of the material properties. If only solid material is allowed in the design, there cannot be any variation to the nominal value of the design variables, since they must be either 0 or 1 at the end of the design. Therefore, it is not

possible to apply the robust design formulation from (2.6) to conventional topology optimization methods such as homogenization and material distribution.

On the other hand, topology optimization based on macrostructure (also known as topological shape optimization) shows the potential to be coupled with robust design formulations. Topological shape optimization methods have been successfully applied to electromagnetic design problems (Kim et al., 2008). In such an optimization method, a topological gradient (TG) provides the sensitivity information of a design with respect to topological changes, e.g. the insertion of a small air hole at any point inside the solid material. To be more precise, the TG indicates the change in the objective function with respect to a potential topology change in the design domain, thus the TG can be used as a decision making tool for the topology optimization process.

A topological shape optimization process usually contains two stages: first, generate topology changes to the domain of the design by creating a small hole of a different material based on the values of the topological gradient; second, optimize the shape of the hole created in the first stage

using a standard shape optimizer. These two steps are repeated in sequence until the optimality conditions are satisfied.

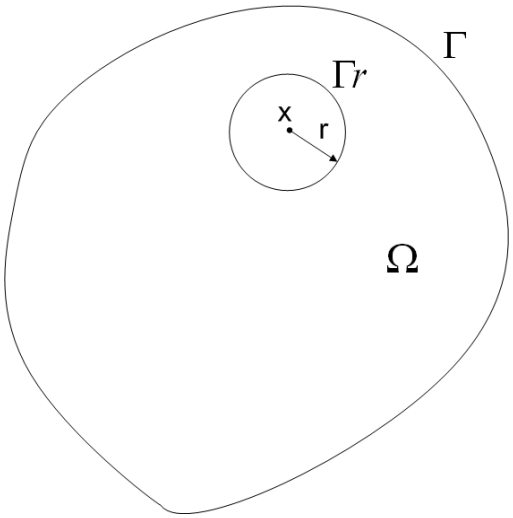

Figure 2.5: A design domain with a small hole

A mathematical formulation of the TG, which originated from the classical shape gradient information, is derived using a topological asymptotic expansion for PDE systems (Masmoudi et al., 2005). Figure 2.5 illustrates a design domain Ω defined on $\mathbb{R}^n$ (n=2 or 3), with an outer boundary Γ. Consider an infinitesimal hole $\phi(x, r)$ in Ω, where x is the center of ϕ and r is the radius of ϕ. The topological gradient G(x) is given as:

$$G(x) = \lim_{r \to o} \frac{\Psi_{obj}(\Omega \setminus \phi(x,r)) - \Psi_{obj}(\Omega)}{\delta(\Omega)}. \qquad (2.9)$$

where Ψ is an objective function defined on Ω and an implicit function of a solution to a partial differential equation, $\Omega \setminus \phi(x, r) = (\forall y \in \Omega, ||y - x|| \leq r)$ is

the domain excluding the small hole ϕ, and $\delta(\Omega) = \Omega \setminus \phi(x, r)$ - Ω is the volume of the hole with a negative sign.

The topological gradient is closely linked with the classical shape gradient. In order to derive the expression of the topological gradient, first, we need recall how to obtain the shape sensitivity on the boundary of the design domain Ω. We consider a perturbation V of the boundary Γ which changes the domain Ω to Ω +V,

$$\Omega + V = \{x + V(x), x \in \Omega\} . \tag{2.10}$$

The general shape sensitivity of the objective function Ψ in the direction of the perturbation V can be expressed in the form of a surface integral as,

$$\Psi'(s) = \int_{\partial\Omega} L(s) V_n ds . \tag{2.11}$$

where L is a function defined on the boundary $\partial\Omega$ and V_n is the normal component of the perturbation V with respect to the boundary, also known as the design velocity.

In the case of the Laplace equation with Neumann boundary conditions, L can be obtained using the primary solution to the PDE defined on Ω and

an adjoint solution, where a detailed definition can be found in (Guillaume and Masmoudi, 1994), used to facilitate the sensitivity calculation, as:

$$L(s) = (\nabla u \cdot \nabla p)(s). \tag{2.12}$$

where u is the primary solution and p is the adjoint solution.

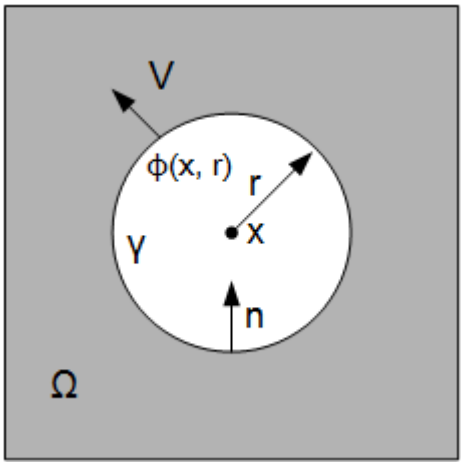

Figure 2.6: Boundary perturbation on the small hole

Now assuming a perturbation V of the boundary of the small hole ϕ(x, r) as shown in figure 2.6, while the external boundary Γ of Ω remains unchanged, let V= -n. Consider a scalar function J(r) = Ψ(Ω\ϕ(x, r), using (2.11) and (2.12) we have,

$$J'(r) = -\int_{\Gamma r} (\nabla u_r \cdot \nabla p_r)(s) ds. \tag{2.13}$$

where u_r and p_r are the primary and adjoint solutions to the PDE, across the boundary respectively.

Using a local asymptotic expansion of the solutions, ∇u_r and ∇p_r, (Cea et al., 2000), J'(r) is approximated as:

$$J'(r) = -4\pi r(\nabla u \cdot \nabla p)(x) + o(r)\,. \tag{2.14}$$

Note that the coefficient $-4\pi r$ is not a result from the integration and substitution of ∇u_r by ∇u and ∇p_r by ∇p, which leads to the result as $-2\pi r$.

The change in the objective function value due to the topology change can be calculated as,

$$\begin{aligned} &\Psi_{obj}(\Omega \setminus \phi(x,r)) - \Psi_{obj}(\Omega) = J(r) - J(0) \\ &= \int_0^r J'(\rho)d\rho = -2\pi r^2(\nabla u \cdot \nabla p)(x) + o(r^2)\,. \end{aligned} \tag{2.15}$$

By substituting the result from (2.15) back into (2.9), with $\delta(\Omega) = -\pi r^2$ in 2-D, the topological gradient G(x) and the relationship between G(x) and the natural extension of the shape gradient *L*(x) is given as:

$$G(x) = 2(\nabla u \cdot \nabla p)(x) = 2L(x)\,. \tag{2.16}$$

Equation (2.16) has some implications on the simultaneous shape and topology optimizations. The variation of the objective function Ψ due to the topological change is proportional to $G(x)\delta(\Omega)$ and the variation due to the shape change of the external boundary of the design domain Ω is

proportional to $L(x)\delta(\Omega) = G(x)\delta(\Omega)/2$. For a topology optimization with a volume constraint imposed, the choice between a shape change or a topological change during the optimization is balanced by this relationship. The implication of (2.16) on the optimality condition will be discussed next. In addition, equation (2.9) can be re-written using a local expansion as:

$$\Psi_{obj}(\Omega \setminus \phi(x,r)) - \Psi_{obj}(\Omega) = \delta(\Omega)G(x) + o(\delta(\Omega)) . \qquad (2.17)$$

It can be observed that if a hole is created ($\delta(\Omega) < 0$ by definition) in the region where G(x) is greater than zero, we have the right-hand side of the equation smaller than zero; hence the left-hand side of the equation, $\Psi(\Omega\setminus\phi(x, r) - \Psi(\Omega) < 0$, and the objective function Ψ is minimized.

For an unconstrained topological shape optimization, an optimum is the state where no more improvement of the performance can be achieved. Thus the following optimality conditions must be satisfied,

$$\begin{aligned} G(x) &= 0 \quad on\ \Gamma = \partial\Omega \\ G(x) &\le 0 \quad in\ \Omega \end{aligned} . \qquad (2.18)$$

In the case of a maximum volume constraint imposed on the problem, the optimality condition for the shape gradient becomes L = c on the boundary Γ with $c \ge 0$. If a topological change and a boundary variation are taking

place simultaneously, the first variation of the objective function J is expressed as:

$$\begin{aligned} \delta J &= G(x)(-\delta m) + \int_{\partial\Omega} L(s) V_n ds \\ &= G(x)(-\delta m) + c(\delta m) = (-G(x) + c)\delta m \end{aligned}, \tag{2.19}$$

where δm is the volume change.

For a local minimum, we have $\delta J \geq 0$, thus the optimality condition is given as:

$$\begin{aligned} G(x) &= 2c \quad on\ \Gamma \\ G(x) &\leq c \quad in\ \Omega \end{aligned}. \tag{2.20}$$

The theory of the topological shape optimization is still in development, and the convergence of the optimization is not guaranteed by the optimality conditions defined in (2.18) to (2.20). In the stopping criterion, both the optimality condition and some dimensional constraints in manufactory (e.g. minimal size of components) are considered.

Based on the optimality condition in (2.18), a simple algorithm for topological shape design, without considering a volume constraint, can be proposed as follows:

1. Set the iteration number k =0.

2. Solve the primary and adjoint systems.

3. Calculate the topological gradient at different points in the design domain.

4. Define the new domain Ω_k by changing the material in a small region ϕ around the point x if TG(x)>0.

5. Apply the standard shape optimization method to determine the shape of the boundary of ϕ.

6. Verify the stopping criteria and exit if the optimality condition is satisfied

7. Set k=k+1

Note that the topological gradient can be obtained at any point inside the design domain; it only requires the primary and adjoint solution of the original problem (without creating the hole).

2.3 Robust Topology Optimization

If a topology change has taken place, the scalar objective function J can be approximated near the point ξ using a first-order local expansion as in (2.15),

$$J(\xi) = \Psi(\Omega \setminus \phi(\xi, d)) = \Psi(\Omega) + TG(\xi) \cdot \delta(d) + o(d^2). \qquad (2.21)$$

Since $\Psi(\Omega)$ and $\delta(d)$ are both constants with respect to ξ (note that $\delta(d)$ has a negative sign), $J(\xi)$ has the largest value where $TG(\xi)$ is the smallest. Therefore, the worst performance of J due to the perturbation of the design variables is determined by the point ξ in the uncertainty set, where $TG(\xi)$ has the smallest value. Hence we can obtain a robust topological gradient as:

$$TG_R(x) = \min_{\xi \in U(x)} TG(\xi). \tag{2.22}$$

Figure 2.7 is used to illustrate the robustness of a topological change. There exist two areas for a potential topological change in the design domain Ω. However, area 1, which has the highest TG value, is close to a large area which has the lowest TG value, i.e. the TG value drops drastically in the neighborhood of area 1. If a topology change is made in area 1, e.g. an air hole in the domain of solid material, a small variation to the boundary of the hole may cause a big change in the objective function value, which implies that the new topology is not robust. Therefore, area 2, which has the second largest TG value, is superior to 1 for a topological change in terms of the topological robustness. This is, in fact, equivalent to the robust topological design using second-order sensitivity analysis (Nam-Kyung et al., 2010).

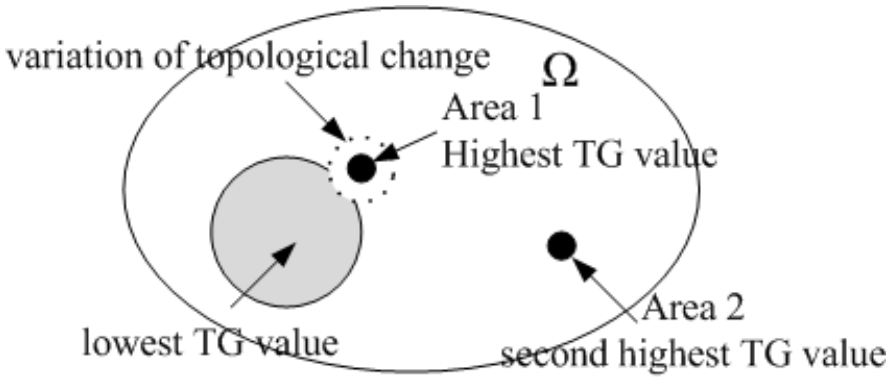

Figure 2.7: Robustness of topological changes

As a result, the robust formulation of the topological gradient TG_R can be computed and used as a decision criterion on the location where the topology changes will take place.

In robust topology optimization, first, we use the robust TG to determine whether a topology change in the problem domain is needed for reducing the objective function value. Then a small hole (of a different material) is created in the area where the robust TG has the highest positive values. After the hole is created in the domain, the boundary of the hole is parameterized and is optimized using a shape optimizer. Thus a new uncertainty set is defined for the new design variables, which are the coordinates of the controlling points on the discretized boundary of the

hole. As shown in figure 2.8, several controlling points are created and the boundary is described using a B-Spline curve.

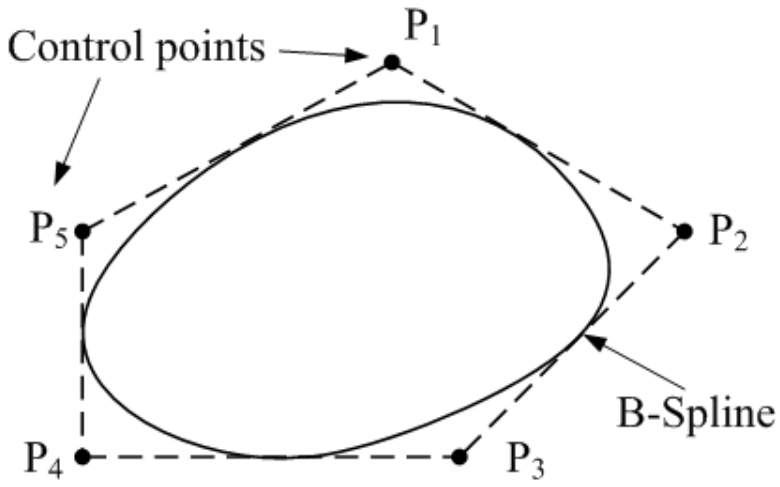

Figure 2.8: Boundary parameterization

The uncertainty set can be defined as the perturbation to the nominal value of P = [P_1, P_2, P_3, P_4, P_5], and the worst performance function remains the same through the entire design process.

An algorithm for robust topology optimization

Finally, a simple algorithm for robust topology optimization based on topological shape optimization is described as follows:

1. Set the iteration number k =0.

2. Calculate the robust topological gradient TG_R at the center of each element.

3. Define the new domain Ω_k where the topology changes take place by removing the material in the region where TG_R is greater than zero.

4. Apply the standard shape optimization method with a robust objective function to determine the shape of the boundary.

5. Verify the stopping criteria and exit if the optimality condition is satisfied

6. Set k=k+1

Uncertainties in both the topology and shape are handled throughout the entire design process.

2.4 Links between Worst-Case Analysis and Multi-Objective Approaches

Some may argue that a robust design approach based on worst-case analysis might be too "conservative", e.g. if the user-defined uncertainty set is too large, the solution to the robust objective function will have a very poor performance compared to the nominal solution. The alternate way to treat the robust design problem is to use a expectancy measure of robustness based on probability, i.e. using a multi-objective optimization formulation that minimizes the mean and the variance of the nominal performance simultaneously, as:

$$\min\begin{bmatrix} E[f(x)] \\ V[f(x)] \end{bmatrix}. \tag{2.23}$$

where E[f(x)] and V[f(x)] are the expectation (mean) and the variance of the performance f based on statistical models, respectively.

While obtaining the mean and variance is still computationally expensive since many function evaluations are needed, we may use the nominal value of f to approximate the mean and the deviation , $f_w - f$, as a surrogate of the variance in the multi-objective formulation (Guimaraes et al., 2006). Thus equation (2.23) is considered equivalent to,

$$\min\begin{bmatrix} f \\ f_w - f \end{bmatrix}. \tag{2.24}$$

In addition, the problem in (2.24) can be solved using a convex combination as:

$$\begin{aligned} \Psi &= (1-\alpha) f(x) + \alpha(f_w(x) - f(x)) \\ &= (1-2\alpha) f(x) + \alpha f_w(x) \\ 0 &\le \alpha \le 1 \end{aligned} \quad . \tag{2.25}$$

If we choose α = 0.5, we have,

$$\Psi = 0.5 f_w(x), \tag{2.26}$$

therefore the worst case scenario is just one of the solutions to the multi-objective optimization problem defined in (2.24).

Using the multi-objective formulation, the robust design problem is treated as a classical conflict design and a *pareto* front of the potential robust solutions can be generated by changing the value of the weighting factor and solving the single objective function successively.

Chapter 3 NON-DESTRUCTIVE TESTING

Non-destructive testing (NDT) technologies play a critical role in many fields of modern day industry, (e.g. to assure the quality and reliability of structural materials). NDT technicians and engineers define and implement tests to detect and locate defects in the material that may affect the reliability of the structure (e.g. small fractures in the body of a plane might cause a plane crash and flaws in a pipe might cause an oil leak). The benefits of NDT are that these tests or inspections can be performed without damaging the test specimen or causing any changes in the future use of them.

3.1 NDT Forward and Inverse Problems

One of the typical applications of topology optimization is the reconstruction of defects in the test specimen from the signals of NDT. Inverse problems are usually formulated as minimizing the squared errors between the measured and the simulated signals. In general, it is more

important to know the number of the flaws and their locations rather than the determination of the exact shape.

NDT systems can be enhanced in conjunction with field analysis software tools. The finite element method (FEM) is employed to perform full 3-D simulations of the testing to obtain more accurate results of the field distribution than purely analytical approaches. While field computations from given sources, material properties and the geometries of the cracks are considered as a forward problem, the reconstruction of the crack shape is defined as an inverse problem for which the goal is to find correct values of specific parameters, such as length, depth and size of the cracks, given particular performance criteria (e.g. the field distribution measured by the sensing device). In fact, the forward problem is solved iteratively until the system output matches the input signals, i.e. a classical feedback control problem.

Conventional solutions to the inverse NDT problem can be categorized as two types: crack reconstruction based on optimization; or signal inversion using artificial neural networks. In the first category, the inverse problems are solved through a standard shape optimization of a parameterized

crack profile with a gradient-based search algorithm (Badics et al., 1998, Hoole et al., 1991) or a topology optimization based on optimal material distribution, assuming different conductivity values in an array of discretized cells (Dyck et al., 1994). However, the drawbacks of the optimization-based methods are that they cannot be applied to real-time detection because of the iterative nature of the problem that requires many evaluations of finite element field problems before the results converge.

On the other hand, the defect profile can be determined by various Artificial Neural Networks using signal inversion. This method is relatively faster than the optimization-based approach, but it requires a large set of training data from the NDT experiments, which may not be available for a particular problem in practice. Also, it cannot provide the information of the exact shape of the cracks, unless an exact match can be found between the measurement and the training data.

A novel solution strategy for the inverse NDT problem, proposed in this thesis, is shown in the following flow chart, figure 3.1. Unlike the conventional iterative procedure of shape optimization (Badics et al.,

1998), in this method, the topological gradient is computed to predict any potential effect of topology changes in the problem domain, i.e. replacing the solid material with air. Note that for NDT problems, usually the external boundary of the problem domain cannot change, thus the shape optimization in the first iteration is ignored. After the topology change to the domain, a sensitivity analysis based shape optimizer is used to determine the exact shape of the boundary of the crack. The global optimality condition defined in (2.18) is checked at the end, and the algorithm terminates when there is no more topology change needed.

.

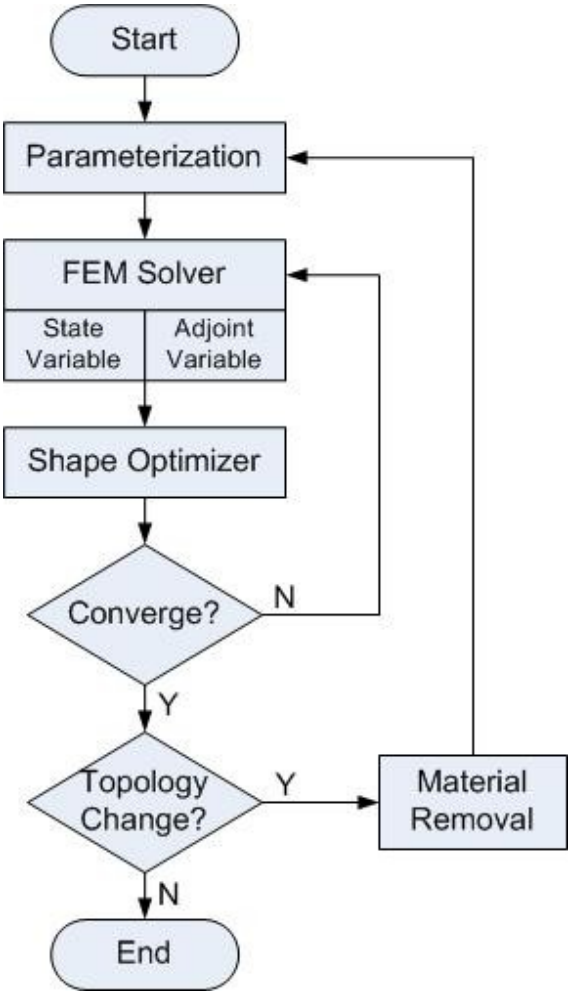

Figure 3.1: A solution to the inverse NDT problem

There are a number of different electromagnetic testing methods and in this chapter we will demonstrate the numerical applications of topological sensitivity analysis to the magnetic flux leakage (MFL) and eddy current testing (ECT) methods.

3.2 Magnetic Flux Leakage type NDT

The magnetic flux leakage method is a fast and reliable non-destructive testing technique that has been widely used for decades. When a piece of metal made of ferromagnetic material is placed in a magnetic field, small defects or flaws in the material cause a significant flux anomaly due to the permeability variation. The anomalous fields are captured by Hall-effect probes or sensing coils, placed close to the surface of the test object, and which generate signals that can be used to identify the defect.

FEM forward model of MFL

Figure 3.2 shows the basic model for MFL testing consisting of two permanent magnet blocks as the excitation source of the magnetic field (Al-Naemi et al., 2006). A test plate, 6mm thick, is placed under the MFL system. A sensor is placed 4.5 mm above the test plate and is moved parallel to the surface of the plate.

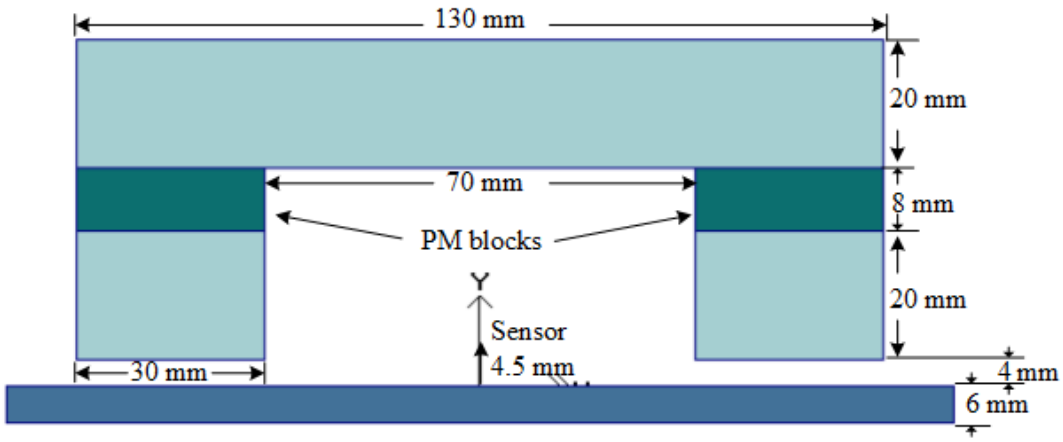

Figure 3.2: MFL test device

In the simulation model, the back yoke and iron arms in the sensing system are made of magnetically linear material. The test plate is made of cold rolled steel which has a nonlinear permeability. The forward MFL model is solved using a 3-D FEM system, MagNet (Infolytica, 2013b). In the reconstruction tests, first, cracks with different shapes and sizes are created in the test plate, and then, MFL signals corresponding to different cracks are generated from the simulation. Those simulated signals are used as the targets (measured results) for the inverse problem of defect identification.

Formulation of the inverse problem

The solution to the inverse problem utilizes a nonlinear optimization scheme in order to identify the size and the shape of the defects in the

material from a given MFL signal profile. An objective function, F, is formulated from the field signals B_{io} captured by MFL sensors (obtained at n sampling points along a line from the simulation model with the defects) and the field values B_i are computed from the FEM solution of the forward model where the shape of the plate is allowed to change at each iteration as the system tries to create the defect shape to minimize F.

$$F = \sum_{i=1}^{n} (B_i - B_{io})^2 \ . \tag{3.1}$$

Topological sensitivity analysis using an adjoint problem

The topological gradient for the MFL field problem (magnetostatic) can be expressed in terms of the field solution of the original problem and an adjoint problem as,

$$\begin{aligned} TG(x) &= 2L(A, \lambda) \\ L(A, \lambda) &= (v_1 - v_2)(\nabla \times A)(\nabla \times \lambda) \end{aligned} \ , \tag{3.2}$$

where ν_1 is the permittivity of the ferromagnetic material, ν_2 is the permittivity of air or the defect; L(A, λ) is the generic shape sensitivity and A and λ are the state variable and adjoint variable from the field solutions. Thus, ∇ X A and ∇ X λ are the magnetic flux densities obtained from the original field solution and adjoint field solution respectively.

In this problem, the calculation of TG requires a solution from the adjoint problem. In the discrete design sensitivity analysis (DDSA) based on a FEM solution, the adjoint variable λ is introduced to avoid the inversion of the system matrix S in the sensitivity calculation (Sundaresan et al., 1995). The adjoint variable λ is given as:

$$\lambda^T S = \frac{\partial F}{\partial A}, \tag{3.3}$$

where S is the system matrix of the FEM, which represents the linear equations to be solved for obtaining the field solution; A is the solution to the FEM and F is the objective function.

While the DDSA method requires obtaining details about the locations of the nodes inside the FEM mesh, a continuum design sensitivity analysis (CDSA) approach is capable of computing the sensitivity independent of any field solution methods. From (3.3) we can define an adjoint system that has the following properties (Kim et al., 2004):

1. A linear problem which has the same geometric and material properties (except for the excitation sources and the boundary conditions) as the original problem.

2. The source for the adjoint problem depends on the objective function used in the design optimization problem.

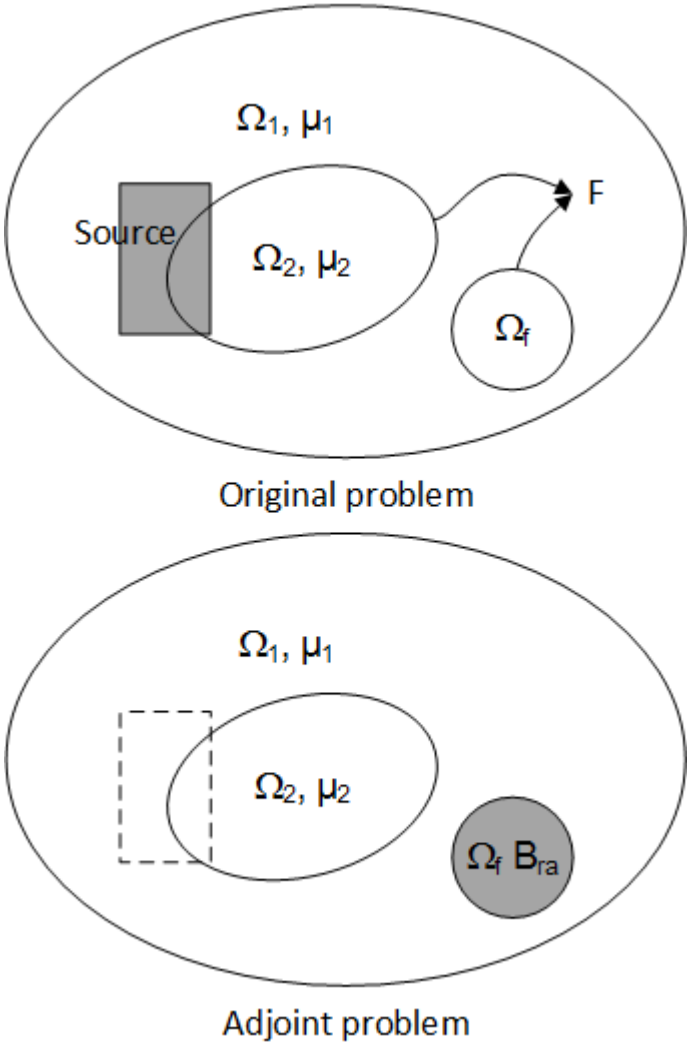

Figure 3.3: Dual systems of sensitivity calculation

Figure 3.3 shows the analogy between the original problem and the adjoint problem. If an objective function is formed as $f = (B_{xi} - B_{xo})^2$, the source term is given as $B_{ra} = \partial f / \partial B$, B is the magnetic flux density, which acts as a magnetic source to the adjoint problem (Kim et al., 2004). B_{ra} is set as the residual flux density for the magnetic source in the area of Ω_f where the field values of the original problem are sampled.

Calculation of the topological gradient

In order to find the location of the defects, the topological gradient is computed over the domain. Based on the asymptotic expansion of (2.17) and the optimality condition (2.18), we would expect that the defects lie in the regions where the topological gradient has the largest positive value.

The use of topological gradient to detect cracks was first tested in 2-D. A region from x = −20 mm to 20 mm in the center of the plate is the domain of interest in the test. It is then divided to 6X40 small blocks (1mmX1mm), and the topological gradient evaluated at the center of each block. The units of the topological gradient do not have any physical meanings, since they depend on the choice of objective functions. Thus, in all the figures for the values of TG, we do not include the units.

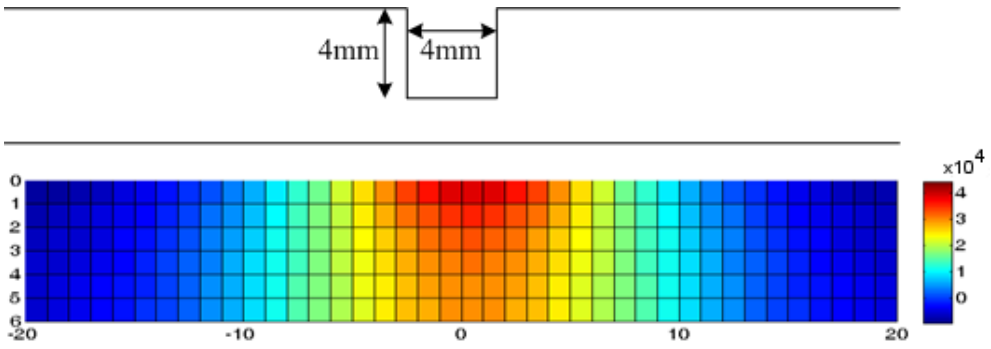

Figure 3.4: Topological gradient plot for one defect in 2-D

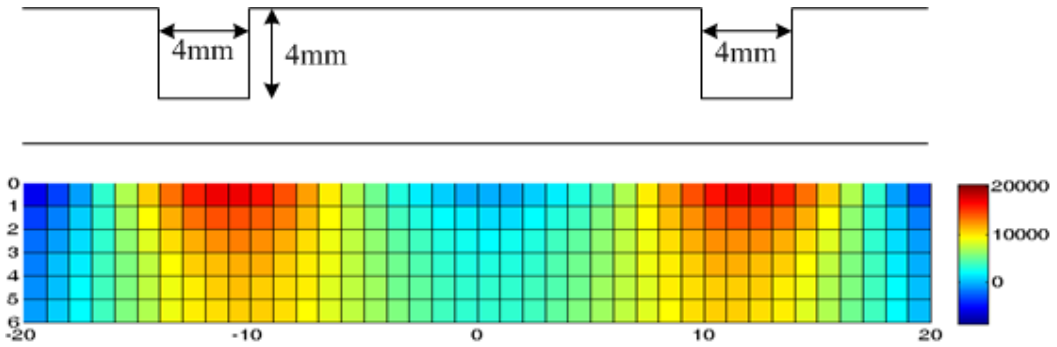

Figure 3.5: Topological gradient plot for two defects in 2-D

Figure 3.4 shows the topological gradient plot for the model with one defect 4 mm wide and 4 mm deep and centered at x = 0. Figure 3.5 shows the topological gradient of a model with two defects, each of them are 4 mm wide and centered at x = −12 mm and x = 12 mm respectively. As can be seen from the figures, the regions of the highest values of topological gradient coincide with the position of the defects.

In addition, the topological gradient is computed for the case of a buried crack in 3-D. The required field values are obtained from a finite element solution on a relatively coarse mesh. A cuboid shape crack of size 6x6 mm and height 5 mm exists at the center of the steel plate, and the topological gradient plot on the bottom surface of the plate is shown in figure 3.6. The highlighted area in the figure matches the location of the defect. TG plots for two and three cracks of the same size in the plate are shown in figures 3.7 and 3.8.

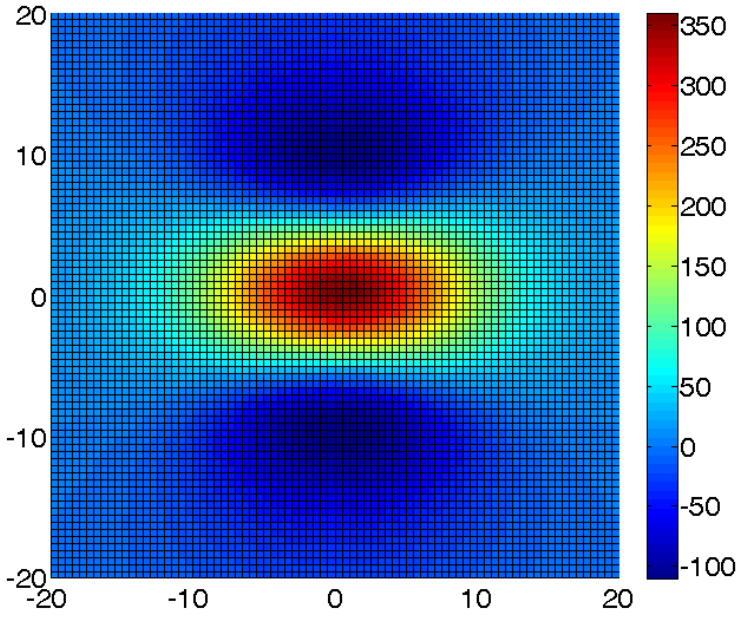

Figure 3.6: Topological gradient plot for one defect in 3-D

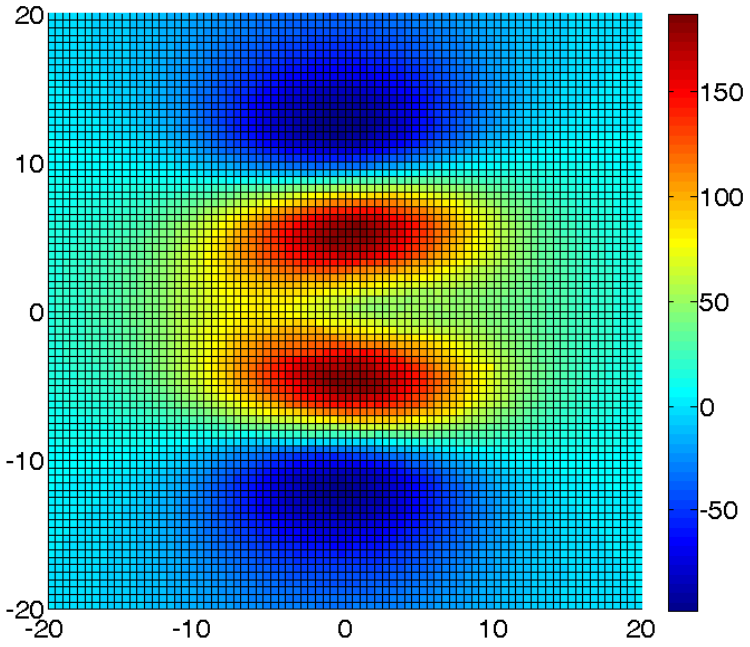

Figure 3.7: Topological gradient plot for two defects in 3-D

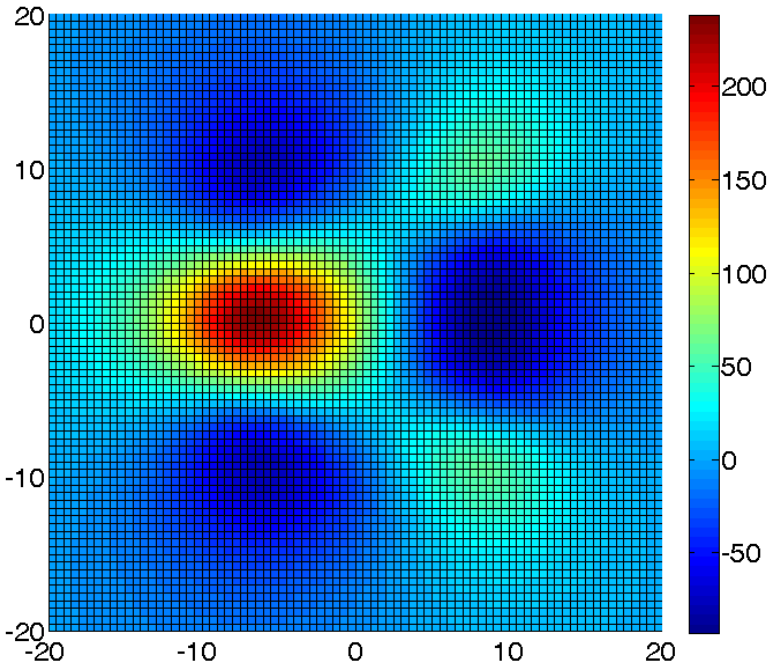

Figure 3.8: Topological gradient plot for three defects in 3-D

As a result, the method based on the topological sensitivity analysis has the potential to be employed to locate the cracks in the test plate fairly quickly.

Determination of defect size and shape

While obtaining the information on the location of the crack involves only one computation of the TG, to reconstruct the shape of the crack from the test signal requires more integrations. The defect prediction based on topological shape optimization method is tested with one crack located on

the near side of a steel plate of 5 mm width and with an average depth equal to 80% (4.8 mm) of the thickness of the plate. First, the topological gradient is computed over the domain of interest consisting of 6X40 blocks. Then, from this calculation, about 5% of the area, which has the highest positive TG values, is removed from the domain. Next, the boundary of the initial crack is discretized with 5 points and expressed using a piecewise linear approximation. Then it can be modified through a shape optimizer based on CDSA. The topology and shape changes in the optimization are illustrated in figures 3.9 and 3.10 for a rectangular shape crack and irregular shape crack respectively. The final shapes of the crack obtained from the topological shape optimization are consistent with those used for producing the test signals.

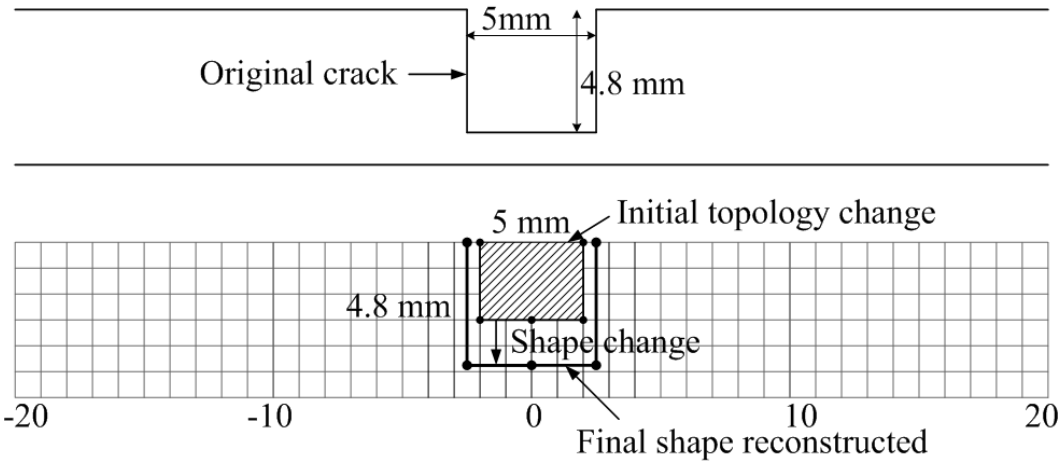

Figure 3.9: Rectangular shape crack reconstruction

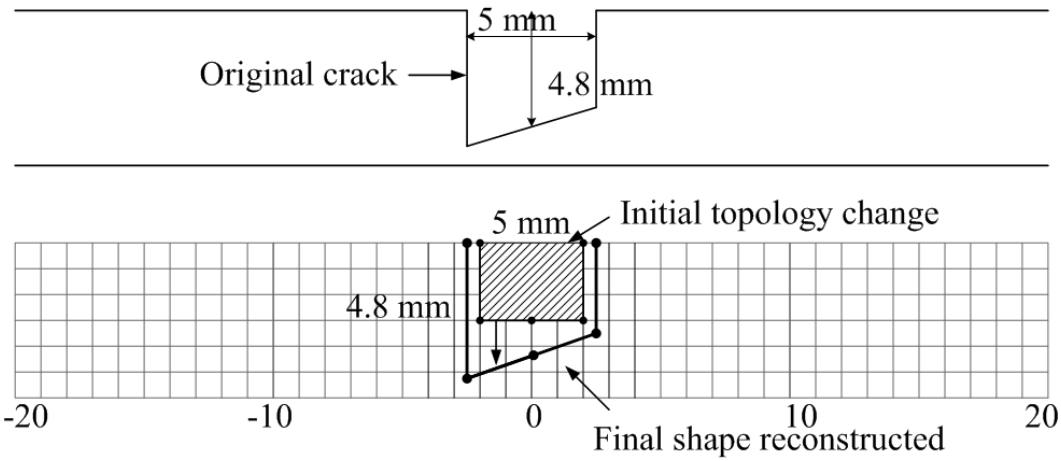

Figure 3.10: Irregular shape crack reconstruction

The values of the objective function F during the topological shape optimization of the rectangular shape crack are shown in figure 3.11. The initial value of the objective is 0.0865 when there is no crack existing in the simulation model. The topological change reduces it to 10% of this value. The remaining improvement is then obtained through shape optimization. Figure 3.11 also shows the convergence of the process if only shape optimization is used. In this particular example, the topological shape optimization process converges in twelve iterations while the conventional shape optimizer takes a lot more iterations and in turn requires more FEM solutions.

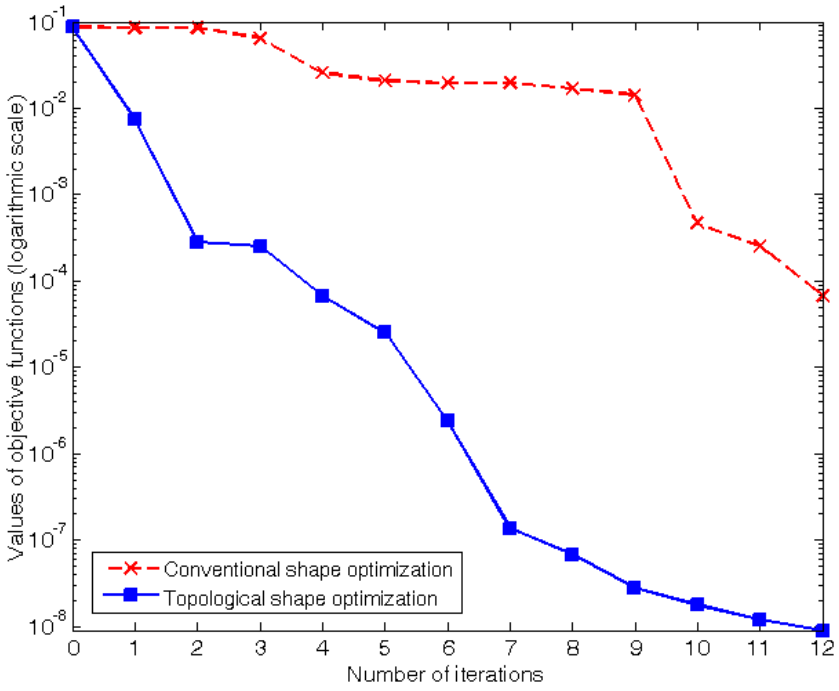

Figure 3.11: Objective function values through the optimization

We should note that given the ill-posed nature of this kind of inverse problem, the shape optimizer is likely to run into a local minimum. In that case, it is still possible to use the topological gradient to look for another topology change in the problem domain and to merge the two holes into a larger hole. Therefore the topological shape optimization is able to find a global minimum by verifying the global optimality condition until no more topology change is necessary to minimize the objective function.

Robustness of the topological gradient

In real MFL tests, noise from the environment (i.e. experimental errors) cannot be avoided, therefore the reconstruction methods must be robust in the presence of random noise. In order to verify the robustness of the topological gradient in the presence of noise, a uniformly distributed random noise signal is created and is added to the original signal obtained for the crack. Figure 3.12 shows the MFL signal corresponding to one surface crack in the test plate. In figure 3.12, the dashed line with cross marker indicates the original signal, the dashed grey line illustrates the noise signal and the solid line with square marker is the summation of the original signal and the noise.

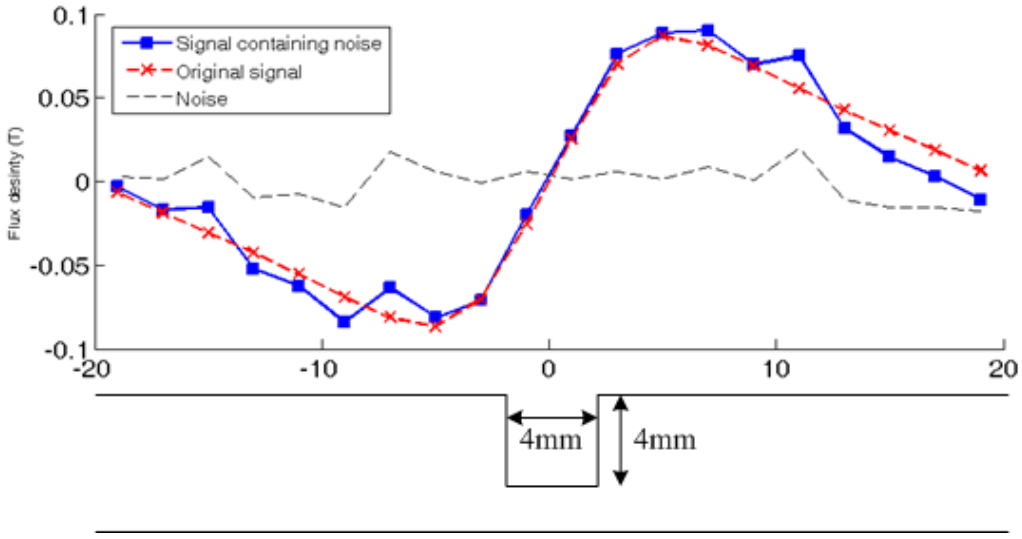

Figure 3.12: Random noise added to the MFL signal

The signal containing noise is then used as the input for the crack reconstruction. The resultant topological gradient plots are compared in figure 3.13. In figures 3.13 a) and 3.13 b), the areas of positive TG values, which indicate the location of the cracks, are almost identical. This implies that the method is relatively robust with respect to a small (less than 20% of the magnitude of the signal) amount of noise.

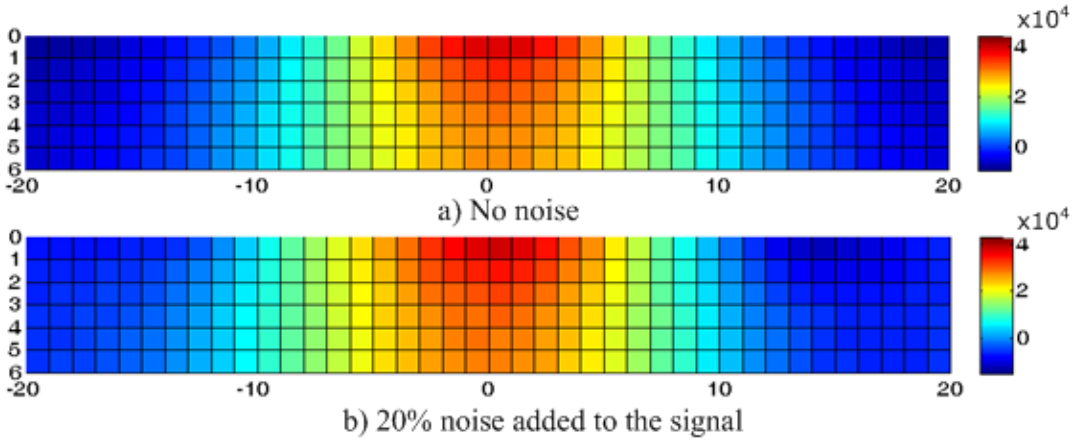

Figure 3.13: Noise effects on the topological gradient plot

Conclusions

In the MFL type NDT inverse problem, the topological gradient can be employed to find any potential topology change that may reduce the objective function value. It provides a fast, but approximate, exploration of the solution space. The initial topology predicted by TG can significantly reduce the value of the objective function, and the shape optimization can then be used to refine the solution from that initial state. Thus, the

topological shape optimization is more efficient compared to conventional methods using pure shape optimization for the inverse problem of crack reconstruction.

This method is able to detect buried defects in 2-D and 3-D. Although the solution to the inverse problem might take a long time to converge, i.e. find the exact shape of the defects, the topology gradient can roughly predict the position and numbers of the defects within one step. In the case where fast detection speed is needed, it can be used to label the position of the defects and the full signal profile can be used later for an accurate description of the cracks.

3.2 Eddy current testing problems

The eddy current non-destructive testing relies on the physical effect called "eddy currents" to inspect the cracks in a conductive specimen. In the eddy current testing (ECT), a coil is usually placed above the test plate. When the coil is excited with sinusoidal current, eddy currents are induced in the body if it is conductive. If a crack exists in the test specimen, the crack will block the eddy currents in the region and this

results in a change of the external magnetic field which can in turn be picked up by some sensing coils.

Derivation of the topological sensitivity for ECT problems

Let Ω be a bounded domain of R^n with an external boundary Γ. The magnetic field, H, is the solution to the following problem:

$$\begin{cases} \nabla \times (\alpha \nabla \times H) - \beta H = 0 \quad in\ \Omega \\ \alpha (\nabla \times H) \times n = b \quad on\ \Gamma \end{cases} . \tag{3.4}$$

where n is a unit vector normal to Γ and α and β are scalar auxiliary functions, defined on Ω, which are used to facilitate the derivation and will be replaced by the coefficients depending on the Maxwell governing equations for the problem.

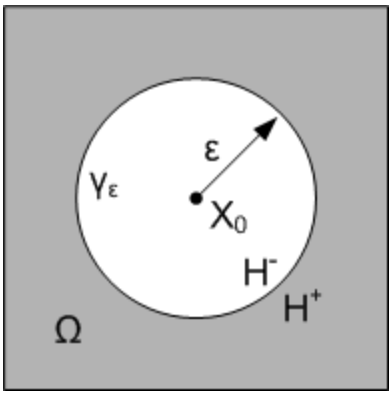

Figure 3.14: Small inhomogeneity in the problem domain

If a small inhomogeneity ϕ_ε, e.g. a different material, bounded by γ_ε is created in domain Ω, as shown in figure 3.14. α and β become piecewise constant functions across the boundary γ_ε, as:

$$\alpha(x) = \begin{cases} \alpha_1 & if\ x \in \Omega \setminus \phi_\varepsilon \\ \alpha_2 & if\ x \in \phi_\varepsilon \end{cases}, \tag{3.5}$$

$$\beta(x) = \begin{cases} \beta_1 & if\ x \in \Omega \setminus \phi_\varepsilon \\ \beta_2 & if\ x \in \phi_\varepsilon \end{cases}. \tag{3.6}$$

Thus the perturbed solution H_ε in the presence of ϕ_ε must satisfy the following equations:

$$\begin{cases} \nabla \times (\alpha_1 \nabla \times H_\varepsilon) - \beta_1 H_\varepsilon = 0 \quad in\ \Omega \setminus \phi_\varepsilon \\ \nabla \times (\alpha_2 \nabla \times H_\varepsilon) - \beta_2 H_\varepsilon = 0 \quad in\ \phi_\varepsilon \\ \alpha_1 (\nabla \times H_\varepsilon)^+ \times n - \alpha_1 (\nabla \times H_\varepsilon)^+ \times n = 0 \quad on\ \Gamma_\varepsilon \\ \beta_1 H_\varepsilon^+ \cdot n - \beta_2 H_\varepsilon^- \cdot n = 0 \quad on\ \Gamma_\varepsilon \\ \alpha_1 \nabla \times H_\varepsilon \times n = b \quad on\ \Gamma \end{cases}. \tag{3.7}$$

where the superscripts + and – represent the limit of field values as the sampling point approaches Γ_ε from outside ϕ_ε and inside ϕ_ε respectively.

The field solution in the absence of ϕ_ε is denoted as H_0 and the variational form associated with H_0 can be expressed as:

$$\alpha_1(H_0, v) = \ell(v) \quad \forall v \in V. \tag{3.8}$$

where ℓ is a bilinear form on V and V is a functional space of all admissible potentials.

In order to compute the variation of an objective function J with respect to the perturbation, we define an adjoint problem in the form of

$$\alpha_\varepsilon(w, v_\varepsilon) = -L_{H_0}(w) \quad \forall w \in V\,. \tag{3.9}$$

where L is the linear term depending on J. Equation (3.9) has a unique solution v_0 when ε is small enough.

From the result proven in (Masmoudi et al., 2005), the topological asymptotic expansion is expressed in terms of the solution H_0 and adjoint state v_0 as:

$$\begin{aligned} &J(\varepsilon) - J(0) \\ &= -4\pi\varepsilon^3 \,\mathrm{Re}\{\frac{\alpha_1(\alpha_2 - \alpha_1)}{\alpha_1 + 2\alpha_2} \nabla \times H_0 \cdot \overline{\nabla \times v_0} + \frac{\beta_1(\beta_1 - \beta_2)}{\beta_2 + 2\beta_1} H_0 \cdot \overline{v_0}\} + o(\varepsilon^3)\,. \end{aligned} \tag{3.10}$$

The governing Maxwell equation for the steady state time harmonic problem is:

$$\nabla \times (\frac{1}{\sigma} \nabla \times H) + j\omega\mu H = 0\,. \tag{3.11}$$

To obtain the topological gradient for the steady state time harmonic problem, α is substituted by 1/σ and β by –jωμ in (3.10). If the material is

nonmagnetic, i.e. it has the same permeability as air, the coefficient of the second term in (3.10) becomes zero, and we obtain:

$$J(\varepsilon) - J(0) = -4\pi\varepsilon^3 \operatorname{Re}\{\frac{\sigma_1(\sigma_1 - \sigma_2)}{2\sigma_1 + \sigma_2} E \cdot \overline{E_A}\} + o(\varepsilon^3), \qquad (3.12)$$

where σ_1 is the electrical conductivity of the material and σ_2 is the electrical conductivity of air. E_A is the electrical field computed from the adjoint problem.

The volume of the small ball ϕ_ε is given as $4/3\pi\varepsilon^3$. Combining (3.12) and the definition in (2.9), finally, the topological gradient is given as:

$$TG = \frac{3\sigma_1(\sigma_1 - \sigma_2)}{2\sigma_1 + \sigma_2} \operatorname{Re}\{E \cdot \overline{E_A}\}. \qquad (3.13)$$

Note that the topological gradient is expressed with field values only and, therefore, the calculation of TG is independent of the field analysis approach and code used, and the TG can be evaluated at any point in the domain using just two field solutions, which could even be from different methods of field calculation.

Inverse procedure of ECT

An objective function F is formulated from the squared errors between the measured signal and simulated signals, as:

$$F = \sum (S^i_{Simulated} - S^i_{Measured})^2 \ , \tag{3.14}$$

where S can be a variety of physical quantities depending on the means of the measurement, such as impedance, voltage or magnetic flux density; and i is the index for different sampling points.

Similar to the crack reconstruction in MFL testing, in ECT, the topological gradient of the objective function F is computed over the domain of interest in order to discover any potential topology changes that may reduce the value of F. The material in the area which has the highest TG values is replaced with air to create an initial crack model. Then the boundary of the initial crack is parameterized and altered through a shape optimizer until both the optimal shape and topology are obtained. The global optimality condition defined in (2.18) is verified at the end. For the problem of detecting multiple cracks, this procedure can be performed repeatedly until all the cracks in the area are found.

Examples of the ECT inverse solution

The topological shape optimization method is tested against several ECT inverse problems, which include the TEAM 15 benchmark problem, the determination of wall thickness of a conductive tube and several crack reconstruction problems.

TEAM 15 benchmark problem

The numerical simulation of an eddy current testing signal requires sophisticated models and accurate field computation. The goal of the benchmark problem is to reconstruct the crack shape using the experimental data from eddy current testing recorded in the TEAM workshop problem 15. The experimental setup is shown in figure 3.15, and consists of a circular coil placed above a conductive test plate of aluminum alloy. There is one rectangular slot in the center of the conductor. The length of the slot is 12.6 mm and the depth is 5 mm. The scan frequency used is 900 Hz, which in turn gives the depth of penetration as 3.04 mm.

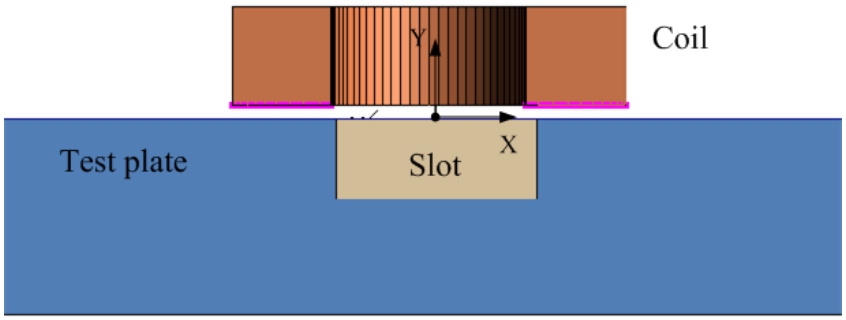

Figure 3.15: Coil configuration of TEAM 15

A numerical model is created with the same geometry as described in the TEAM problem 15 (Compumag, 2013). The forward field problem is solved with a 3D time harmonic FEM solver from MagNet (Infolytica, 2013b).

The inverse procedure starts with an assumption of no cracks. Hence, the objective function F in (3.14) is evaluated using the values taken from TEAM problem 15 as the measured signal and the values computed from a simulation of an aluminum plate free of flaws. Figure 3.16 shows the dimensions of the crack and the topological gradient is computed and plotted in figure 3.17.

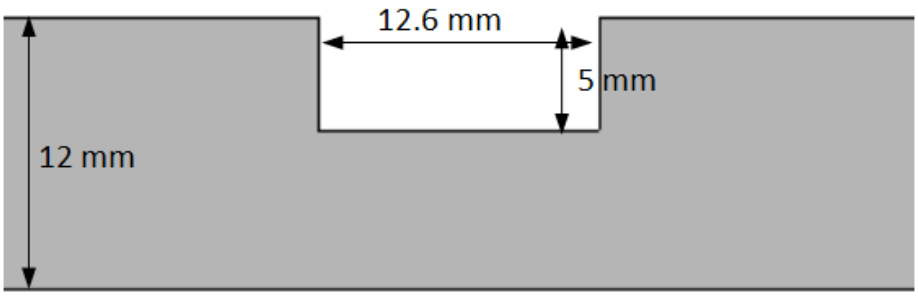

Figure 3.16: Dimensions of the crack

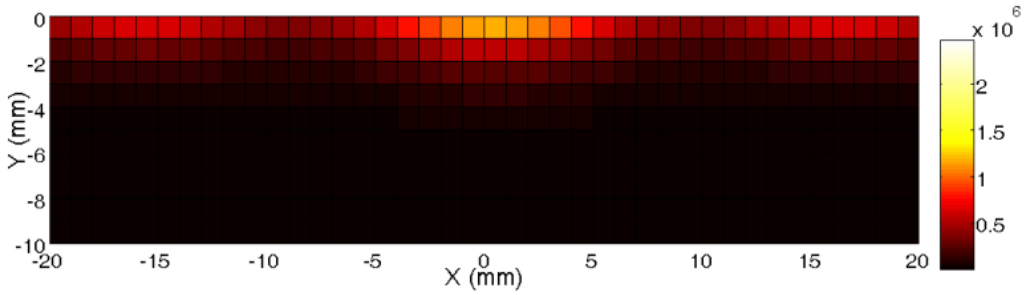

Figure 3.17: Topological gradient plot for a rectangular slot

As shown in the above figure, the regions of the highest values of topological gradient (represented by the light area) coincide with the position of the slot in the plate. The topological sensitivity analysis indicates a topology change in the domain of interest. Figure 3.18 shows the discretization of the problem domain and it demonstrates that we can create an initial slot of air in the test plate and parameterize the boundary of this slot with five control points. The precise shape of the slot is then determined using a shape optimization based on CDSA. The final shape

of the crack matches the dimensions of the slot, indicated in figure 3.16, used in the TEAM 15 experiment.

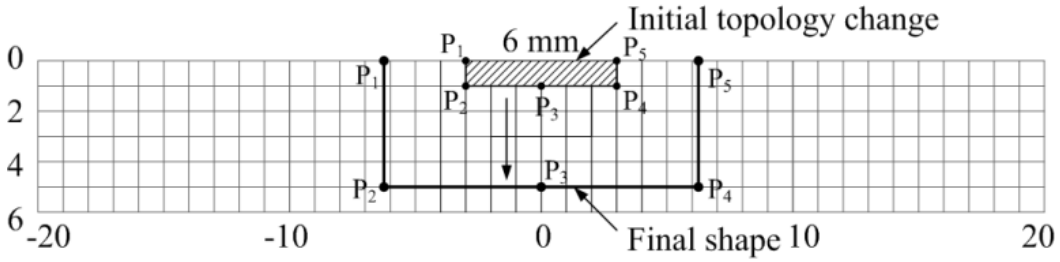

Figure 3.18: Final shape of the reconstructed slot

The measured signal used in the reconstruction is the change of the voltage in the coil. The magnitude and phase of the impedance change can be computed as:

$$|\Delta Z| = \sqrt{(\Delta R)^2 + (\Delta X_L)^2}\,, \qquad (3.15)$$

where $\Delta X_L = \omega \Delta L$.

The signal of impedance changes calculated from the reconstructed shape is compared to the experimental results from TEAM 15 in figure 3.19.

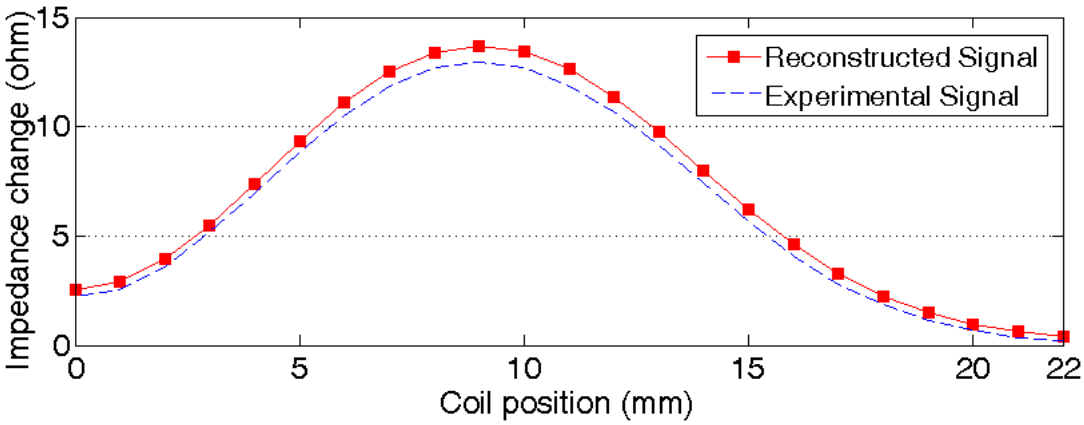

Figure 3.19: Impedance signal of the reconstructed slot

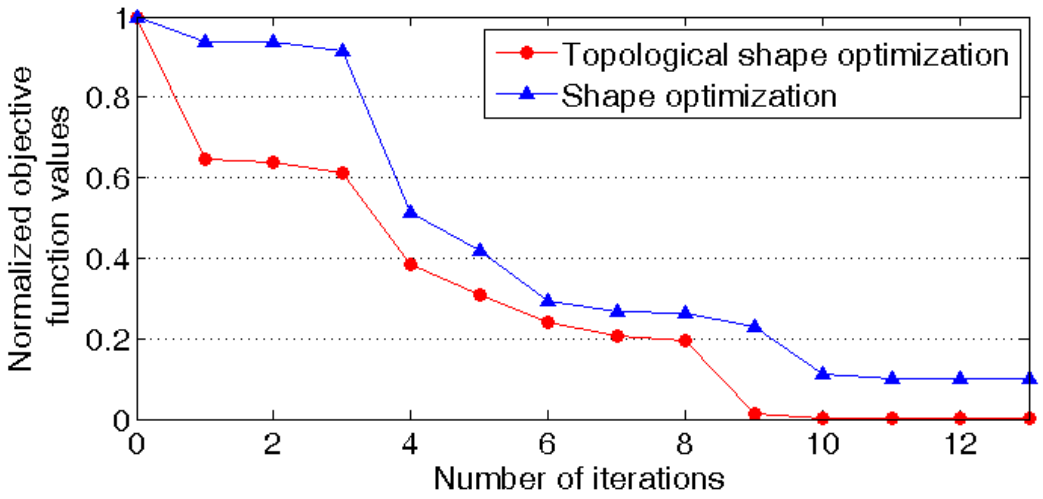

Figure 3.20: Performances of two optimization models

Figure 3.20 shows the changes of the objective function values during the inverse procedure of crack reconstruction using the topological shape optimization and a pure shape optimization procedure as presented in (Badics et al., 1998). As can be seen in figure 3.20, the topological shape optimization has a better performance than shape optimization alone. This

may result from the fact that the topological sensitivity analysis can provide a better starting point for the shape optimization algorithm. The value of the objective function is reduced by four orders of magnitude in 13 iterations.

A conductive tube with eccentric walls

Eddy current NDT can also be used in the test of wall eccentricity of cylindrical tubes with coaxial internal and external surfaces (Diserens and Sullivan, 1994), (Theodoulidis and Bowler, 2008), (Skarlatos and Theodoulidis, 2010), (Theodoulidis and Bowler, 2010). In such tests, an air-cored bobbin coil is placed in the center of a conductive, nonmagnetic tube. Eddy currents in the tube are induced by the coil whose axis is parallel to the axis of the tube. Therefore if there is a deviation from the coaxial geometry (eccentricity) or there is a change in the wall thickness, the change of the eddy currents will result in a change of the magnetic field which can be picked up by the coil. However, if the test problem is modeled using conventional formulations based on FEM, the huge computational cost may be an disadvantage for obtaining the inverse solution (Skarlatos and Theodoulidis, 2010).

The topological gradient is applied to the ECT of a conductive tube with eccentric walls. The TG is calculated using an objective function of the impedance changes. Figure 3.21 a) shows the set up of the problem, a coil inside a conductive tube with an outer diameter of 12 cm. As we can see from the result in figure 3.21 b), TG can identify the wall thickness correctly as the highest values of TG correspond to the area where the tube wall is the thinnest. Therefore, the TG-based method can be used to detect the changes in the wall thickness or the eccentricity without intensive computational cost since only one FEM solution is required.

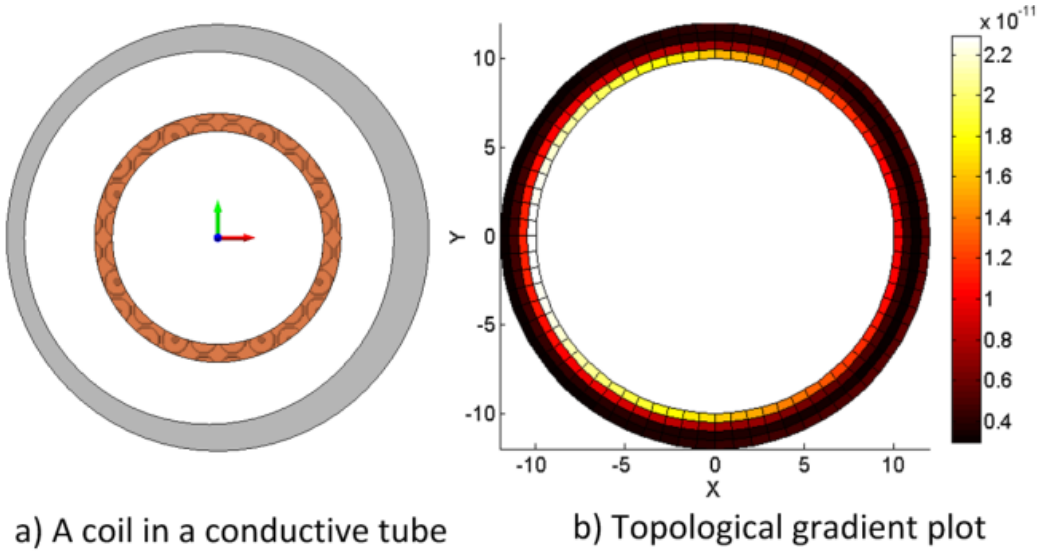

Figure 3.21: TG plot for a conductive tube with eccentric walls

Buried flaw reconstruction

One advantage of the ECT technique is the ability to detect flaws buried under the surface. Figure 3.22 shows an ECT imaging system consisting

of five parallel coils and an aluminum block containing a buried flaw. A 2-D model of the ECT system is used for crack reconstruction instead of the full 3-D simulation, for the reason of faster field calculation. The thickness of the conductive plate is 10 mm. An excitation frequency of 60 Hz is used in the coils for a deep enough penetration of the induced eddy currents.

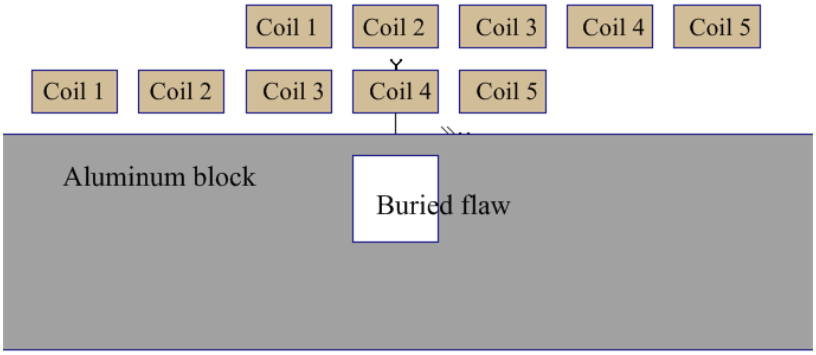

Figure 3.22: Eddy current imaging system in 2D

When one of the coils is excited with a current, the induced voltages of all five coils are measured. The goal of the inverse problem is to reconstruct the flaw by matching the target signal with the reconstructed signal. Thus, the objective function is formulated as:

$$F = \frac{1}{2}\sum_{i=1}^{5}\sum_{i=1}^{5}(V_{ij} - V_{ij}^{Measured})^2 , \qquad (3.16)$$

where V_{ij} denotes the voltage of coil i induced by coil j. The ECT physical problem is modeled using MagNet (Infolytica, 2013b) and the field solutions are obtained using a FEM time harmonic solver. The target

(measured) signals are also obtained from the simulation of the model with pre-defined cracks.

The topology gradient is calculated for one crack of 4x4 mm centered at (0,−3), as shown in figure 3.22, and the TG is plotted in figure 3.23. The location of the flaw is clearly indicated by TG in figure 3.23.

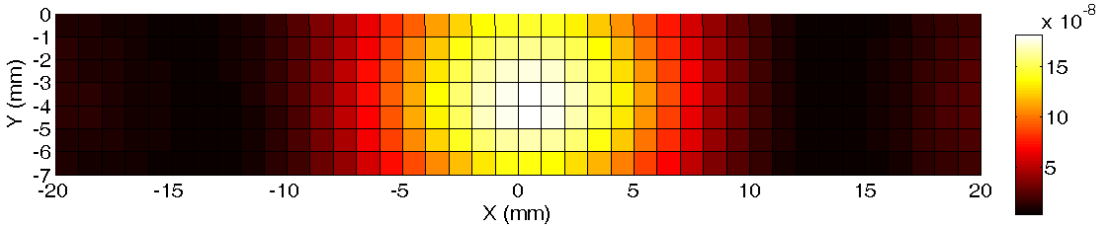

Figure 3.23: Topological gradient plot for one buried flaw

Figure 3.24 shows the shape reconstruction of buried flaws with different sizes and shapes. The dashed line indicates the reconstructed flaw while the solid line defines the original crack.

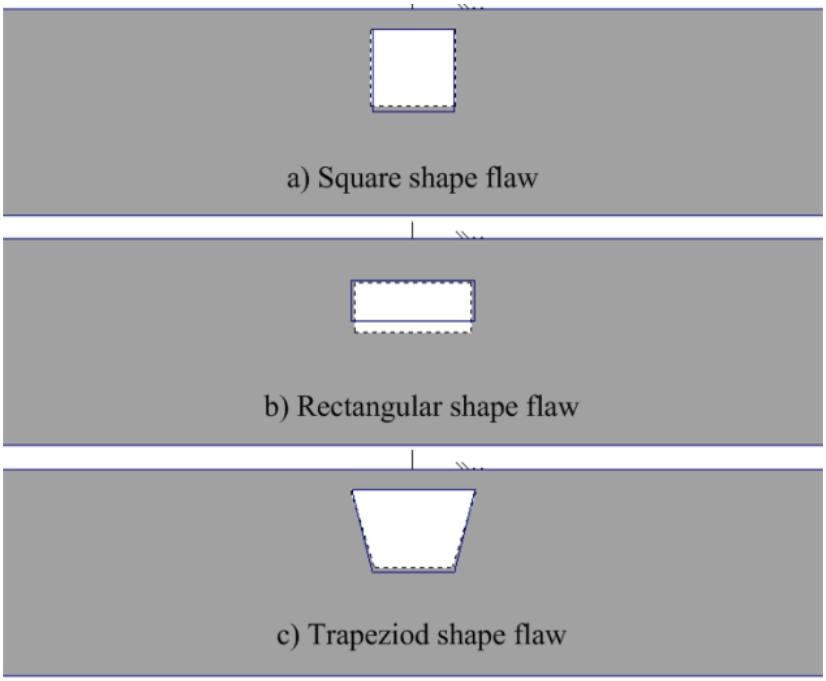

Figure 3.24: Shape reconstruction of buried flaws

Multiple flaws reconstruction

The inverse problem involving multiple flaws is much more complicated than single defect reconstruction due to the ill-posed nature of the inverse problem structure (Hoole et al., 1991). The same eddy current imaging system model as in figure 3.22 is employed. The topology gradient is calculated for the problem of a test plate containing two defects of 4x4 mm, centered at (−12,−4) and (2,−4) respectively as in figure 3.25.

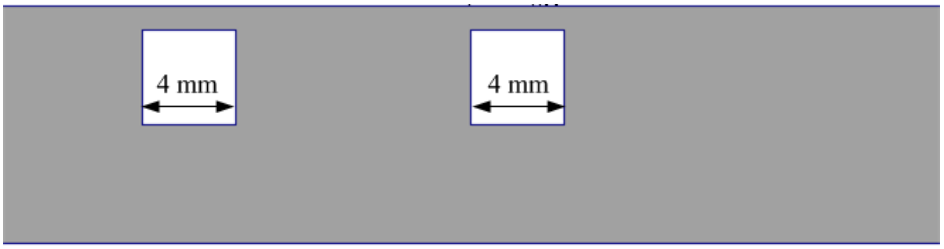

Figure 3.25: Test plate containing two cracks

First, the TG plot indicates that two flaws may exist in the test block, as shown in figure 3.26.

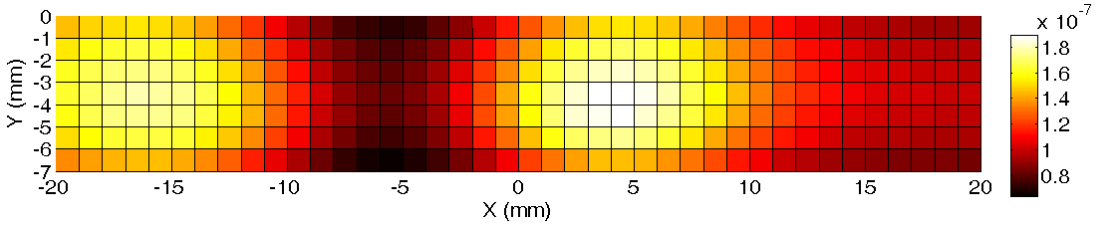

Figure 3.26: Topological gradient plot for two cracks

A first hole is created in the left region of high TG values. Its boundary is optimized until no improvement can be achieved. This is a local minimum for the inverse crack reconstruction problem. The final result of the shape optimization is shown in figure 3.27.

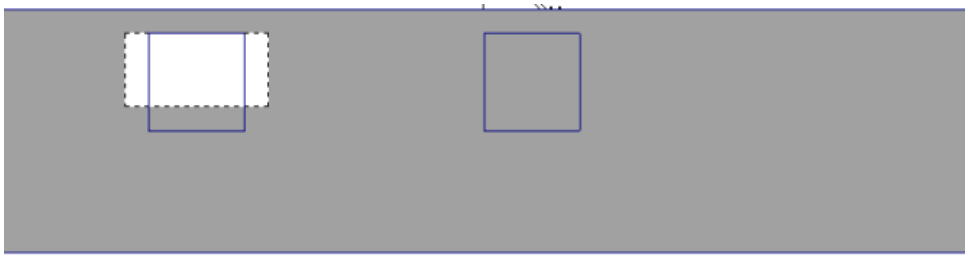

Figure 3.27: Shape optimization of the left hole

Then the TG is computed again for the domain shown in figure 3.27 against the measured signal obtained from the cracks model. And we can see, in figure 3.28, another region of positive TG values, which corresponds to the location of the second crack.

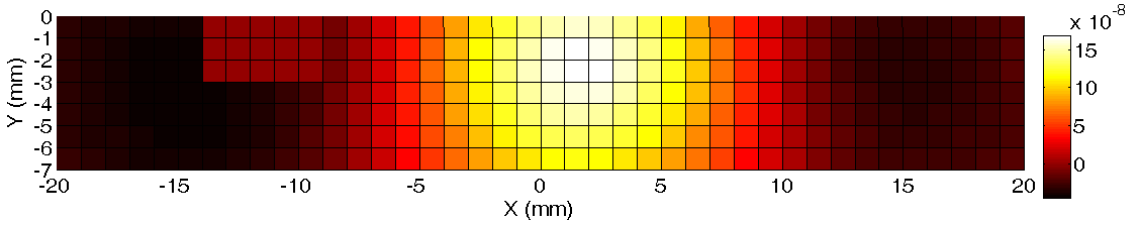

Figure 3.28: Topological gradient plot

Therefore, a second hole is created in the region indicated by the TG in figure 3.28, and the boundaries of both holes are optimized simultaneously. The final result achieved from the shape optimization is given in figure 3.29.

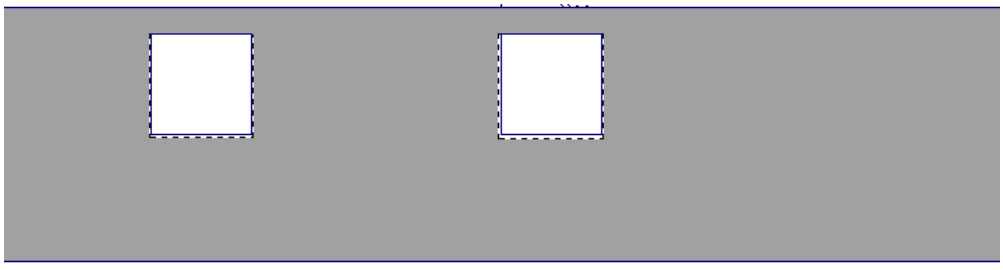

Figure 3.29: Final shape for two flaws

Comparison of ECT crack reconstruction methods

There exist many different methods to solve the ECT inverse problem, such as the method of pure topology optimization based on optimal material distribution (OMD), a pure shape optimization or signal inversions using artificial neural networks. We are only interested in comparing the topological shape optimization with the inverse solutions from different optimization methods. In OMD methods, the results are limited to the spatial resolution while the smooth boundary topological shape optimization can be used to match the cracks of any size. If a pure shape optimization model is employed to reconstruct the crack, certain assumptions must be made in order to decide the initial shape of the crack. Given the ill-posed nature of the inverse problem, the pure shape optimization model has a high probability of encountering a local minimum. On the other hand, TSO can be used to detect the crack anywhere free of any assumptions. The topology sensitivity analysis changes the objective function value drastically and thus brings a huge performance improvement to this inverse strategy.

Conclusions

In this section, an equation for the topological gradient was derived for a steady state time harmonic problem. The TG formula contained only the field values and therefore it can be evaluated independent of any field solution method. Topological sensitivity analysis can be used to predict any potential topological changes in the problem domain and provide a better starting point for the optimization algorithm.

The topological gradient based method has been shown to be very efficient in the application to eddy current non-destructive testing. It can be used to detect the locations of multiple cracks in the test plate with a relatively low computational cost. Good crack reconstruction results were achieved from various testing problems, including a benchmark test problem from the TEAM workshop.

3.3 Examples of robust topology optimization

In topology optimization of solid structures, a topology is defined by the features of the space, such as the connectivity of the domain and the number and locations of holes in the domain (Bendsoe and Sigmund,

2003). Therefore, we may define a robust topology as that in which the connectivity of the domain does not change or is the least sensitive to small variations to the topology or shape of the domain. Figure 3.30 shows some examples of non-robust topology under the definition above. On the left side of the figure, the domain has two holes, however, if there is a small variation to the boundary of the holes, they will connect with each up and become one hole. On the right, the domain contains only one hole, but under some variations, the two parts of the large hole will be disconnected thus changing the connectivity of the domain.

Figure 3.30: Final shape for two flaws

Reconstruction of two cracks close together

The robust topology optimization method for ECT problems is tested against a crack reconstruction problem with two cracks close together using the same ECT imaging system setting as mentioned in figure 3.22.

The test specimen contains two cracks close together as shown in figure 3.31. The size of both cracks is 4 mm by 4 mm, and the distance between the cracks is 6 mm.

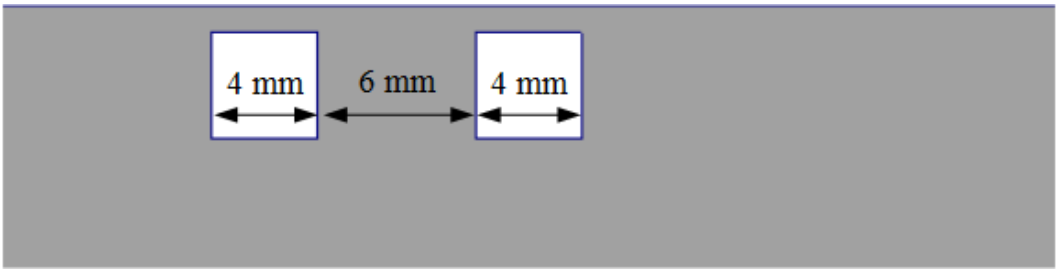

Figure 3.31: Two cracks at a close distance

In the ECT, when two cracks exist in a close distance and are scanned simultaneously within the detection range of the coils, the response voltage signals from the different cracks can interact with each other. In fact, the signals generated by the second crack can be considered as a noise source in the signals from the first crack. This presents a challenge for the crack reconstruction.

The robust topological gradient given in (2.22) is computed in order to estimate the location of the potential crack in the problem domain and to provide an initial crack for the robust shape optimization which in turn optimizes the shape of the crack. The value of the robust TG is determined by the lowest values of the TG in the neighboring cells in the

discretized domain for TG calculation as shown in figure 3.26. Figure 3.32 shows the contour plot of both non-robust and robust topological gradient values.

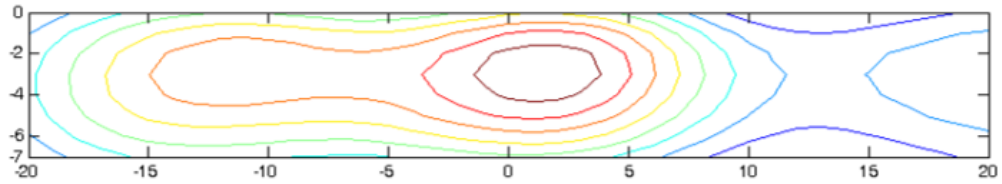

a) Non-robust TG contour plot

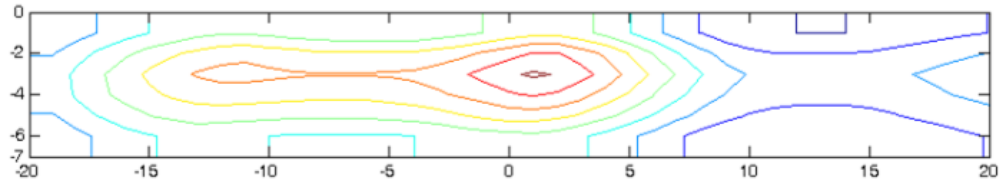

b) Robust TG contour plot

Figure 3.32: Topological gradient contour plots.

As can be seen in figure 3.32 b), there are two peaks in the values of the robust TG which correspond to the location of the two cracks in the test plate. While in figure 3.32 a), the non-robust TG plot only showed one significant peak, which implies only one crack may exist in the test plate. If the shape optimization is applied, different reconstruction results will be achieved for the two different initial topologies indicated by the TG plots in figure 3.32 a) and b); and the results are displayed in figure 3.33, with the target crack shape displayed by solid lines and the reconstructed crack shapes indicated by dashed lines.

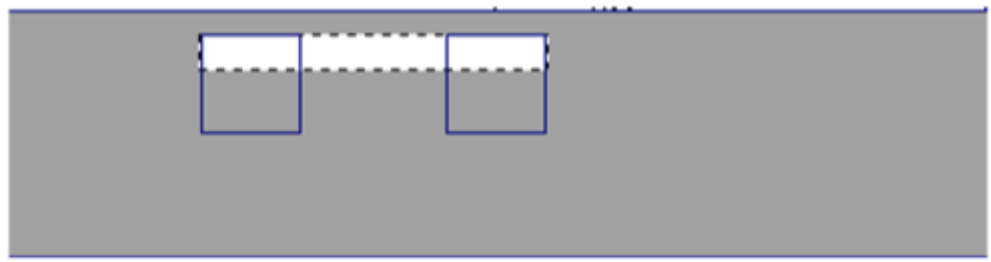

a) Crack reconstruction by a non-robust formulation

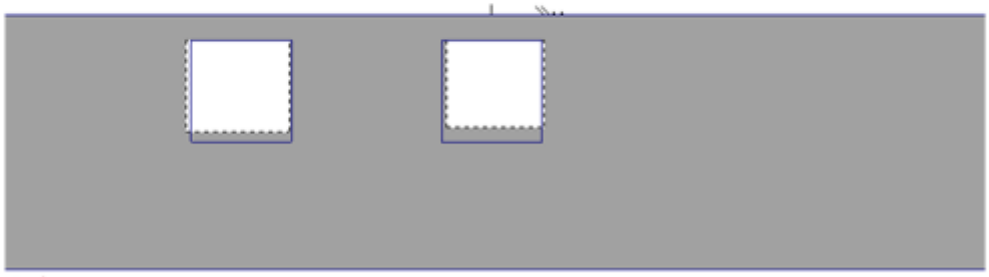

b) Crack reconstruction by a robust formulation

Figure 3.33: Reconstruction of two cracks.

The reconstruction result from figure 3.33 a) shows that the non-robust formulation is unable to differentiate the two cracks. The reconstructed shape of the shallow and wide crack produces the closest matching signals for the target, based on the initial topology generated by the non-robust topological gradient. On the other hand, the robust topology optimization method demonstrates the capability to distinguish the two cracks in the presence of noise, i.e. signal caused by the other crack in the test plate. The topology, a domain with two cracks, as determined by the robust TG, is considered as a more robust topology than that with only one crack in this problem. And the robust estimated initial topology

eventually leads to a successful reconstruction of the shapes of the two cracks.

Conclusions

The robust topology optimization (RTO) was illustrated using an example of the ECT crack reconstruction problem, while the uncertainties are caused by the presence of a second crack in the testing system. In chapter 2, a robust objective function was defined using the worst response due to the variations of the design variables in the topological design. The robustness of the design can be evaluated during the entire design process through the topological shape optimization where the topology and shape of the object are being optimized simultaneously.

Topology optimization is often used as conceptual design tools in the early stage of a design. The example of the ECT inverse problem has shown that if the initial topology is incorrect, the shape optimization applied later to the detailed design may produce wrong results as well. Therefore, it is critical to introduce the robustness evaluation in the early stage of the solution process of the inverse problem, i.e. the topological design. In addition, the calculations of the robust TG for the ECT problem showed

that it is possible to find a robust topology through the topological sensitivity considering variations to the topology. This method also has a large computational advantage since the worst performance caused by the variations of the design parameters can be predicted using the topological gradient without the evaluation of the cost function. Numerical applications of RTO to eddy current crack reconstruction problems showed that this method can provide reliable results in the presence of significant noise.

Chapter 4 SENSITIVITY BASED TORQUE CALCULATION FOR ELECTRICAL MACHINES

4.1 Introduction

The general purpose of electric motors is to provide torques or forces from the conversion of electromagnetic energy into mechanical effects. As a result, in the design and analysis of such machines, the accurate computation of electromagnetic forces and torques at both the global and local level is crucial. It is generally accepted that two major approaches exist for the numerical evaluation of electromagnetic forces and torques.

The first one is based on the Maxwell stress tensor (MST), which is in the form of a surface integral evaluated in the air region surrounding the body of interest. Numerical examples of MST based torque calculations of electric motors can be found in (Mizia et al., 1988) (Howe and Zhu, 1992) (Salon et al., 1997). Despite that the MST torque expression is quite simple and only relies on the field values, the torque calculation requires accurate results of the tangential field in the air gap, thus the resultant

torques are sensitive to the discretization (Salon et al., 1997). Therefore, the integration contour must be carefully chosen in order to avoid the area with large numerical errors in the field solution (McFee and Lowther, 1987), (McFee et al., 1988).

The second category of torque/force calculation methods is based on the principle of virtual work, where the force or torque on a component in a certain direction can be found by computing the changes in the system energy with respect to a virtual displacement of the body in the same direction. The basic virtual work algorithms require the energy in a system in each of two positions. Coulomb first applied the design sensitivity analysis to finite element field analysis and his approach was able to compute the virtual work forces using only one FEM mesh and solution (Coulomb, 1983), (Coulomb and Meunier, 1984). Later a method based on the direct differentiation of the finite element co-energy was developed by Aronson and Brauer to compute the force as a derivative of co-energy. (Aronson and Brauer, 1989). Local forces were computed through a formulation of the virtual nodal displacement with edge elements (Kameari, 1993). Unfortunately, the implementation of the nodal force formulae is quite cumbersome and involves the Jacobian matrix of

coordinate transformation which results in a relatively heavy computational cost. Recently papers by Kim suggested using a continuum design sensitivity analysis (CDSA) approach to determine the virtual work forces through a single field solution (Kim et al., 2005), (Kim et al., 2007). The CDSA approach was demonstrated and validated on a simple electrostatic problem in (Li et al., 2008), where it has the advantage over MST of not requiring a virtual air gap. The accuracy and mesh dependency issues were discussed in (Li and Lowther, 2009).

The CDSA based force formulation, while based on the values of the fields in the problem, is similar to, but differs from, the Maxwell stress result in two ways. First, the sensitivity analysis computes a force which is generated whenever a boundary between two materials having different magnetic properties is moved; and, second, since the approach effectively provides a virtual movement of every point individually, it can provide the local stress distribution. In fact, the approach could be applied inside a body wherever there is a change in permeability such as might happen as saturation occurs. This effect cannot be recognized by the Maxwell stress approach as has been pointed out in (Bossavit and Verite, 1983).

In this chapter, the CDSA based virtual work torque calculation is applied to the problems of rotating machines. In the CDSA based torque calculation, a vector of a local torque component is obtained through the decomposition of the local CDSA force component, normal to the interface between two different materials, in the direction of the rotation. And the total torque of the system is the summation of these local torque vectors. The first example is the comparison of the Maxwell stress and CDSA approaches of torque calculation for a simple rotating actuator made of linear material. The second example involves an interior permanent magnet (IPM) motor. The CDSA based approach is able to determine not only the global torques but also the distributed torques in three different areas: torque distributions on the surface of the rotor, on different parts inside the rotor (such as the permanent magnet and the flux barriers) and the distributions inside the rotor body of saturated nonlinear steel. The capability to predict the distributed torques is particularly important for the design of IPM motors for which we can separate the effects caused by the external excitation or the reluctance change. This can be used for the topological design of electric motors where the optimal material distribution is to be determined for a desired model of motor.

4.2 Torque Calculation Formulae

The MST torque calculation

The tangential component of the Maxwell stress tensor is used to find the torque density on a rotating part of the motor:

$$f_t = \frac{B_n B_t}{\mu_0}. \tag{4.1}$$

where B_n and B_t are the normal and tangential components of the flux density respectively and μ_0 is the permeability of air.

The torque is obtained as a surface integral on a contour l surrounding the body in the air:

$$T = w \cdot (r \times \int_l f_t dl), \tag{4.2}$$

where r is the displacement vector (from the origin of the torque to the point where f_t is computed) and l is the length of integration path and w is the depth of the 2-D model of the electrical machine.

The virtual work torque calculation

Torques can also be computed using the virtual work principle as the derivative of the system co-energy W' with respect to a virtual displacement angle θ (under the assumption of constant flux), as:

$$T = -\frac{\partial W'}{\partial \theta}. \tag{4.3}$$

The conventional virtual work torque calculation employs a finite difference approach, therefore two FEM field solutions corresponding to the two positions of the rotor are needed, and this is quite expensive in terms of computational cost. In addition, the conventional virtual work approach does not support the calculation of local torque, i.e. it cannot provide the value of torque at a desired point.

The CDSA torque calculation

Figure 4.1 shows a two-dimensional magnetostatic problem containing two domains Ω_1 and Ω_2 with different material properties (e.g. air and iron). γ is the interface boundary between Ω_1 and Ω_2.

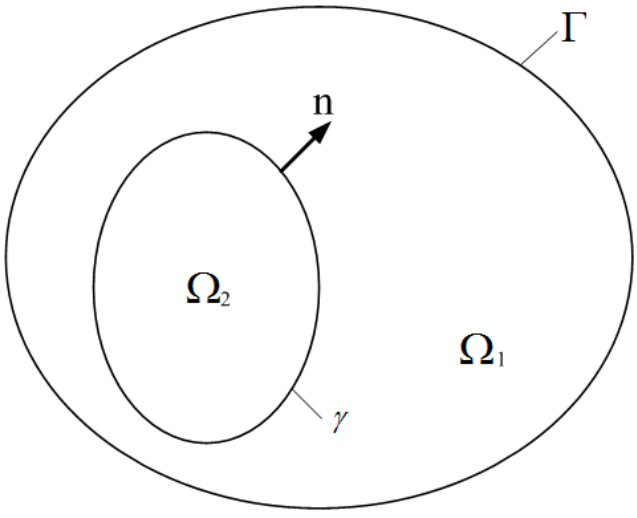

Figure 4.1: A 2-D shape design problem

The CDSA based force calculation method is derived from the shape sensitivity analysis (Park et al., 1993) for electromagnetic design problems, which computes the derivative of an objective function G with respect to the boundary shape change using an adjoint variable as:

$$\frac{dG}{dp} = \int_{\gamma} L(A,\lambda) V_n d\gamma + \int_{\Omega_2} \frac{dg}{dp} d\Omega$$

$$\begin{aligned} \frac{dW}{dp} &= \int_{\gamma} [(v_1 - v_2) B_1 \cdot B_2] V_n d\gamma \\ &+ \int_{\Omega_1} [\nabla v_1 \cdot V(B_1 \cdot B_1)] d\Omega \\ &+ \int_{\Omega_2} [\nabla v_2 \cdot V(B_2 \cdot B_2)] d\Omega \\ &+ \int_{\gamma} [(M_2 - M_1) \cdot B_2] V_n d\gamma \\ &+ \int_{\gamma} [(J_2 - J_1) \cdot A_2] V_n d\gamma \end{aligned} \quad , \tag{4.4}$$

where L(A,λ) is a function of the magnetic vector potential A and an adjoint variable λ determined by g(x), p is the variable describing the boundary change.

Let the system energy, W, be the objective function. In this case, the problem becomes self adjoint (i.e. A = λ), and there is no need to solve the adjoint problem. Therefore, the sensitivity of the energy with respect to boundary perturbation variables p, for a magnetostatic problem, is given in (Kim et al., 2007) as:

$$\frac{dW}{dp} = \int_{\gamma} [(v_1 - v_2)B_1 \cdot B_2]V_n d\gamma + \int_{\Omega_2} [\nabla v_2 (B_2 \cdot B_2)]d\Omega + \int_{\gamma} [M_2 - M_1] \cdot B_2]V_n d\gamma + \int_{\gamma} [J_2 - J_1] \cdot A_2]V_n d\gamma$$

$$\frac{dW}{dp} = \int_{\gamma} [(v_1 - v_2)B_1 \cdot B_2]V_n d\gamma + \int_{\Omega_1} [\nabla v_1 \cdot V(B_1 \cdot B_1)]d\Omega + \int_{\Omega_2} [\nabla v_2 \cdot V(B_2 \cdot B_2)]d\Omega + \int_{\gamma} [(M_2 - M_1) \cdot B_2]V_n d\gamma + \int_{\gamma} [(J_2 - J_1) \cdot A_2]V_n d\gamma \quad , \qquad (4.5)$$

where all values with subscript indices 1 and 2 correspond to the two sub-domains Ω_1 and Ω_2 containing different materials, ν is the material reluctivity, B is the vector of flux density, A is the magnetic vector potential, M is the permanent magnetization, J is the current density.

If the design variable, p, is set as the virtual displacement, the force and torque formulae based on the virtual work principle can be derived using the energy sensitivity in (4.5). For a ferromagnetic material, the magnetic force consists of a surface force distribution due to the reluctivity change across the surface and a volume force due to the gradient of the reluctivity inside the body Ω_2,

$$T = r \times F = \int_{\gamma} r \times [\frac{1}{2}(v_1 - v_2)B_1 . B_2]V_n d\gamma + \int_{\Omega_2} r \times [\frac{1}{2}\nabla v_2 (B_2 . B_2)]d\Omega . \qquad (4.6)$$

In addition, the force and torque acting on a permanent magnet is calculated as:

$$T = r \times F = \int_{\gamma} r \times [(M_2 - M_1).B_2]V_n d\gamma \; F = \int_{\gamma} [(M_2 - M_1) \cdot B_2]V_n d\gamma. \quad (4.7)$$

And the force and torque acting on a conductor containing a current is given as: $F = \int_{\gamma} [(J_2 - J_1) \cdot A_2]V_n d\gamma$

$$T = r \times F = \int_{\gamma} r \times [(J_2 - J_1).A_2]V_n d\gamma \; . \quad (4.8)$$

The CDSA torque formulation can can be applied to a boundary between any two materials having different magnetic properties and it does not require a closed contour in the air region as in the case of the MST method.

The CDSA force calculation with a field solution

The CDSA force can be computed based any field solutions obtained by not only the finite element solver but also other approaches of field analysis. Figure 4.2 shows the B field (flux density) on different sides of an interface boundary, γ, between two domains (Ω_1 and Ω_2) of different materials . In the following description, all the fields and material properties of one side of the boundary are assigned the subscript 1 and those on the other side of the boundary are assigned the subscript 2.

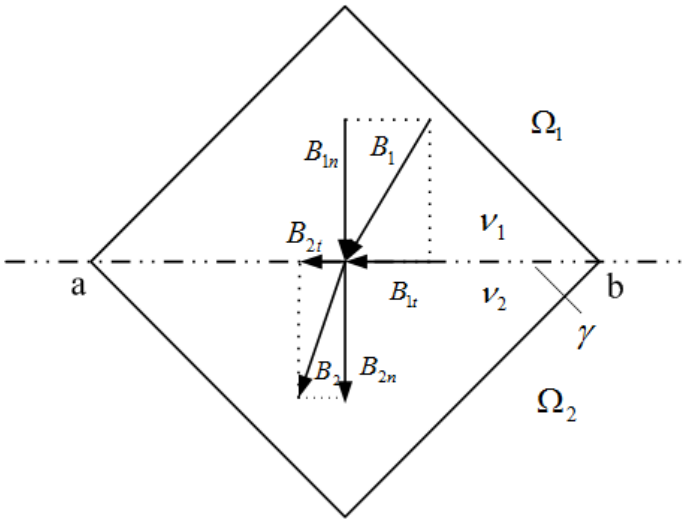

Figure 4.2: Fields on different sides of a boundary

In the CDSA based force calculation, the unit force exerted on a point on the boundary is given by:

$$f_s = \frac{1}{2}(\nu_1 - \nu_2) B_1 \cdot B_2 . \tag{4.9}$$

In the problem shown in figure 4.2, the tangential component of the flux density field presents a discontinuity on each side of the boundary while the normal components of B remains the same across the boundary. Therefore, to evaluate f_s in (4.9), B_1 and B_2 cannot be directly obtained at any point on the boundary, but inside the domains on each side of the boundary.

The total force acting on one element edge, from point a to b, is computed as:

$$\vec{f}_i = \frac{1}{2}\int_a^b (v_1 - v_2)(B_{1n}B_{2n} + B_{1t}B_{2t})dx \,. \tag{4.10}$$

The global force is obtained by summing up all the local forces:

$$\vec{F} = \sum_{i=1}^{N} \vec{f}_i \,, \tag{4.11}$$

where N is the total number of element edges that form the entire boundary of the body.

4.3 Torque Calculation Examples

Two numerical models for torque calculation were studied. Both models were solved using the commercial finite element field analysis software (Infolytica, 2013b). The MST torques were provided by MagNet using a tunable volume integration formulation based on MST (McFee et al., 1988). The CDSA torques were computed using exactly the same field solutions.

Example 1 – Torques on a rotating block

The first model for the CDSA torque verification consists of a simple C-core and a rotating block. The core and the rotating block are both made of a linear material with a relative permeability of 1000.

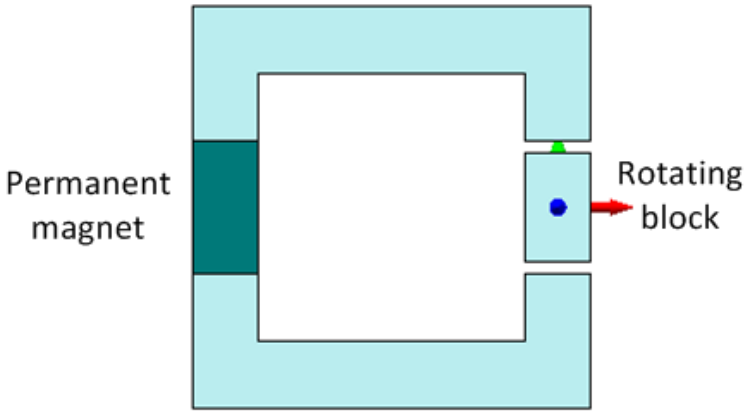

Figure 4.3: C-core with a rotating block

The surface force distributions produced by the CDSA approach are illustrated in figure 4.4 for two different positions of the block. According to the CDSA, large forces are distributed at the corner of the block where high magnetic fields are present.

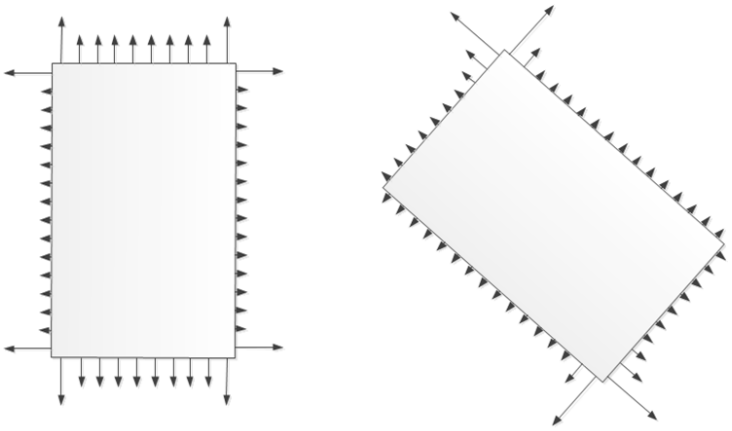

a) Rotation angle = 0 degree b) Rotation angle = 45 degree

Figure 4.4: Force distributions by the CDSA

The total torque of the CDSA is obtained by integrating the distributed torque on the boundary of the rotating block. The CDSA torques are computed at seven positions of the block: 0, 15, 30, 45, 60, 75, 90 degrees and are compared to the results provided by MagNet in figure 4.5. We can observe a good agreement between the two results, and the slight discrepancy may be a result of the numerical errors in the field solutions.

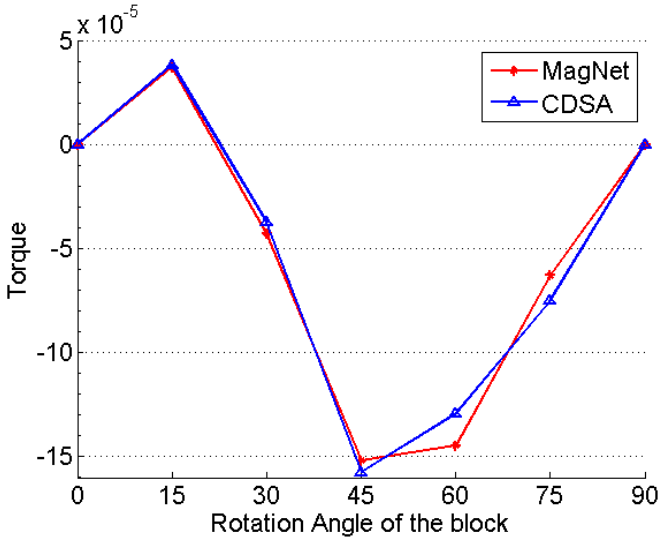

Figure 4.5: Torques vs. rotation angles

Example 2 – Torques of an IPM machine

This example looks at the calculation of torques generated by a 3-phase, 4-pole interior permanent magnet (IPM) machine. The detailed structure of

the IPM machine is shown in figure 4.6. Only a quarter of the motor is modeled in order to reduce the computational cost. The rotor contains three different materials, a NdFeB (neodymium iron boron) magnet bar, two flux barriers of air, and the rest of the rotor is made of M19 steel, which is also used in the stator.

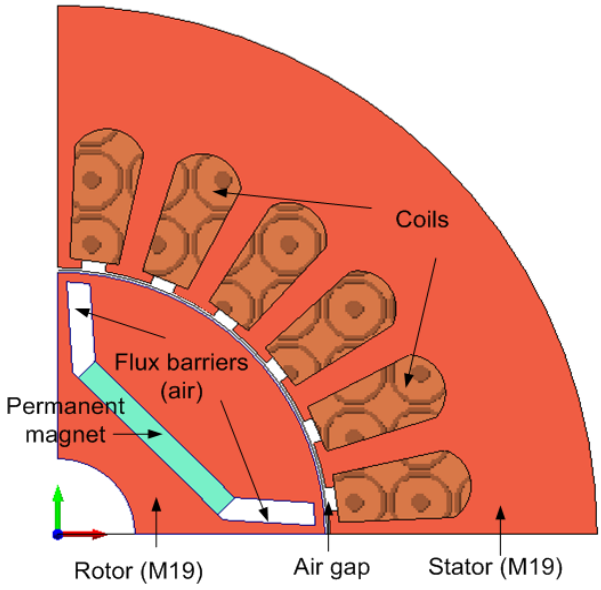

Figure 4.6: A quarter of an IPM machine

Figure 4.7 shows the geometries of the IPM components. The values of all the parameters are given in table 4.1.

Table 4.1: Parameters of the IPM motor

Symbol	Value
R	27.75 mm
r	8 mm

L	20.5 mm
d	2.5 mm
H	12 mm
θ	2 deg

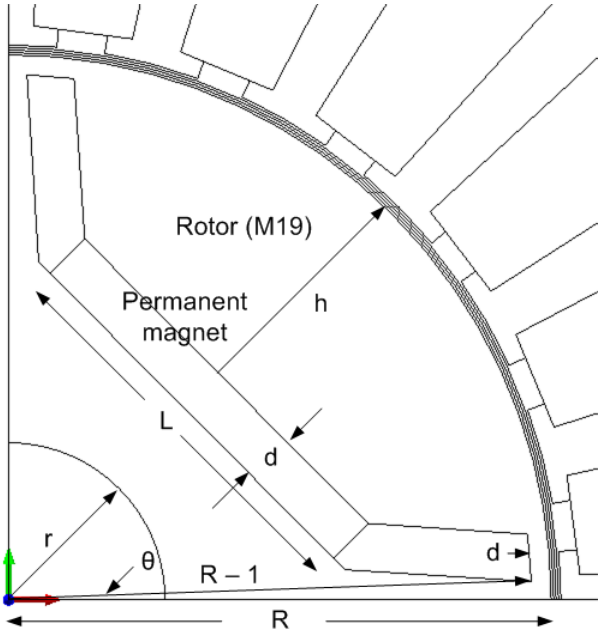

Figure 4.7: Geometries of the IPM motor

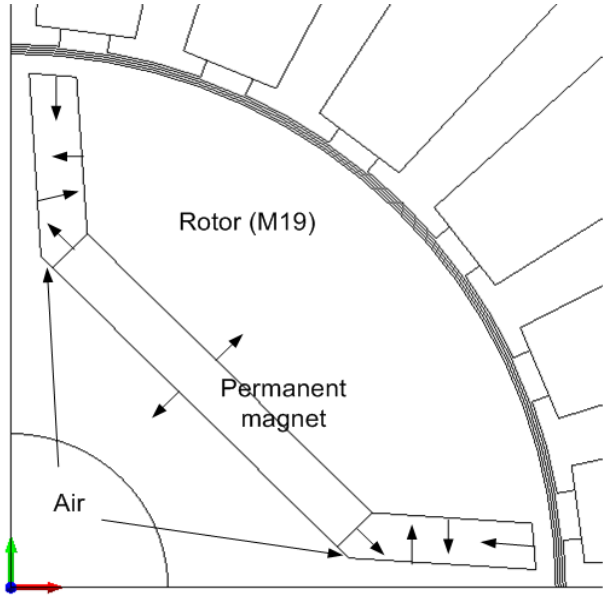

Figure 4.8: Illustration of local force directions

Based on the CDSA force equations (4.7) and (4.8), the local force components appear on and are normal to the boundaries between any two different materials (e.g. iron and air or permanent magnet and iron). The directions of the distributed forces inside the rotor are indicated in figure 4.8. The global torque is obtained as the summation of all local distributed torques on the rotor surface and inside the rotor body.

The IPM motor model is solved for 31 positions of the rotor, starting at zero degrees and increasing at one degree each time. Torques are computed at each position and plotted against the rotor angle.

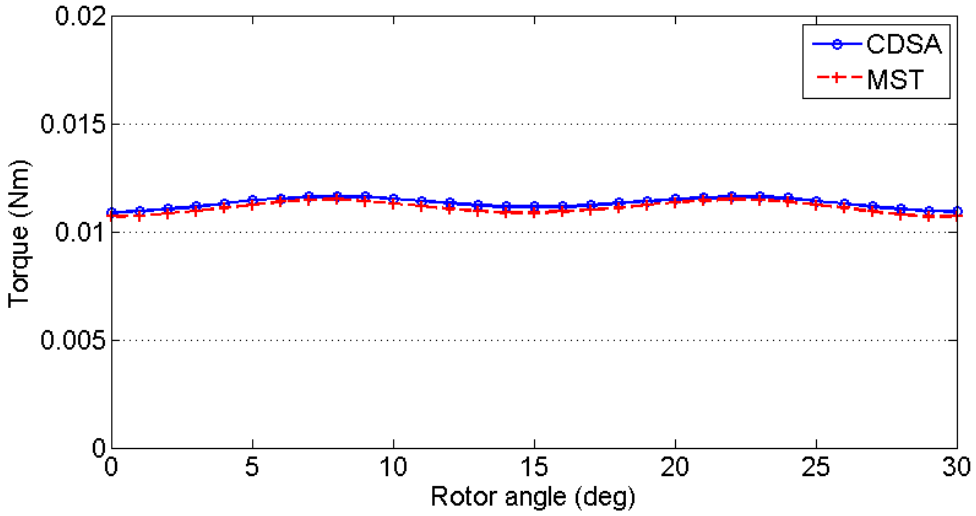

Figure 4.9: Torques against rotor position of a linear core

If a linear material is used instead of the M19 in the rotor, the volume integral in the CDSA disappears, thus only the surface torques distributed between the different components of the rotor account for the global torque. As shown in figure 4.9, the CDSA torque agrees with the MST torque in every position.

If the rotor core is made of nonlinear material, part of the rotor is saturated in the magnetic field as shown in figure 4.10. Forces distributed between the saturated and non-saturated area cannot be ignored.

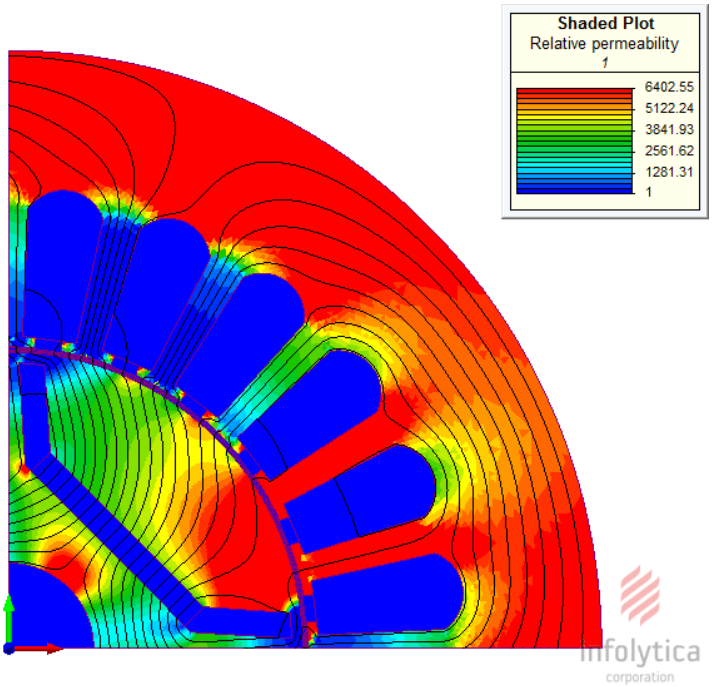

Figure 4.10: Plot of relative permeability distribution

Figure 4.11 shows the comparison of the MST torques and the CDSA torques computed from the surface integral for a non-linear rotor core. Large discrepancies are observed and this results from the reluctance torque due to the saturation in the material.

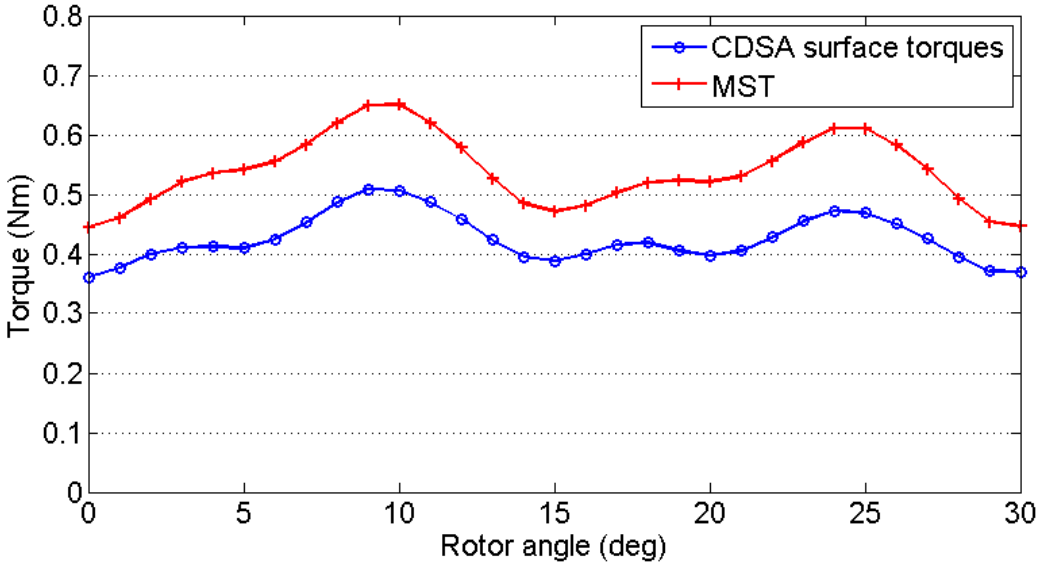

Figure 4.11: Torques against rotor position of a non-linear core

The CDSA volume torques are evaluated using a fine mesh. The model has a total of more than 90,000 elements in the rotor where the maximum element size is set to 0.1 mm. In order to simplify the calculation, we used first order elements inside which the relative permeability is a constant. The distributed torques are computed on the three sides of every element in the mesh. The volume torques are shown in figure 4.12 for 31 positions of the rotor.

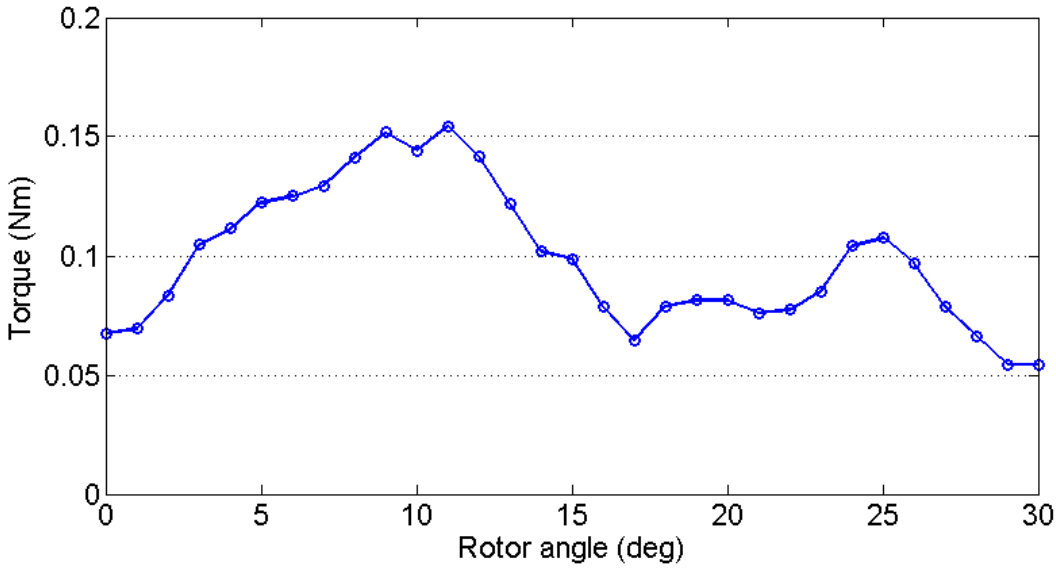

Figure 4.12: Volume torques against rotor position

The combination of the surface torque and the volume torque makes up the CDSA total torque. The CDSA total torques are compared with the MST torques in figure 4.13. As we can see, the volume torque has made up for the discrepancy and the results of the two approaches are very close. The small difference between the two torques for rotor angles after 16 degrees may be result from the discretization error of the finite element model.

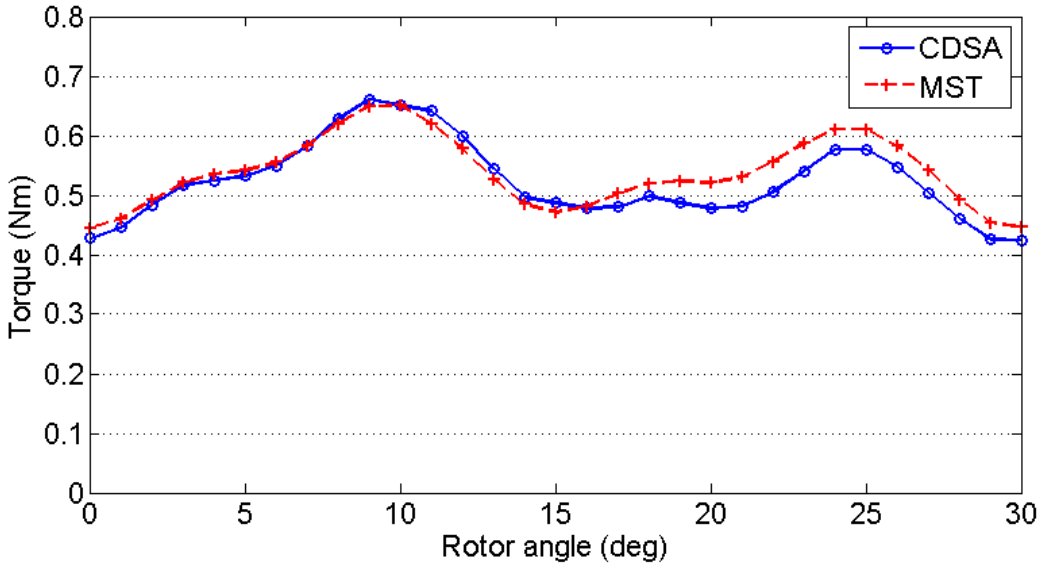

Figure 4.13: MST vs. CDSA total torques

4.4 Conclusion

A CDSA based method is applied to the calculation of torques of electrical machines. The results are verified by MagNet which uses a MST based torque calculation. Unlike the MST, the CDSA force calculation method can be applied directly to the boundary between two different materials. The CDSA method also produces the surface force distributions and internal force distributions inside a body where different materials (or different value of reluctivity within one material) exist. Thus this method has the potential to be applied to coupled structural-magnetic analysis

problems such as are encountered in deformation and vibration computations.

In the case of a non-linear problem, the CDSA needs to evaluate both the surface integral and the volume integral for the total torque while the MST torque calculation is relatively simpler. On the other hand, the CDSA torque formulation defines different components of the torque. The volume integral accounts for the torque caused by the reluctance change inside the rotor due to the saturation. It provides an important piece of information for the design optimization of IPM and other motors.

Finally, the evaluation of the CDSA torque is as efficient as that of the MST. And we may use the subtraction of the CDSA surface integral from the MST torque to compute the torque due to internal permeability changes indirectly and thus avoiding the direct evaluation of the volume integral. However, if this is done, the internal distribution of local torques cannot be determined.

Chapter 5 ROBUST TOPOLOGY OPTIMIZATION OF ELECTRICAL MACHINES

5.1 Introduction

Permanent magnet (PM) synchronous motors have been used in many industries as an alternative to induction motors in recent years. PM synchronous machines have many advantages such as high efficiency, high power density and easy speed control over some other types of electrical machines (Staunton et al., 2004). Thus, they have shown great promise in the application of hybrid electric vehicle (HEV) traction drive systems.

There are two major categories of PM synchronous motors: surface mounted PM (SPM) motors and interior PM (IPM) motors where PMs are embedded inside the rotor cores. There are certain features of the IPM model that make it more attractive than the SPM model. One significant advantage of the IPM is its suitability for high-speed operations. When operated at high speeds, an IPM can produce a reluctance component to

the torque in addition to the magnetic torque (alignment torque between different directions of magnetization of the stator windings and the PM in the rotor), which can improve the constant-power speed range of the machine. The manufacturing processes of IPMs are much simpler and more robust than those of SPMs, because IPMs use less expensive rectangular PM blocks rather than arc magnets glued to the surfaces of the rotors of SPMs. In addition, in an IPM, the permanent magnet blocks are not directly exposed to the magnetic field from the excitation coils. Thus, the magnet flux is shielded by the rotor iron which provides a protection from demagnetization.

The finite element method (FEM) is often applied to the analysis and design of IPM motors to provide accurate performance estimation. FEM analyses were combined with genetic algorithm based optimization (Sim et al., 1997), (Bianchi and Canova, 2002), or analytical approaches (Liu et al., 2002) to look for efficient IPM designs. An investigation on the performance of various IPM rotor structures with flux barriers can be found in (Stumberger et al., 2008). In order to match a specific torque-speed curve for an IPM, a multi-objective optimization scheme is employed for which torques produced at different currents are treated as different

objectives (Ray and Lowther, 2009). In addition to the analyses, various optimization methods have been applied to the design of the IPM in order to improve its performance, e.g. torque ripple reduction. Ohnishi and Takahashi have built a FEM model considering the rotation of the motor, and conducted the design of the motor using an experimental design method (Ohnishi and Takahashi, 2000). The shape of the surface of the iron core in an IPM motor has been optimized to reduce the cogging torque using a continuum design sensitivity analysis (CDSA) approach in (Kim et al., 2003a). While in (Kim et al., 2003a), only the surface of the rotor is allowed to change within a small range, Takahashi et al. proposed a new design scheme using the ON/OFF method in order to find new magnetic circuits of IPM motors (Takahashi et al., 2010). Two designs have been presented in (Takahashi et al., 2010), one is through surface optimization and the other is the design of the field barrier using topology optimization. In (BATISTA et al., 2012), the topological design of the rotor of an IPM was treated as a combinatorial problem and the ant colony optimization (ACO) method is applied to find the best rotor structure for producing the maximum output torque. However, the resultant structures obtained from the conventional topology optimization do not have smooth

boundaries, thus these designs require some post-processing tools or they are not practical for manufacture.

5.2 IPM Design using Topological Sensitivity Analysis

Field analysis model of an IPM

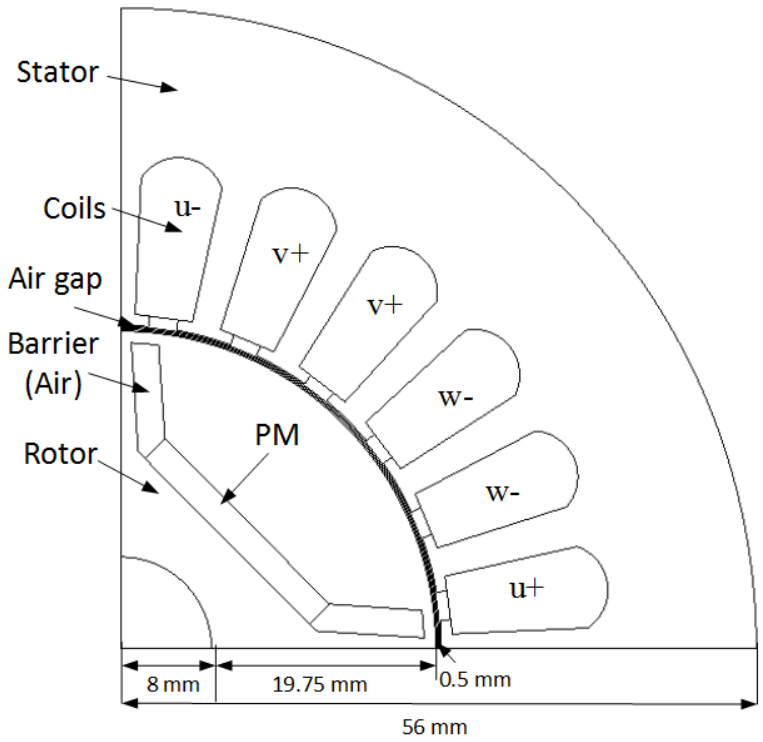

Figure 5.1: A sample model of an IPM motor

Figure 5.1 shows a 3-phase, 4-pole single-barrier interior permanent magnet (IPM) motor. The radius of the motor shaft is 8 mm, the outer radius of the rotor is 27.75 mm and the stator outer radius is 56 mm. The

currents I_u, I_v and I_w in the stator winding are three-phase sinusoidal, and have the form given by:

$$\begin{cases} I_u = I\sin(\omega t + \theta) \\ I_v = I\sin(\omega t + \theta + 2/3\pi) \\ I_w = I\sin(\omega t + \theta + 4/3\pi) \end{cases}, \tag{5.1}$$

where θ is the advance angle of the stator pole.

This model is solved using a 2-D nonlinear FEM solver from MagNet (Infolytica, 2013b). The periodic torque is obtained by solving the motor model for 30 different positions where the rotor angle changes one degree at each step.

Topological design of the rotor

The optimal design of an IPM machine is not a single target problem (Ohnishi and Takahashi, 2000). A feasible design must satisfy several different objectives at the same time, such as high average torque and low torque ripple. If the topological design of an IPM starts from an empty space, made of pure iron or air, the torque ripple can be very small for that design but the essential torque is zero. Therefore we must change the design strategy first to increase the average torque to meet the minimal torque requirement for a practical machine, and then other parameters

can be optimized for reducing the torque ripple. Thus, at the beginning of the design, an objective function of maximizing the torque T (i.e. minimizing -T) is used,

$$F = \min(-\mathrm{T}) . \tag{5.2}$$

The topological gradient of a torque based objective function can be derived as:

$$TG_T = \frac{\partial T}{\partial P} = \frac{\partial W}{\partial \theta \partial P} = \frac{\partial W}{\partial P \partial \theta} = \frac{\partial TG_w}{\partial \theta} , \tag{5.3}$$

where TG_w is the topological gradient of the system co-energy. In this phase of design, the topological design of the motor starts with an empty design space.

The design region is the entire rotor core, discretized into a 45x39 grid. The topological design of the rotor starts with an empty space free of assumptions. The topological design process is divided into two phases, finding the optimal source distribution (OSD) and then finding the optimal material distribution (OMD).

Design phase 1: OSD

At the beginning of this phase, the domain of design is a quarter of the rotor core filled with nothing else but iron, e.g. M19 silicon steel, thus the initial torque is extremely small (ideally this will be zero in the absence of permeability variations). The goal of the OSD design is to use the material of the excitation source, e.g. a NdFeB magnet, to replace part of the iron in the design region in order to increase the output torque, i.e. finding the optimal distribution of the excitation source for the design.

The topological gradient of the system energy can be written as:

$$TG_w = 2(M_2 - M_1)\cdot B + (v_1 - v_2)B^2$$

$$\begin{aligned}\frac{dW}{dp} &= \int_\gamma [(v_1 - v_2)B_1 \cdot B_2]V_n d\gamma \\ &+ \int_{\Omega_1}[\nabla v_1 \cdot V(B_1 \cdot B_1)]d\Omega \\ &+ \int_{\Omega_2}[\nabla v_2 \cdot V(B_2 \cdot B_2)]d\Omega \\ &+ \int_\gamma [(M_2 - M_1)\cdot B_2]V_n d\gamma \\ &+ \int_\gamma [(J_2 - J_1)\cdot A_2]V_n d\gamma\end{aligned} \quad , \tag{5.4}$$

where v_1 and v_2 are the reluctivity of the material before and after the topological change, and M_1 and M_2 are the magnetization of the material before and after the topological change.

In (5.4), the term associated with the magnetization is responsible for the energy or torque change due to the introduction of the permanent magnet as an excitation source, thus the TG for OSD is given as:

$$TG_{OSD} = 2(M_2 - M_1)\cdot\frac{\partial B}{\partial \theta} \qquad \begin{aligned} \frac{dW}{dp} &= \int_{\gamma} [(v_1 - v_2)B_1 \cdot B_2]V_n d\gamma \\ &+ \int_{\Omega_1}[\nabla v_1 \cdot V(B_1 \cdot B_1)]d\Omega \\ &+ \int_{\Omega_2}[\nabla v_2 \cdot V(B_2 \cdot B_2)]d\Omega \\ &+ \int_{\gamma} [(M_2 - M_1)\cdot B_2]V_n d\gamma \\ &+ \int_{\gamma} [(J_2 - J_1)\cdot A_2]V_n d\gamma \end{aligned} \quad , \qquad (5.5)$$

$\partial B/\partial\theta$ is evaluated using a finite-difference approach using a second field solution of the problem where the rotor angle changes by a small amount.

The robust TG is computed on a 45x39 mesh in the design region with the fields due to the stator excitation, and is plotted in figure 5.2. The unit of the TG depends on the objective function defined for the optimization, thus it has no physical meaning.

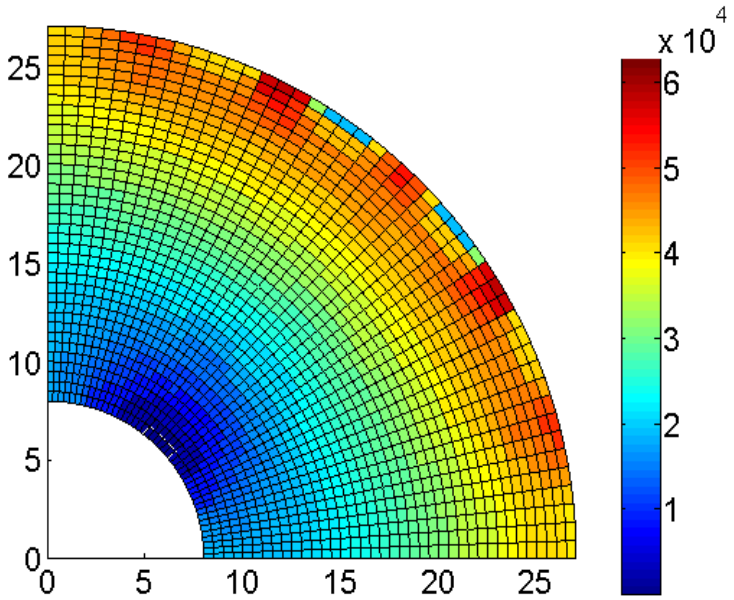

Figure 5.2: TG plot for OSD

The region with the highest values of TG is shown in a light color, which suggests a material swap in the area on the surface of the rotor. This corresponds to the structure of a surface mount permanent magnet (SPM) motor. However, as mentioned earlier, one of the advantages of IPM motors over SPM motors is the capability of creating reluctance variation of the rotor while keeping the air gap length constant. A significant amount of the output torque comes from the reluctance change inside the rotor body due to the magnetic field of the permanent magnet. Also, the PM bars need to be shifted away from the stator excitation field in order to prevent eddy current losses and demagnetization. Therefore, the

minimum distance between the PM bars and the surface of the rotor is imposed as a constraint on the system which ignores the TG values in the surface layer of the rotor. As a result, a topology change to the design domain is performed by changing the material from iron to PM below the surface layer in the regions indicated by the TG. Next, the size and the location of the PM block are optimized using a shape optimizer. The final layout of the rotor with a PM after OSD design is shown in figure 5.3.

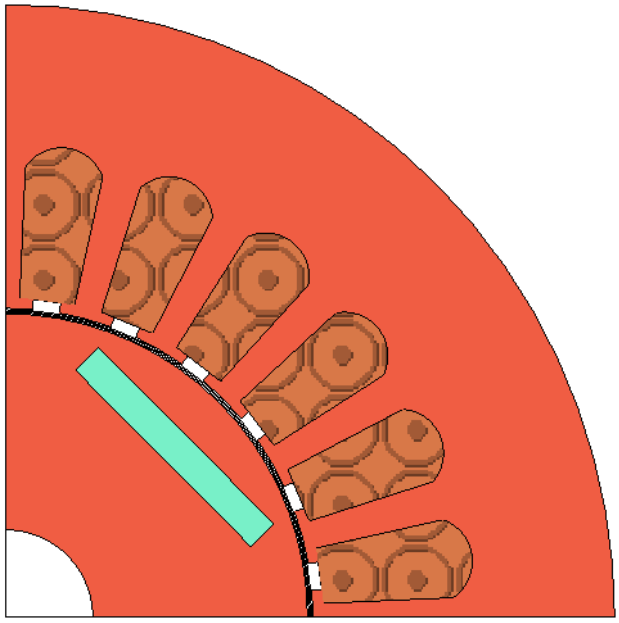

Figure 5.3: Optimized size and location of the PM by OSD

The output torques of the optimal IPM layout by OSD are plotted against the rotor angle in figure 5.4. This is a huge improvement of the motor performance over the initial structure.

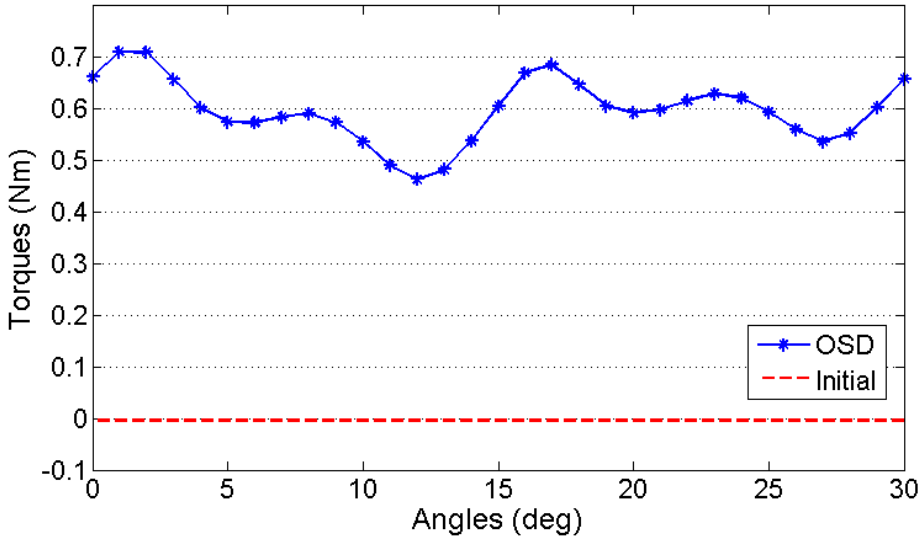

Figure 5.4: Optimized torques vs. rotor angle (phase 1)

Design phase 2: OMD

At the OMD design stage, a third material, air, is introduced. The topological gradient for the OMD is expressed based on the second term in (5.4), as:

$$TG_{OMD} = 2(v_1 - v_2)B \cdot \frac{\partial B}{\partial \theta} \qquad \begin{aligned} \frac{dW}{dp} &= \int_\gamma [(v_1 - v_2)B_1 \cdot B_2]V_n d\gamma \\ &+ \int_{\Omega_1} [\nabla v_1 \cdot V(B_1 \cdot B_1)]d\Omega \\ &+ \int_{\Omega_2} [\nabla v_2 \cdot V(B_2 \cdot B_2)]d\Omega \\ &+ \int_\gamma [(M_2 - M_1) \cdot B_2]V_n d\gamma \\ &+ \int_\gamma [(J_2 - J_1) \cdot A_2]V_n d\gamma \end{aligned} \quad . \qquad (5.6)$$

The TG for the OMD is calculated over the design domain to determine whether there is any potential topological change which may improve the performance, as shown in figure 5.5.

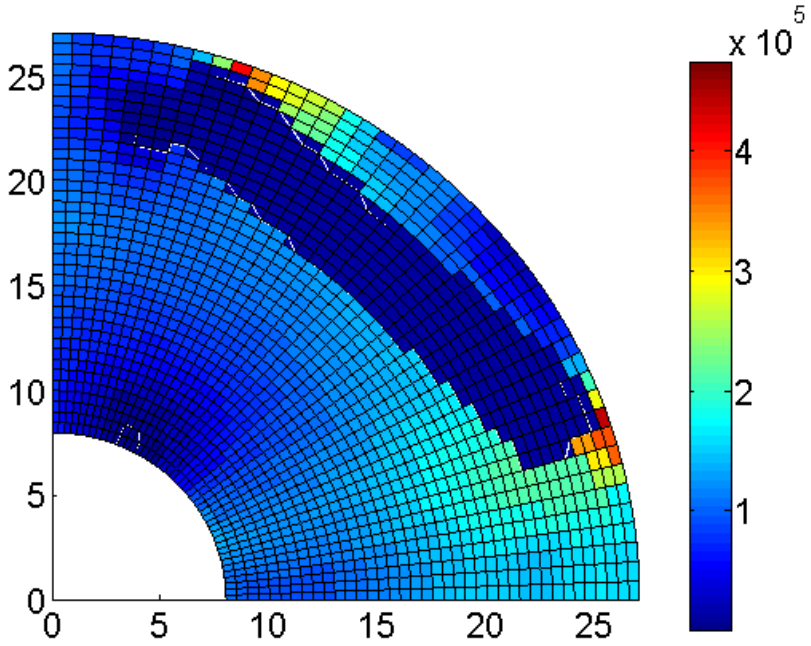

Figure 5.5: TG plot for OMD

In this stage of the rotor design, two physical constraints based on a human expert's knowledge about the manufacturing must be taken into account. First, the rotor structure is usually symmetric. Second, the surface of the rotor is round and the air-gap length between the rotor and stator must be constant in order to reduce the vibration. As a result, when we decide to create an air region (flux barrier) in the rotor based on the TG values, the area with the highest values is ignored since it touches the surface of the rotor. Instead, we choose the area that has lower positive values of the TG around the corner of the PM bar and create another air region on the other side of the PM bar due to the symmetry. Therefore, a

new topology of the rotor core is produced according to the TG values from figure 5.5. Figure 5.6 shows the rotor layout generated by OMD which also corresponds to a common design of IPM motors with flux barriers.

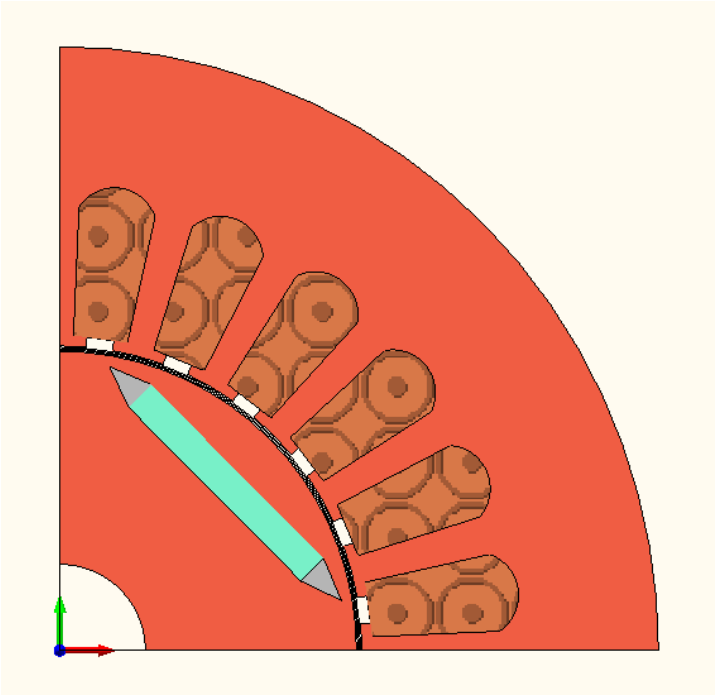

Figure 5.6: Rotor layout produced by OMD

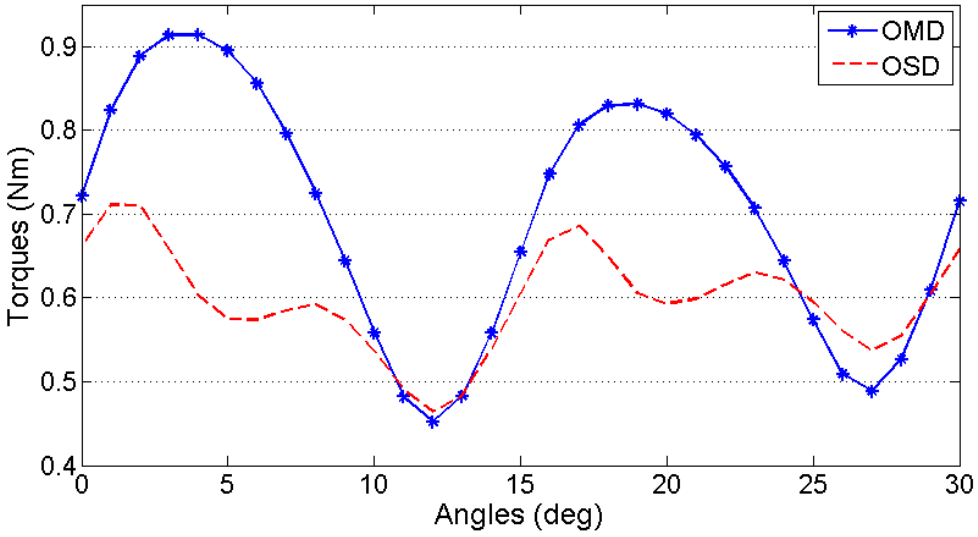

Figure 5.7: Torques vs. rotor angles (phase 2)

Figure 5.7 shows the torques obtained from the model determined by OSD, and yet another performance improvement can be observed, although with a fairly large torque ripple. After design phase 2, the average output torque obtained is 0.70 Nm. Now we have obtained a feasible design that can be carried on to the next design phase with a different objective.

Design phase 3: Reduction of the torque ripple

The goal of design in this phase is to optimize the shape and size of the magnet and flux barrier in order to reduce the torque ripple, while maintaining an adequate average torque. The objective function is defined

using the output torques T_i at every rotor angle from 0 to 30 degrees and the average torque T_{avg} as:

$$F = \sum_{i=0}^{30} \left(\frac{T_i - T_{avg}}{T_{avg}}\right) \quad s.t.\ T_{avg} \geq 0.5Nm \tag{5.7}$$

The second objective, the average output torque, is now treated as a constraint in this optimization. The rotor layout, as shown in figure 5.6, has gone through a standard shape optimizer, and the final design of the IPM is shown in figure 5.8.

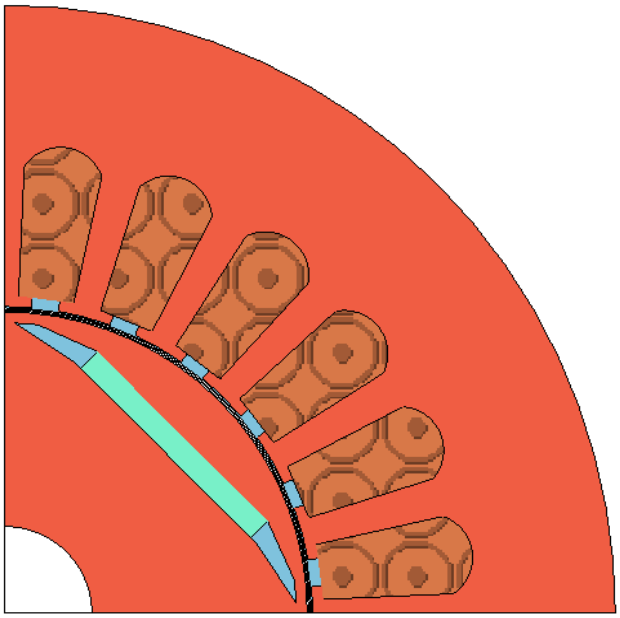

Figure 5.8: Final design of the IPM

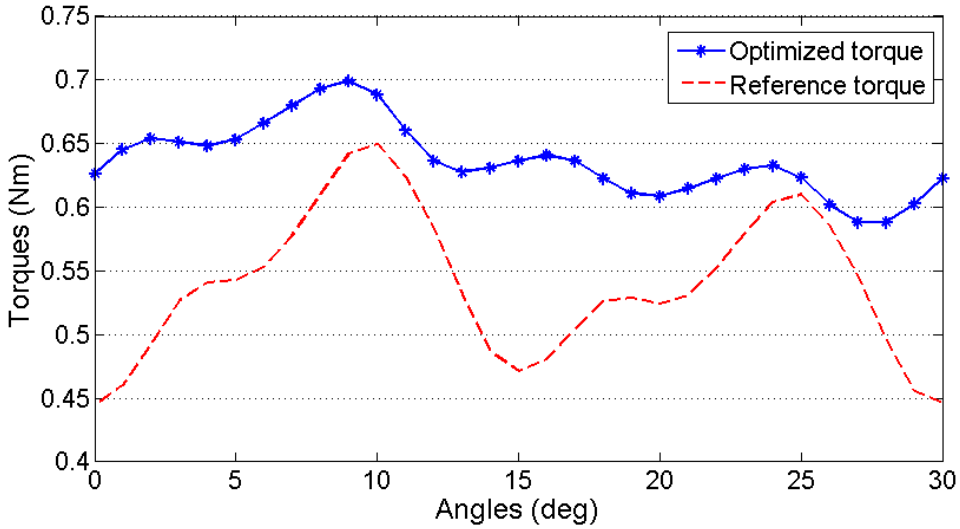

Figure 5.9: Final torques vs. rotor angle

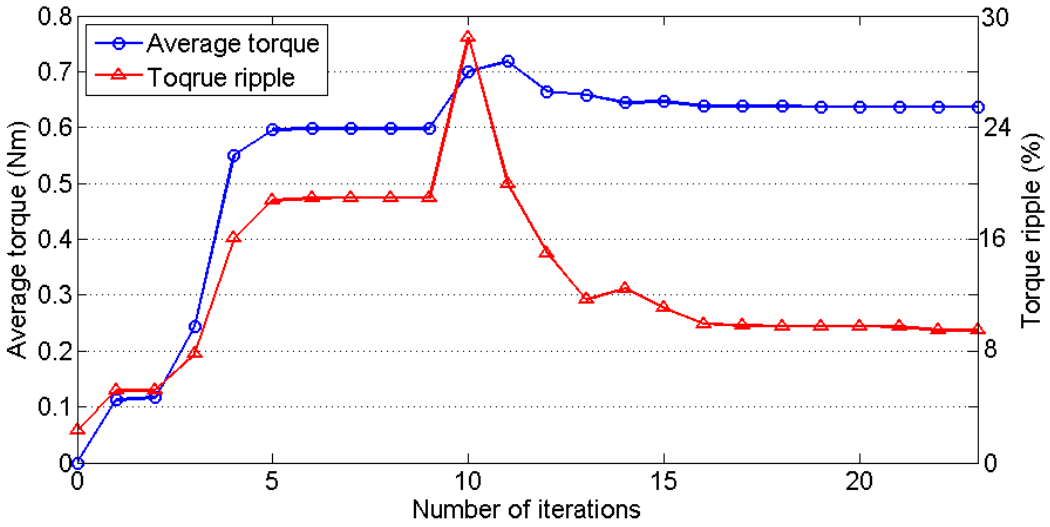

Figure 5.10: Variation of objective functions values with optimization iterations

The target torque curve of the final design is compared to the initial IPM motor model used in (Infolytica, 2013a), which has the same rotor and stator size, and the same excitation current, in figure 5.9. The final optimal design has an average torque of 0.63 Nm and a torque ripple of 9.78%

which has been improved by 50% compared to the reference model. The changes of the objective function values during the entire design process are shown in figure 5.10.

5.3 Robust Design of an IPM

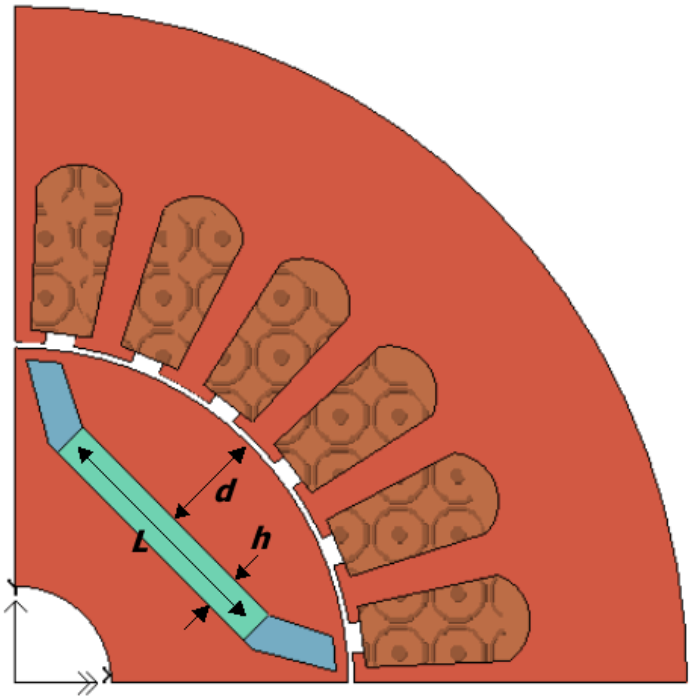

Figure 5.11: Design variables of an IPM motor

Design variables

Figure 5.11 shows a quarter of a 3-phase 4-pole IPM machine and the design variables chosen for the robust design optimization: the length of the permanent magnet, L, the width of the PM, h, and the distance from the PM to the surface of the rotor, d. A robust objective function can be defined, considering the manufacturing uncertainties, as,

$$\begin{aligned} &\min \ \max_{U(x)} \sum_i \left(\frac{T_i - T_{avg}}{T_{avg}}\right) \\ &s.t \quad \min_{U(x)} (T_{\min}) > 0.4Nm \,. \\ &x = [L, h, d]^T \end{aligned} \tag{5.8}$$

Results of robust design

In section 5.2, we employed the robust topological gradient to find a rotor structure with one PM bar and two flux barriers. This can be used as the starting point of the shape optimization process with the robust objective function. The system optimizes the shape of the boundaries between different materials in order to achieve more accurate values of the geometries.

Table 5.1: Values of design variables of the nominal and robust optima

Design variables	Unit	Initial Values	Nominal Optimal	Robust Optimal
H	mm	2.5	1.588	1.616

L	mm	22.5	18.33	19.879
D	mm	12	13.426	12.243
Nominal performance	%		0.2358	0.2583
Worst performance	%		0.2709	0.2791
Feasibility robustness			No	Yes

Table 5.1 shows the values of the design variables, the nominal performance, the worst performance and the feasibility robustness of the non-robust optimal and the robust optimal. The uncertainty is set to as 5% of the design variables. Although the nominal solution has a better performance, but the variations to the design variables violate the constraint. On the other hand the robust optimal satisfies the constraint on the entire uncertainty set. Also the difference between the worst performance and the nominal performance of the robust solution is smaller than that of the non-robust solution, which implies that the performance of the robust design is less sensitive than the nominal design.

5.4 Conclusion

A topological shape optimization scheme has been successfully applied to the design of an IPM motor and a novel design layout is obtained. Robust objective functions were used and the robust TG was computed to handle the topological uncertainties. The performances of both targets, the average running torque and the torque ripple, were improved compared to a reference model. The values of TG provided suggestions for design decision making in accordance with the knowledge from design experts. The final IPM layout obtained through the optimal design process has a much more practical structure than that developed from a conventional topology optimization based the ON/OFF method. The proposed method is very efficient since the objective function converges much faster than a stochastic optimization approach.

The robust topology optimization method employs a deterministic search based on the topological gradient and the shape sensitivity, and the method is very efficient and fast to converge. However, as mentioned earlier in chapter 2, the robust objective function defined in (2.20) is not necessarily partially differentiable and this may pose some difficulties to

the optimization. Also, the convexity of the objective function is not guaranteed, thus the worst performance point may be found inside the uncertainty set instead of on the corner. The worst performance prediction is only an approximation.

Chapter 6 DISCUSSION AND CONCLUSION

6.1 Re-Statement of the Objective

The research objective of this thesis was to create an automated topological design system for low frequency electromagnetic device design. The first step towards this goal has been achieved by successfully implementing the code using MATLAB and MagNet software. Several design or inverse engineering problems were tested by the automated design system and very satisfactory results were obtained.

The implemented system has the following features:

1. It does not require any knowledge of the shape or topology of the target device; but works on the first principles of physical laws. On the other hand, if design knowledge is available, it can be applied to reduce the size of the search space and thus used to accelerate the search process.

2. The system does not require a prototype, and it can start with an empty space free of assumptions (on topology or shape). Also different materials

can be introduced to the design in the form of topology changes. This feature breaks the limitation of the conventional shape design optimization which only improves the performance of the design through altering the design variables defined on the boundary of the design domain. In the context of systematic engineering design (Pahl et al., 2007), the automated system forms a cycle between the stages of conceptual and embodiment design until an optimal design can be achieved.

3. The system also takes advantage of the design sensitivity information; thus it is quite efficient compared to the algorithms based on the stochastic search such as genetic algorithms or evolutionary algorithms.

6.2 Most Significant Contributions of the Thesis

Besides several publications based on the work described in this thesis, the contributions of this thesis are stated as follows:

1. The method based on the topological gradient is applied to the design of low frequency electromagnetic devices. The concepts of topological gradient and topological shape optimization were adopted from the study of mechanical engineering while the derivation of the sensitivity formulae

was adapted for the governing equations of Maxwell in electrical engineering. The algorithm for the topological shape optimization was also improved by the author in order to better serve the purpose of electrical machine design.

2. The idea of combining the robust design formulation and the topological optimization is original from this thesis. A definition of the robustness of a topology was introduced by the author to the research. This allows the examination of a topology for robustness before applying any shape changes to the domain. Then the robustness evaluation can be extended to the shape design variables of the topological shape optimization. The robust target function does not change through the entire design process.

3. The topological shape optimization is applied to the inverse problem of crack reconstruction in non-destructive testing, including MFL and ECT problems. The method can quickly identify and locate the crack in the test specimen through the values of the topological gradient computed using field solutions generated from any numerical or analytic method. The exact shape of the crack can be obtained through a parameterization of the boundary of the initial crack and a shape optimizer. In addition, the

method is capable of dealing with uncertainties caused by noise in the test signals using a robust target function, and the results are proven to be more robust than those from conventional methods.

4. A design sensitivity based torque calculation was demonstrated in this thesis. The torque equations are derived based on virtual work principles and are able to predict the local torque densities as well as the global torque. The method has been applied to the torque calculation of an interior permanent magnet motor where two torque components are revealed, the torque due to the excitation source (windings and/or permanent magnets) and the torque due to the reluctance change inside the rotor core. This is crucial to the design of electric motors where the two torque components can be treated as different objectives and the trade-off between the torques can be analyzed.

6.3 Future Work

Multi-objective formulation of robust design

This thesis used a robust objective function based on the worst case scenario which is sometimes considered as "too conservative". An

extension of such kind of robust design formulation is the multi-objective robust design formulation (Gimaraes 2006) which minimizes the worst case of the original objective and the performance variation (the difference between the worst case and the nominal value of the original objective function) simultaneously. The single objective robust target function used in this thesis is just one special case of the multi-objective robust design formulation. The result obtained from the method in the thesis is only one point on the *pareto* front and the entire *pareto* front may be obtained by altering the weighting factors for the two objectives.

Robust design for multi-objective problems

Some design problems have two or more objectives and they may be conflicting objectives. For instance, in the case of an IPM design, three objectives, the maximization of the output torque, the minimization of the torque ripple and the minimization of the cost (by restricting the use of rare earth permanent magnet material) must be taken into account at the same time. In addition, a robust design may focus on the robustness of each objective or a global robustness of the design defined on all the design variables. This is an interesting research area that needs further investigation.

Combination with stochastic search algorithms

Stochastic search algorithms have many advantages such as global exploration and avoiding local minima. Although a stochastic search algorithm does not necessarily need the gradient information, the topological and shape sensitivity can help enhance the performance of those algorithms. For instance, a topological gradient can quickly examine the meta design space in the global exploration stage and a shape gradient can provide an efficient solution in the local exploitation stage by converging to the local minimum very quickly. Therefore, a hybrid method combining the advantages of the stochastic method and the sensitivity analysis can be proposed in the future.

LIST OF REFERENCES

AL-NAEMI, F. I., HALL, J. P. & MOSES, A. J. 2006. FEM modelling techniques of magnetic flux leakage-type NDT for ferromagnetic plate inspections. *Journal of Magnetism and Magnetic Materials,* 304.

AL-WIDYAN, K. & ANGELES, J. 2005. A model-based formulation of robust design. *Journal of Mechanical Design, Transactions of the ASME,* 127**,** 388-396.

ALOTTO, P., MAGELE, C., RENHART, W., WEBER, A. & STEINER, G. 2003. Robust target functions in electromagnetic design. *COMPEL: The International Journal for Computation and Mathematics in Electrical and Electronic Engineering,* 22**,** 549 - 560.

ARONSON, E. A. & BRAUER, J. R. 1989. Magnetic torque or force calculation by direct differentiation of finite element coenergy. *Magnetics, IEEE Transactions on,* 25**,** 3578-3580.

BADICS, Z., KOMATSU, H., MATSUMOTO, Y. & AOKI, K. 1998. Inversion scheme based on optimization for 3-D eddy current flaw reconstruction problems. *Journal of Nondestructive Evaluation,* 17**,** 67-78.

BATISTA, L., LI, M., CAMPELO, F., GUIMARÃES, F., LOWTHER, D. & RAMÍREZ, J. ANT COLONY OPTIMIZATION FOR THE TOPOLOGICAL DESIGN OF IPM MACHINES. 12th International Workshop on Optimization and Inverse Problems in Electromagnetism (OIPE), 2012 Ghent.

BELEGUNDU, A. D. & ZHANG, S. 1992. Robustness of Design Through Minimum Sensitivity. *Journal of mechanical design,* 114**,** 213-217.

BENDSOE, M. P. 1989. Optimal shape design as a material distribution problem. *Structural Optimization,* 1**,** 193-202.

BENDSOE, M. P. & KIKUCHI, N. 1988. Generating optimal topologies in structural design using a homogenization method. *Computer Methods in Applied Mechanics and Engineering,* 71**,** 197-224.

BENDSOE, M. P. & SIGMUND, O. 2003. *Optimization of Structural Topology, Shape, and Material,* Germany, Springer.

BIANCHI, N. & CANOVA, A. FEM analysis and optimisation design of an IPM synchronous motor. Power Electronics, Machines and Drives, 2002. International Conference on (Conf. Publ. No. 487), 4-7 June 2002 2002. 49-54.

BIDDLECOMBE, C. S., SYKULSKI, J. K. & TAYLOR, S. C. 1994. Design environment modules for non-specialist users of EM software. *Magnetics, IEEE Transactions on,* 30**,** 3625-3628.

BOSSAVIT, A. & VERITE, J. 1983. The "TRIFOU" Code: Solving the 3-D eddy-currents problem by using H as state variable. *Magnetics, IEEE Transactions on,* 19**,** 2465-2470.

BYUN, J.-K., HAHN, S.-Y. & PARK, I.-H. 1999. Topology optimization of electrical devices using mutual energy and sensitivity. *Magnetics, IEEE Transactions on,* 35**,** 3718-3720.

BYUN, J.-K., LEE, J.-H., PARK, I.-H., LEE, H.-B., CHOI, K. & HAHN, S.-Y. 2000. Inverse problem application of topology optimization method with mutual energy concept and design sensitivity. *Magnetics, IEEE Transactions on,* 36**,** 1144-1147.

BYUN, J.-K., PARK, I.-H. & HAHN, S.-Y. 2002. Topology optimization of electrostatic actuator using design sensitivity. *Magnetics, IEEE Transactions on,* 38**,** 1053-1056.

CAMPELO, F., OTA, S., WATANABE, K. & IGARASHI, H. 2008. Generating Parametric Design Models Using Information From Topology Optimization. *Magnetics, IEEE Transactions on,* 44**,** 986-989.

CEA, J., GARREAU, S., GUILLAUME, P. & MASMOUDI, M. 2000. The shape and topological optimizations connection. *Computer Methods in Applied Mechanics and Engineering,* 188**,** 713-726.

CHOI, S. H. E., LOWTHER, D. A. & DYCK, D. N. 1998. Determining boundary shapes from the optimized material distribution system. *Magnetics, IEEE Transactions on,* 34**,** 2833-2836.

CIOFFI, M., FORMISANO, A. & MARTONE, R. 2004. Stochastic handling of tolerances in robust magnets design. *Magnetics, IEEE Transactions on,* 40**,** 1252-1255.

COMPUMAG. 2013. *Rectangular Slot in a Thick Plate: A Problem in Non-Destructive Evaluation* [Online]. Available: http://www.compumag.org/jsite/images/stories/TEAM/problem15.pdf.

COULOMB, J. 1983. A methodology for the determination of global electromechanical quantities from a finite element analysis and its application to the evaluation of magnetic forces, torques and stiffness. *Magnetics, IEEE Transactions on,* 19**,** 2514-2519.

COULOMB, J. L. & MEUNIER, G. 1984. Finite element implementation of virtual work principle for magnetic or electric force and torque computation. *Magnetics, IEEE Transactions on,* 20**,** 1894-1896.

DISERENS, N. J. & SULLIVAN, S. P. 1994. Simulation of a remote field eddy current detector in eccentric thin-walled non ferrous tubes using a 3D finite-element program. *Magnetics, IEEE Transactions on,* 30**,** 3737-3740.

DONG-HUN, K., SYKULSKI, J. K. & LOWTHER, D. A. 2005. A novel scheme for material updating in source distribution optimization of magnetic devices using sensitivity analysis. *Magnetics, IEEE Transactions on,* 41**,** 1752-1755.

DYCK, D. N. & LOWTHER, D. A. 1996. Automated design of magnetic devices by optimizing material distribution. *Magnetics, IEEE Transactions on,* 32**,** 1188-1193.

DYCK, D. N., LOWTHER, D. A. & FREEMAN, E. M. 1994. A method of computing the sensitivity of electromagnetic quantities to changes in materials and sources. *Magnetics, IEEE Transactions on,* 30**,** 3415-3418.

ESCHENAUER, H. A., KOBELEV, V. V. & SCHUMACHER, A. 1994. Bubble method for topology and shape optimization of structures. *Structural and Multidisciplinary Optimization,* 8**,** 42-51.

ESCHENAUER, H. A. & OLHOFF, N. 2001. Topology optimization of continuum structures: A review. *Applied Mechanics Reviews,* 54**,** 331-389.

FRENCH, M. J. 1999. *Conceptual design for engineers*, Springer.

GUILLAUME, P. & MASMOUDI, M. 1994. Computation of high order derivatives in optimal shape design. *Numerische Mathematik,* 67**,** 231-250.

GUIMARAES, F. G., LOWTHER, D. A. & RAMIREZ, J. A. 2006. Multiobjective approaches for robust electromagnetic design. *Magnetics, IEEE Transactions on,* 42**,** 1207-1210.

HAN, J. S. & KWAK, B. M. 2004. Robust optimization using a gradient index: MEMS applications. *Structural and Multidisciplinary Optimization,* 27**,** 469-478.

HOOLE, S. R. H. & SUBRAMANIAM, S. 1992. Higher finite element derivatives for the quick synthesis of electromagnetic devices. *Magnetics, IEEE Transactions on,* 28**,** 1565-1568.

HOOLE, S. R. H., SUBRAMANIAM, S., SALDANHA, R., COULOMB, J. L. & SABONNADIERE, J. C. 1991. Inverse problem methodology and finite elements in the identification of cracks, sources, materials, and their geometry in inaccessible locations. *Magnetics, IEEE Transactions on,* 27**,** 3433-3443.

HOWE, D. & ZHU, Z. Q. 1992. The influence of finite element discretisation on the prediction of cogging torque in permanent magnet excited motors. *Magnetics, IEEE Transactions on,* 28**,** 1080-1083.

INFOLYTICA. 2013a. *IPM design example* [Online]. Available: http://www.infolytica.com.

INFOLYTICA. 2013b. *MagNet user's manual* [Online]. Available: http://www.infolytica.com.

KAMEARI, A. 1993. Local force calculation in 3D FEM with edge elements. *International journal of applied electromagnetics in materials,* 3**,** 231-240.

KIM, D.-H., LEE, S. B., KWANK, B. M., KIM, H.-G. & LOWTHER, D. A. 2008. Smooth Boundary Topology Optimization for Electrostatic Problems Through the Combination of Shape and Topological Design Sensitivities. *Magnetics, IEEE Transactions on,* 44**,** 1002-1005.

KIM, D.-H., LOWTHER, D. A. & SYKULSKI, J. K. 2005. Efficient force calculations based on continuum sensitivity analysis. *Magnetics, IEEE Transactions on,* 41**,** 1404-1407.

KIM, D.-H., LOWTHER, D. A. & SYKULSKI, J. K. 2007. Efficient Global and Local Force Calculations Based on Continuum Sensitivity Analysis. *Magnetics, IEEE Transactions on,* 43**,** 1177-1180.

KIM, D.-H., PARK, I.-H., LEE, J.-H. & KIM, C.-E. 2003a. Optimal shape design of iron core to reduce cogging torque of IPM motor. *Magnetics, IEEE Transactions on,* 39**,** 1456-1459.

KIM, D.-H., PARK, I.-H., SHIN, M.-C. & SYKULSKI, J. K. 2003b. Generalized continuum sensitivity formula for optimum design of electrode and dielectric contours. *Magnetics, IEEE Transactions on,* 39**,** 1281-1284.

KIM, D.-H., SHIP, K. S. & SYKULSKI, J. K. 2004. Applying continuum design sensitivity analysis combined with standard EM software to shape optimization in magnetostatic problems. *Magnetics, IEEE Transactions on,* 40**,** 1156-1159.

KIM, D. H., SYKULSKI, J. K. & LOWTHER, D. A. 2009. The Implications of the Use of Composite Materials in Electromagnetic Device Topology and Shape Optimization. *Magnetics, IEEE Transactions on,* 45**,** 1154-1157.

KOHN, R. V. & STRANG, G. 1986. Optimal design and relaxation of variational problems, I. *Communications on Pure and Applied Mathematics,* 39**,** 113-137.

KOMKOV, V., CHOI, K. K. & HAUG, E. J. 1986. *Design Sensitivity Analysis of Structural Systems,* New York, NY, Academic Press.

LI, M., KIM, D.-H., LOWTHER, D. A. & SYKULSKI, J. K. 2008. A Sensitivity Approach to Force Calculation in Electrostatic MEMS Devices. *Magnetics, IEEE Transactions on,* 44**,** 1610-1613.

LI, M. & LOWTHER, D. A. 2009. Local Electromagnetic Force Computation in the Presence of Numerical Field Errors. *Magnetics, IEEE Transactions on,* 45**,** 1344-1347.

LIU, Q., JABBAR, M. A. & KHAMBADKONE, A. M. Design optimisation of wide-speed permanent magnet synchronous motors. Power Electronics, Machines and Drives, 2002. International Conference on (Conf. Publ. No. 487), 4-7 June 2002 2002. 404-408.

LOWTHER, D. A. 2003. Automating the design of low frequency electromagnetic devices - A sensitive issue. *COMPEL - The International Journal for Computation and Mathematics in Electrical and Electronic Engineering,* 22**,** 630-642.

LOWTHER, D. A., MAI, W. & DYCK, D. N. 1998. A comparison of MRI magnet design using a Hopfield network and the optimized material distribution method. *Magnetics, IEEE Transactions on,* 34**,** 2885-2888.

MASMOUDI, M., POMMIER, J. & SAMET, B. 2005. The topological asymptotic expansion for the Maxwell equations and some applications. *Inverse Problems,* 21**,** 547-564.

MCFEE, S. & LOWTHER, D. A. 1987. Towards accurate and consistent force calculation in finite element based computational magnetostatics. *Magnetics, IEEE Transactions on,* 23**,** 3771-3773.

MCFEE, S., WEBB, J. P. & LOWTHER, D. A. 1988. A tunable volume integration formulation for force calculation in finite-element based computational magnetostatics. *Magnetics, IEEE Transactions on,* 24**,** 439-442.

MICHELL, A. G. M. 1904. LVIII. The limits of economy of material in frame-structures. *Philosophical Magazine Series 6,* 8**,** 589-597.

MIZIA, J., ADAMIAK, K., EASTHAM, A. R. & DAWSON, G. E. 1988. Finite element force calculation: comparison of methods for electric machines. *Magnetics, IEEE Transactions on,* 24**,** 447-450.

MOHAMMED, O. A., LOWTHER, D. A., LEAN, M. H. & ALHALABI, B. 2001. On the creation of a generalized design optimization environment for electromagnetic devices. *Magnetics, IEEE Transactions on,* 37**,** 3562-3565.

MOHAMMED, O. A., MERCHANT, R. S. & ULER, F. G. 1993. Utilizing Hopfield neural networks and an improved simulated annealing procedure for design optimization of electromagnetic devices. *Magnetics, IEEE Transactions on,* 29**,** 2404-2406.

NAM-KYUNG, K., DONG-HUN, K., DONG-WOOK, K., HEUNG-GEUN, K., LOWTHER, D. A. & SYKULSKI, J. K. 2010. Robust Optimization Utilizing the Second-Order Design Sensitivity Information. *Magnetics, IEEE Transactions on,* 46**,** 3117-3120.

NGUYEN, T. N. & COULOMB, J. L. 1999. High order FE derivatives versus geometric parameters. Implantation on an existing code. *Magnetics, IEEE Transactions on,* 35**,** 1502-1505.

OHNISHI, T. & TAKAHASHI, N. 2000. Optimal design of efficient IPM motor using finite element method. *Magnetics, IEEE Transactions on,* 36**,** 3537-3539.

PAHL, G., WALLACE, K. & BLESSING, L. 2007. *Engineering Design: A Systematic Approach*, Springer.

PARK, I.-H., LEE, B.-T. & HAHN, S.-Y. 1991. Sensitivity analysis based on analytic approach for shape optimization of electromagnetic devices: interface problem of iron and air. *Magnetics, IEEE Transactions on,* 27**,** 4142-4145.

PARK, I. H., COULOMB, J. L. & HAHN, S. Y. 1993. Implementation of continuum sensitivity analysis with existing finite element code. *Magnetics, IEEE Transactions on,* 29**,** 1787-1790.

PARKER, C. F., SYKULSKI, J. K., TAYLOR, S. C. & BIDDLECOMBE, C. S. 1996. Parametric environment for EM computer aided design. *Magnetics, IEEE Transactions on,* 32**,** 1433-1436.

PARKINSON, A., SORENSEN, C. & POURHASSAN, N. 1993. A General Approach for Robust Optimal Design. *Journal of mechanical design,* 115**,** 74-80.

PREIS, K., MAGELE, C. & BIRO, O. 1990. FEM and evolution strategies in the optimal design of electromagnetic devices. *Magnetics, IEEE Transactions on,* 26**,** 2181-2183.

PREIS, K. & ZIEGLER, A. 1990. Optimal design of electromagnetic devices with evolution strategies. *COMPEL - The International Journal for Computation and Mathematics in Electrical and Electronic Engineering,* 9**,** 119-122.

RAMIREZ, J. A., FREEMAN, E. M. & LOWTHER, D. A. Application of sensitivity analysis to the calculation of electromagnetic field quantities. Computation in Electromagnetics, 1994. Second International Conference on, 1994. 223-226.

RAY, S. & LOWTHER, D. A. 2009. Multi-Objective Optimization Applied to the Matching of a Specified Torque-Speed Curve for an Internal Permanent Magnet Motor. *Magnetics, IEEE Transactions on,* 45**,** 1518-1521.

REN, Z., PHAM, M.-T. & KOH, C. S. 2013a. Robust Global Optimization of Electromagnetic Devices With Uncertain Design Parameters: Comparison of the Worst Case Optimization Methods and Multiobjective Optimization Approach Using Gradient Index. *Magnetics, IEEE Transactions on,* 49**,** 851-859.

REN, Z., ZHANG, D. & KOH, C.-S. 2013b. An Improved Robust Optimization Algorithm: Second-Order Sensitivity Assisted Worst Case Optimization. *Magnetics, IEEE Transactions on,* 49**,** 2109-2112.

SALON, S., BHATIA, S. & BUROW, D. 1997. Some aspects of torque calculations in electrical machines. *Magnetics, IEEE Transactions on,* 33**,** 2018-2021.

SIGMUND, O. 1999. On the Optimality of Bone Microstructure. *IUTAM Symposium on Synthesis in Bio Solid Mechanics.*

SIM, D.-J., CHO, D.-H., CHUN, J.-S., JUNG, H.-K. & CHUNG, T.-K. 1997. Efficiency optimization of interior permanent magnet synchronous motor using genetic algorithms. *Magnetics, IEEE Transactions on,* 33**,** 1880-1883.

SKARLATOS, A. & THEODOULIDIS, T. 2010. Impedance Calculation of a Bobbin Coil in a Conductive Tube With Eccentric Walls. *Magnetics, IEEE Transactions on,* 46**,** 3885-3892.

SOKOLOWSKI, J. & ZOCHOWSKI, A. 1999a. On the topological derivative in shape optimization. *SIAM Journal on Control and Optimization,* 37**,** 1251-1272.

SOKOLOWSKI, J. & ZOCHOWSKI, A. 1999b. Topological derivatives for elliptic problems. *Inverse Problems,* 15**,** 123-134.

SPAGNUOLO, G. 2003. Worst case tolerance design of magnetic devices by evolutionary algorithms. *Magnetics, IEEE Transactions on,* 39**,** 2170-2178.

STAUNTON, R., NELSON, S., OTADUY, P., MCKEEVER, J., BAILEY, J., DAS, S. & SMITH, R. 2004. *PM motor parametric design analyses for a Hybrid Electric Vehicle traction drive application*, United States. Department of Energy.

STEINER, G., WEBER, A. & MAGELE, C. 2004. Managing uncertainties in electromagnetic design problems with robust optimization. *Magnetics, IEEE Transactions on,* 40**,** 1094-1099.

STEPHANE, G., PHILIPPE, G. & MOHAMED, M. 2001. The Topological Asymptotic for PDE Systems: The Elasticity Case. *SIAM Journal on Control and Optimization,* 39**,** 1756-1778.

STUMBERGER, B., STUMBERGER, G., HADZISELIMOVIC, M., MARCIC, T., VIRTIC, P., TRLEP, M. & GORICAN, V. 2008. Design and Finite-Element Analysis of Interior Permanent Magnet Synchronous Motor With Flux Barriers. *Magnetics, IEEE Transactions on,* 44**,** 4389-4392.

SUNDARESAN, S., ISHII, K. & HOUSER, D. R. 1995. A ROBUST OPTIMIZATION PROCEDURE WITH VARIATIONS ON DESIGN VARIABLES AND CONSTRAINTS. *Engineering Optimization,* 24**,** 101-117.

TAGUCHI, G. 1989. *Introduction to Quality Engineering*, American Supplier Institute.

TAGUCHI, G. 1993. *Taguchi on Robust Technology Development,* New York, ASME Press.

TAGUCHI, G., CHOWDHURY, S. & TAGUCHI, S. 2000. *Robust Engineering,* New York, McGraw-Hill.

TAKAHASHI, N., YAMADA, T. & MIYAGI, D. 2010. Examination of Optimal Design of IPM Motor Using ON/OFF Method. *Magnetics, IEEE Transactions on,* 46**,** 3149-3152.

TELLEGEN, B. 1952. A general network theorem, with applications. *Philips Research Reports,* 7**,** 259-269.

TENNANT, G. 2001. *Six Sigma : SPC and TQM in Manufacturing and Services*, Gower Publishing, Ltd.

THEODOULIDIS, T. & BOWLER, J. R. 2010. Interaction of an Eddy-Current Coil With a Right-Angled Conductive Wedge. *Magnetics, IEEE Transactions on,* 46**,** 1034-1042.

THEODOULIDIS, T. P. & BOWLER, J. R. 2008. Impedance of an induction coil at the opening of a borehole in a conductor. *Journal of Applied Physics,* 103**,** 024905-024905-9.

WANG, S. & KANG, J. 2002. Topology optimization of nonlinear magnetostatics. *Magnetics, IEEE Transactions on,* 38**,** 1029-1032.

WEEBER, K. & HOOLE, H. 1992a. A structural mapping technique for geometric parametrization in the optimization of magnetic devices. *International Journal for Numerical Methods in Engineering,* 33**,** 2145-2179.

WEEBER, K. & HOOLE, S. R. H. 1992b. Geometric parametrization and constrained optimization techniques in the design of salient pole synchronous machines. *Magnetics, IEEE Transactions on,* 28**,** 1948-1960.

WEEBER, K. & HOOLE, S. R. H. 1992c. The subregion method in magnetic field analysis and design optimization. *Magnetics, IEEE Transactions on,* 28**,** 1561-1564.

XIAO, S., ROTARU, M. & SYKULSKI, J. K. 2012. Exploration versus exploitation using kriging surrogate modelling in electromagnetic design. *COMPEL - The International Journal for Computation and Mathematics in Electrical and Electronic Engineering,* 31**,** 1541-1551.

XIAO, S., ROTARU, M. & SYKULSKI, J. K. 2013a. Adaptive Weighted Expected Improvement With Rewards Approach in Kriging Assisted Electromagnetic Design. *Magnetics, IEEE Transactions on,* 49**,** 2057-2060.

XIAO, S., ROTARU, M. & SYKULSKI, J. K. 2013b. Strategies for balancing exploration and exploitation in electromagnetic optimisation. *COMPEL - The International Journal for Computation and Mathematics in Electrical and Electronic Engineering,* 32**,** 1176-1188.

YOO, J.-H. 2004. Modified method of topology optimization in magnetic fields. *Magnetics, IEEE Transactions on,* 40**,** 1796-1802.

YOON, S.-B., JUNG, I.-S., HYUN, D.-S., HONG, J.-P. & KIM, Y.-J. 1999. Robust shape optimization of electromechanical devices. *Magnetics, IEEE Transactions on,* 35**,** 1710-1713.